Computational Models of Organotin-Mediated Alkylation of Diols

by

Simiao Lu

Submitted in partial fulfilment of the requirements
for the degree of Master of Science

at

Dalhousie University
Halifax, Nova Scotia
August 2013

To My Parents,
And To My Teachers.

TABLE OF CONTENTS

List of Tables

List of Figures

List of Schemes

Abstract

Dialkylstannylene acetals are tin-containing species employed extensively as intermediates to facilitate high-yielding and regioselective monosubstitution reactions of diols or polyols with various electrophiles, which is an important application of organotin compounds in organic synthesis. Although an abundance of experimental studies of these reactions have been reported, the mechanism of the reaction has not been well defined. The regioselectivities of these types of reactions are controlled by complex stannylene structures, the presence of added nucleophiles, and stereochemical factors, all of which are difficult to elucidate experimentally.

High-level theoretical methods are used in this thesis to investigate the chemistry of organotin systems at a molecular level. This involves the exploration of the geometry characteristics of the gas-phase structures along the reaction paths in order to understand the mechanism of the organotin-mediated alkylations of diols. An unexpected thermochemical problem was observed and a corresponding benchmarking study was carried out to determine a relatively reliable level of theory for the further research. Alkylation reactions which require strict conditions can be dramatically enhanced by the presence of nucleophiles. The effects of added nucleophiles were examined computationally by comparing reaction profiles obtained for alkylations of dimethylstannylene acetals in the presence of different nucleophiles.

List of Abbreviations and Symbols Used

Abbreviations

B3	Becke's three-parameter exchange functional
BO	Born-Oppenheimer
BSIE	Basis set incompleteness error
BSSE	Basis set superposition error
CI	Configuration interaction
CP	Counterpoise
D3	D3 version of Grimme's dispersion correction
DA	Dialkylstannylene acetal
DFT	Density functional theory
DMF	N, N-dimethylformamide
ECP	Effective core potential
GGA	Generalized gradient approximation
GTO	Gaussian-type orbital
HF	Hartree-Fock
IRC	Intrinsic reaction coordinate
KS	Kohn-Sham
LANL2	Effective core potential developed by Hay and Wadt
LCAO	Linear combination of atomic orbitals
LDA	Local density approximation
LYP	Lee-Yang-Parr correlation functional
M05-2X	Hybrid functional of Truhlar and Zhao
M06-2X	Hybrid functional of Truhlar and Zhao
MBPT	Many-body perturbation theory
MP2	Second-order Møller-Plesset pertubation
MPn	Møller-Plesset perturbation theory
NMR	Nuclear magnetic resonance
PES	Potential energy surface
PGTO	Primitive Gaussian-type orbital
SCF	Self-consistent field
STO	Slater-type orbital
STQN	Synchronous transit-guided quasi-Newton method
TS	Transition state
TST	Transition state theory
XDM	Exchange-hole dipole moment correction
ZPE	Zero-point energy

Symbols

Ψ	Total/Molecular wavefunction
$\hat{H}$	Hamiltonian operator
E	Total/Molecular energy
$\hat{T}$	Kinetic energy operator
$\hat{V}$	Potential energy operator
∇^2	Laplacian operator
Ψ_N	Slater determinant of N spin orbitals
E_0	Ground state energy
ε	Energy eigenvalue
$\hat{F}$	Fock operator
$\hat{J}$	Coulomb operator
$\hat{K}$	Exchange operator
φ	Basis function, atomic orbital
C	Basis function expansion coefficient
S	Overlap matrix
P	Density matrix
$(\mu\vartheta\|\lambda\sigma)$	Two-electron integral
ζ	Orbital exponent
r	Distance between the nucleus and electron
N	Normalization constant
$d_{\mu s}$	Contraction coefficient
g_s	Primitive Gaussian function
E_{HF}	Hartree-Fock energy
E_{corr}	Correlation energy
c_i	Coefficients on Slater determinant
λ	Perturbation paramenter
$\rho(\vec{r})$	Electron density
$V_{ext}(\vec{r})$	External field potential
Ψ_i^{KS}	Kohn-Sham Orbital
E_{XC}	Exchange-correlation energy functional
E_X	Exchange functional
E_C	Correlation functional
c	Speed of light
m	Mass of electron
v	Speed of electron

Acknowledgements

I would like to thank my supervisors in the first place, Dr. Russell J. Boyd and Dr. T. Bruce Grindley for their patience, encouragement and guidance. It is very lucky of me to work under their supervision, experiencing both theoretical and experimental chemistry fields. Also, I would like to acknowledge my committee members Dr. Axel D. Becke and Dr. Mark Stradiotto.

I am grateful to have a great group and lovely members. Especially, I would like to give my thanks to Laura Albrecht and Saptarshi Chowdhury. Although we have different cultural backgrounds, it is always happy time for me to chat with you guys, no matter opinions on science, culture, politics or even small daily things.

I also appreciate the Natural Sciences and Engineering Research Council (NSERC) and Dalhousie University for financial support, and gratefully acknowledge the Atlantic Computational Excellence Network (ACEnet) and Western Canada Research Grid (WestGrid) for providing computer resources for me to carry out this research.

At last, thanks to my wonderful parents for their understanding and long-distance mental support. Without their efforts and persistence, I will never have an opportunity to study abroad.

Chapter 1: Introduction

1.1 Organotin Chemistry

An organotin compound contains at least one Sn-C bond which belongs to part of an organic group (R), forming a compound of the formula R_nSnY_{4-n}, where n may vary from one to four, and Y may be a hydrogen, a metal or a group bonded to the tin atom through oxygen, sulfur, nitrogen, halogen or other atoms.[1] Both tin(II) and tin(IV) compounds can be formed but this thesis will deal only with tin(IV) compounds. Organotin chemistry has played an increasingly active role in organometallic chemistry since the discovery of its various applications.[2,3] In the last 30 years, the development of their utility in organic synthesis has been of considerable interest to organic chemists.[2,4,5] An area of organotin chemistry that has been developed extensively consists of compounds in which tin is bonded to one or more oxygen atoms. These organotin derivatives, which include trialkylstannyl ethers and dialkylstannylene acetals, are used extensively as intermediates that facilitate regioselective monosubstitution of diols, polyols and carbohydrates.[4,6,7] Marked improvements have been made in structural predictions and exploration of reaction pathways. The mechanisms of these reactions had been considered to be well understood[4,6,7] but have recently become controversial.[8,9]

1.2 Computational Tin Chemistry

Theoretical studies on organotin chemistry use computational methods to solve chemistry problems in organotin systems. Experimental studies of these organotin intermediates in association with computational techniques have become increasingly popular in current publications.[10-12] Most recently, a number of studies on structural optimizations[13-15] and reaction mechanisms[12,14,16] including thermochemistry have appeared from a purely theoretical point of view.

This document evaluates the mechanisms of the monoalkylation reaction of the dimethylstannylene acetal of ethylene glycol by theoretical methods through both the monomeric and dimeric forms of the tin derivatives.

1.3 Dialkylstannylene Acetals

Organotin derivatives where tin is bonded to oxygen atoms are widely used in synthesis. Compounds with one oxygen atom attached are termed tin ethers or stannyl ethers, whereas those with two oxygen atoms attached are termed stannylene acetals, particularly if the two oxygen atoms are part of a single molecule, resulting in a ring incorporating tin. Dialkylstannylene acetals are widely used as intermediates in reactions of diols and polyols with electrophiles because they give monosubstituted products reliably, often with specific regioselectivity. In comparison to the same reactions with the parent diols, these tin-containing species react at a higher rate, under milder conditions,

giving much more selective monosubstitution and providing much better regioselectivity.[4,6,7]

1.3.1 Preparation of Dialkylstannylene Acetals

Dialkylstannylene acetals are relatively simple to synthesize in high yield. They are usually prepared by reaction of diols (**1**) with dibutyltin oxide or dibutyltin dimethoxide in methanol with heating, or in benzene or toluene with azeotropic removal of water (Scheme 1.1). The afforded acetals (**2**) act as nucleophiles towards various types of electrophiles in reactions such as alkylation, acylation, sulfonylation, oxidation, phosphorylation, and glycosylation.[17-19]

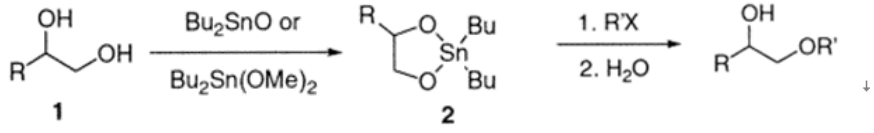

Scheme 1. 1: Regioselective monosubstitution of a diol via a dibutylstannylene acetal intermediate.[19]

1.3.2 Structures of Dialkylstannylene Acetals

In trialkyltin ethers, the tin atoms remain tetracoordinate under all conditions.[2,20] When two oxygen atoms are attached to tin in dialkyldialkoxytin derivatives, the tin atom has been observed to expand its coordination number to five or six. The extent to which this happens depends on the nature of the substituents, the state, the temperature, and the

solvent. Neat or in solution at room temperature, dibutyltin dialkoxides exist as dimers with pentacoordinate tin when the alkoxides are methoxide or primary alkoxides, as monomers with tetracoordinate tin when the alkoxides are tertiary, and as monomer-dimer mixtures when the alkoxides are secondary.[11,20] As mentioned before, if the two oxygen atoms are part of the same molecule, the formation of the organotin derivative results in a ring, a stannylene acetal. If the oxygen atoms are on adjacent carbons, i.e. 1, 2-diol, the resulting ring is five-membered and the O-Sn-O angle observed in the solid state is 78-80°.[21] This small bond angle is caused by the geometry constraint imposed by having two sides (Sn-O bonds) of the five-membered ring being much longer than the others (C-O and C-C bonds). The geometryally enforced decrease in bond angle from the tetrahedral geometry of tin of monomeric acyclic species with 109.5° O-Sn-O bond angles to <80^{o} stabilizes dimerization. The bond angle at tin can be close to the 90^{o} angle that is possible with pentacoordinate geometry, or oligomerization, where all bond angles are 90^{o}, if the tin atom is hexacoordinate. In the solid state, dibutylstannylene acetals with limited substitution are polymers with octahedral tin.[22-24] In more substituted compounds, such as carbohydrate derivatives, structures of stannylene acetals ranging from dimers to pentamers have been observed in the solid.[21,25,26]

In solution, ^{119}Sn NMR spectroscopy has shown that the less substituted derivatives are less aggregated than in the solid state, existing as temperature dependent mixtures of dimers and oligomers up to the pentamers.[24,27,28] More substituted derivatives, such as

carbohydrate-derived stannylene acetals, are largely dimers with some contributions from trimers, as shown by ^{119}Sn NMR spectroscopy and mass spectral studies.[19,29-31]

To form a dimer, coordination of one oxygen atom from each monomer to the tin atom of the other monomer produces a four-membered ring containing two pentacoordinate tin atoms and two tricoordinate oxygen atoms (Figure 1.1). Higher oligomers with hexacoordinate tin atoms are produced if the pentacoordinate tin atom coordinates to an additional oxygen atom. In the dimer, a stannylene acetal five-membered ring is formed from two oxygen atoms attached to the same tin atom. One of the oxygen atoms adopts an equatorial position at the trigonal bipyramidal tin atom, while the other adopts an axial position. Within the extended oligomers, tin atoms have octahedral geometries and all O_2Sn_2 four-membered rings between two units lie in the same plane. Stannylene acetal rings on alternative tin atoms stretch outwards in the opposite directions, connected by the O_2Sn_2-defined planes.[6] Thus, the stannylene rings on every second unit are placed on the same side. Bulky ligands on the tin atom hinder the formation of oligomers, which will be discussed in more detail in the steric effects section.

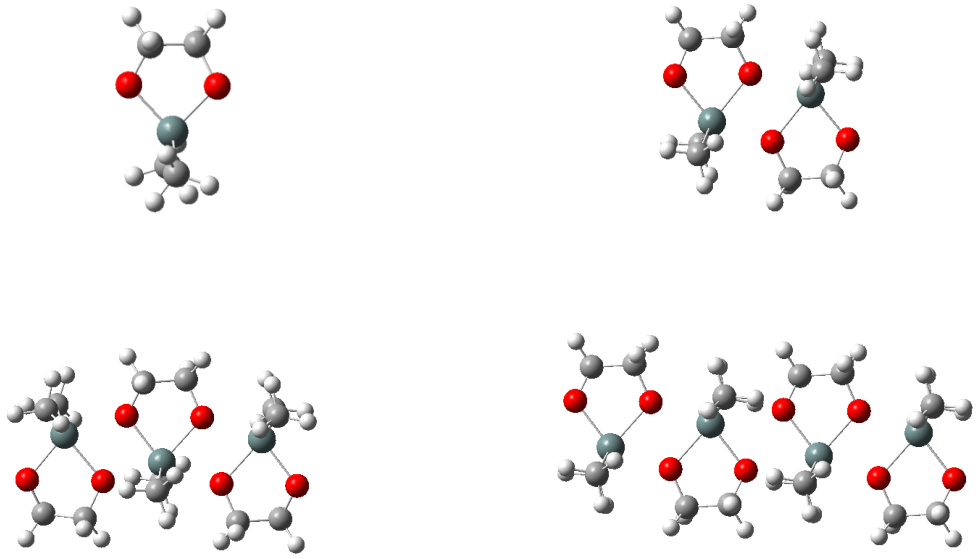

Figure 1. 1: Structure of monomer, dimer, trimer and tetramer dimethylstannylene acetals.

Dimeric species are the most populated in the mixture of dialkylstannylene acetals. In the formation of a dimer, there are two kinds of oxygen atoms: one is dicoordinate attached to the tin atom and the carbon atom, the other is tricoordinate with an extra bond to another tin atom of the next acetal unit. Tricoordinate oxygen atoms are less reactive than dicoordinate ones due to the deactivation of an additional attachment to the tin atom.[4] There are three possible dimeric structures of dialkylstannylene acetals derived from primary-secondary 1, 2-diols (Figure 1.2): a primary, primary dimer (p,p dimer), a primary, secondary dimer (p,s dimer) and a secondary, secondary dimer (s,s dimer).[31]

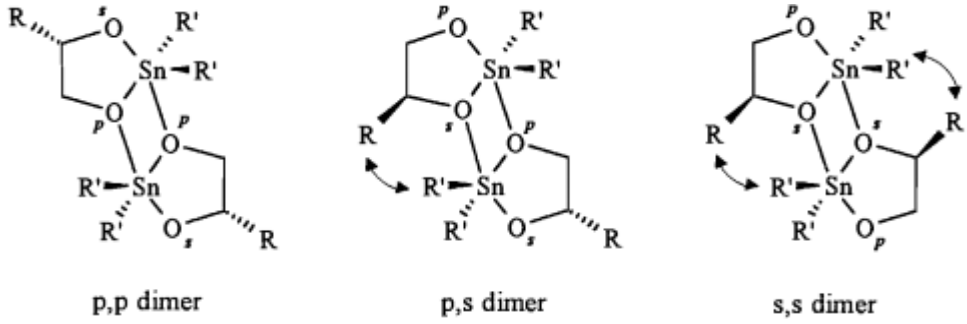

Figure 1. 2: Dimeric structures of dialkylstannylene acetals derived from primary-secondary 1, 2-diols. Dimer nomenclature is based on the types of the tricoordinate oxygen atoms.[31]

Based on the relative stabilities, the p,p dimer is the most populated one, followed by the p,s dimer and s,s dimer. From the point of view of steric effects, the p,p dimer is the only dimeric structure to fully avoid steric interactions. Therefore, steric effects are the major factor in determining the dimer populations in solution. Also, steric effects are one of the factors that influence regioselectivity in the reactions of organotin intermediates.

1.4 Causes of Regioselectivity

The factors that influence the regioselectivity of monosubstitution obtained from dialkylstannylene acetals are complicated. In general, the selectivity depends on the structure of the substrate, the reaction conditions, the presence of added nucleophiles, and the nature of the electrophile.[7] Some reactions are kinetically controlled, e.g. oxidation, alkylation, and sulfonation, but are thermodynamically controlled in others, e.g. silylation,[32] or benzoylation.[33] The causes of the regioselectivity can co-exist and affect each other in different cases. However, the conclusions are surprisingly similar in

most circumstances.[8] This section focuses on the first two causes involved in the reactions with diols through the monomeric or dimeric intermediates.

A significant factor is the structure of the intermediates and relative reactivity of the dominant oligomeric species (mostly the dimer) in solution.[7,34,35] The stereochemical relationships between secondary hydroxyls on pyranose sugars influence the regioselectivity of the reactions. If a *cis*-diol is present, as for mannose and galactose derivatives, one hydroxyl will be equatorial and one will be axial. For *trans*-diols, both hydroxyls are either equatorial or axial.[4,6] When both *cis*-diols and *trans*-diols are exposed, reaction takes place on the *cis*-diol. These reactions and those where only *cis*-diols are exposed, usually give major products substituted on the equatorial oxygen atom. In the reaction of dibutylstannylene acetals of terminal diols, the preference of substitution is usually on the primary oxygen atom. It is well known that the primary hydroxyl group is more chemically active than the secondary hydroxyl group in S_N2 reactions. Consequently, monosubstitutions occurring on the primary hydroxyl group in a diol or polyol unit is one of the factors related to the structure of the intermediates that influences the regioselectivity. Nevertheless, several examples are known with contrary results. For example, dibutylstannylene acetals of *cis*-diols on the pyranose ring have provided predominant products from reaction on the axial oxygen atom,[36,37] and acetals of terminal 1, 2-diols have reacted at the secondary oxygen atom.[31,34-36,38] The mechanisms of reactions of dialkylstannylene acetals have been discussed both in terms of monomeric and dimeric structures. It has been suggested that monomers are less likely

to be the intermediate due to their lower populations in the oligomeric equilibrium and probably lower reactivity. However, monomeric dialkylstannylene acetals are commonly employed as intermediates[8,9] and there is no adequate proof to support the contention that the more populated dimers are the reaction intermediates.

In the dimer of a dialkylstannylene acetal (Figure 1.3), the apical dicoordinate oxygen atom is more reactive than the other tricoordinate one for several reasons. The latter oxygen atom is deactivated by the third coordination with the tin atom and sterically hindered by two alkyl groups on both of the tin atoms.[7,31] Also, the apical position is preferred with higher reactivity in the trigonal bipyramid at tin.[4] This preference can be supported by the suggested reaction mechanism of the cleavage of the apical Sn-O bond and simultaneous formation of a bond between the tin atom and an electrophile.[6]

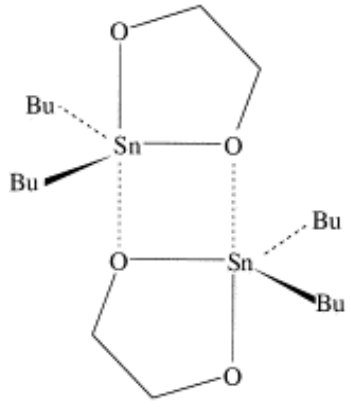

Figure 1. 3: An idealized structure of dimer of a dibutylstannylene acetal.[39]

Steric effects have an important impact on the intermediate structures, especially dimers, and further affect the regioselectivity of reactions.[30,31,34,40] In other words, steric

effects determine the predominant dimeric species in solution. The typical causes of these effects are the size of the substituents on the secondary hydroxyl group and the size of the alkyl groups on the tin atom (Figure 1.3). According to ^{119}Sn NMR spectroscopy, the increasing size of the alkyl groups reduces the reactivity of the dicoordinate oxygen atom on the secondary positions more than that on the primary positions because the former ones are already sterically hindered(Figure 1.2).[31] On the other hand, the introduction of bulky alkyl groups on the tin atom increases the selectivity of the secondary oxygen atom in the reaction. In both cases, the populations of p,s dimer and s,s dimer decrease due to increased steric hindrance on the tricoordinate oxygen atom and the tin atom at the same time(Figure 1.2). Based on the analysis of steric effects, the p,p dimer is the most stable dimeric species.[31]

The second factor that plays a key role in the regioselectivity is reaction conditions, such as concentration, temperature, physical state, the presence of an added nucleophile, solvation effects and other conditions. A 1991 publication by Nagashima and Ohno[41] contained an investigation of the influences of various factors. They studied the regioselectivity of benzylation of unsymmetrical diols (1-phenylethanediol) through dibutylstannylene acetals under different conditions, such as benzyl halides, metal fluorides (added nucleophile), solvent and temperature (Scheme 1.2). It was shown that the reaction rate increased in the order of benzyl fluoride (actually no reaction), benzyl chloride, benzyl bromide and benzyl iodide, that is, the normal S_N2 order.

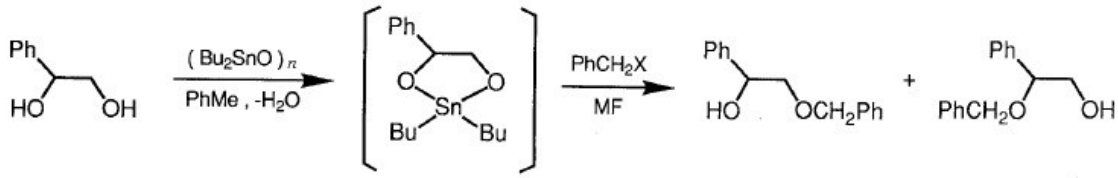

Scheme 1. 2: Monoalkylation of phenyl-1, 2-ethanediol through the dibutylstannylene acetal.[41]

The differences in the regioselectivity were further investigated by performing reactions with cesium fluoride and potassium fluoride (fluoride is the added nucleophile). Different solvent effects and temperatures were also observed. The best reaction conditions concluded in this research were benzyl iodide and cesium fluoride in N, N-dimethylformamide (DMF) at 0 ^{o}C, similar to those used earlier by Danishefsky.[42]

Temperature and solvent effects are also very influential in these reactions. The population of a certain dimeric species that favors a particular regioisomer will change with varying temperature. Equilibria that involve association of two monomers to a dimer are highly temperature dependent because of the negative entropy term involved in the aggregation. Thus, as the temperature is raised the monomers increase in population. Different regioselectivities have been observed in different solvents, as well as associated with other conditions. For instance, in the nonpolar solvents and in the absence of added nucleophiles, dialkylstannylene acetals exist as a mixture of dimer and higher oligomers, in which a dimer is the predominant species. Minor dimers will also be more populated as the temperatures increases from 0 to 100 °C.[27]

In the present computational study, the monomeric and dimeric forms of the acetal

of ethylene glycol with added nucleophiles were modeled in the gas-phase using density functional theory (DFT). In order to concentrate on the study of the mechanism of monoalkylation reaction through these organotin intermediates, relatively simple systems were chosen. Based on these facts, two main factors of regioselectivity were considered: the intermediate structures and the presence of added nucleophiles. Solvent effects should be taken into account in future studies because of the probability of their contribution to the stabilization of intermediate structures.

1.5 Presence of Added Nucleophiles

The presence of added nucleophiles, for example halides, can influence regioselectivity because the geometry structures of intermediates and perhaps the mechanism are changed by their presence. This factor enhances reaction rates, markedly accelerates monosubstitution[41-44] and can dramatically influence regioselectivity.[37,45,46] Many nucleophiles are effective, including cesium fluoride,[42,47] *N*-methyllimidazole,[48] and tetrabutylammonium halides.[43,49] One postulated role of nucleophiles coordinated to the tin atom is to enhance the nucleophilicity of both oxygen atoms and weaken the Sn-O interaction by the elongation of the bond.[8] Another explanation of the rate acceleration is an ease of approach of electrophiles with reduced steric hindrance. In solution, it is probable that the dimer stannylene acetals react with the added nucleophiles, forming monomer complexes with pentacoordination at the tin site as intermediates.[7] The

reaction mechanisms were suggested involving dimeric intermediates[4,31] and monomeric ones.[8,9,50-52]

Alkylation reactions are the slowest reactions of stannylene acetals and often occur with less regioselectivity compared to acylation and oxidation reactions. In the absence of added nucleophiles, these reactions only occur at increased temperatures above room temperature, giving low yields even with the most active alkylating reagents. Since the discovery that added nucleophiles increase reaction rates, it is normal practice to add nucleophiles when performing alkylation reactions.[42-44,47]

1.6 Regioselective Alkylation Reactions of Diols through Dialkylstannylene Acetals

1.6.1 One Suggested Mechanism

Many alkylation reactions through dialkylstannylene acetals with added nucleophiles were performed to support the splendid advancement in the reaction rate. The regioselectivity observed in the alkylation reaction using a monomeric intermediate is connected to the presence of an added nucleophile. Gingras *et al.* suggested that the fluoride anion (nucleophile) attacks the tin center of the stannylene acetal of a diol to generate a pentacoordinate complex, which results in the formation of a highly reactive alkoxide anion.[53] This anion possesses greater nucleophilicity than the original acetals, which contributes to the successful reactions with alkyl halides. According to this

discussion, a suggested mechanism based on the benzylation reaction (in DMF) of a dibutylstannylene acetal with an added fluoride (cesium fluoride) is shown below. (Scheme 1.3).[41]

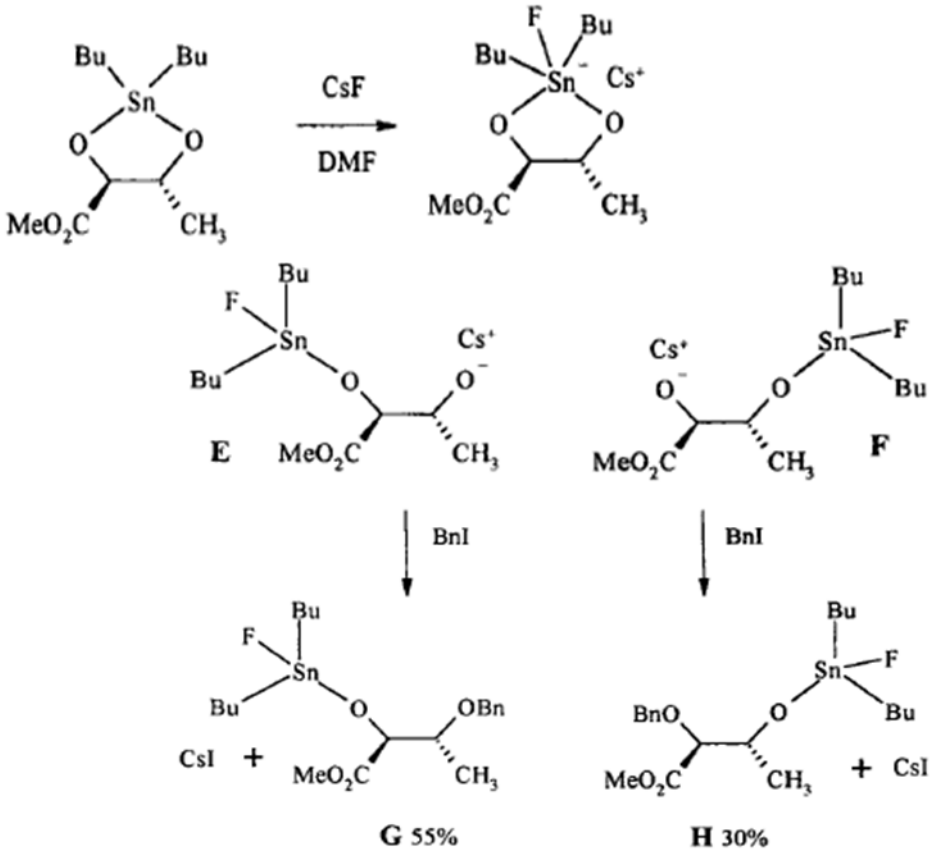

Scheme 1. 3: A suggested mechanism for benzylation reaction of dibutylstannylene acetals with an added fluoride.[41]

1.6.2 Thesis Summary

This thesis elaborates the exploration of the mechanism of the monoalkylation reaction through organotin intermediates by using computational methods. Chapter 2 briefly introduces some of the methods of computational chemistry including density functional theory (DFT) and Møller-Plesset perturbation theory (MPn). Furthermore, because tin is

a relatively heavy element, relativistic effects and effective core potentials (ECP) are described.

Chapters 3 and 4 describe predictions of the geometry structures and reaction mechanisms, and demonstrate the necessity of choosing an appropriate basis set for the thermochemistry of organotin systems.

Chapter 5 examines the mechanisms and the effects of added nucleophiles for monoalkylation reaction pathways of diols with various added nucleophiles on the organotin intermediates including structural optimizations and thermochemistry.

Chapter 6 summarizes the results and conclusions of this study, and proposes possible directions for future research on organotin systems.

Chapter 2: Theoretical Background

Theoretical chemistry provides an ability to tackle real chemical problems by using mathematical methods combined with fundamental laws of physics. With the dramatic advance of computer technologies, various methods have been developed and are available in many software packages. These methods are not "perfect" due to the many approximations and assumptions inherent in the methods. Therefore, it is essential to understand the background theory and to analyze the drawbacks and limitations of computational methods. This chapter introduces Hartree-Fock (HF) theory, Møller-Plesset perturbation theory (MPn) and density functional theory (DFT). Since the reaction paths investigated in this thesis involve heavy-element systems, the basic principles of relativistic effects and effective core potentials (ECP) are provided. The last topic briefly describes the optimization techniques applied in this study.

2.1 The Schrödinger Equation

The Schrödinger equation is the fundamental equation of physics used to describe quantum mechanical behavior. It combines de Broglie's relation with the conservation of energy from classic mechanics, which is also a wave equation in terms of its wavefunctions (Ψ). This equation is simplified by considering only time-independent solutions and shown in short-hand operator form (Eq. 2.1),[54] which includes the Hamiltonian operator ($\hat{H}$) of the wavefunction (Ψ) and the associated eigenvalue (E), the

total energy of the system.

$$\hat{\mathrm{H}}\Psi = E\Psi \qquad (2.1)$$

The wavefunction is capable of exactly describing the behaviors of atomic particles, such as electrons, photons and atoms.[55] Wavefunctions are required to be single-valued, continuous and finite; they must be normalized in order to integrate to the exact number of electrons present in the system, and they must be antisymmetric to satisfy the Pauli exclusion principle.

An essential part of solving the Schrödinger equation is the Born-Oppenheimer (BO) approximation,[56] which allows for a separation of the motion of the nuclei and the electrons. Based on this assumption, the electronic Hamiltonian operator ($\hat{H}$) can be written as the sum of kinetic energy operator for the electrons ($\widehat{T_e}$), the potential energy operator for the interaction between the electron and nuclei ($\hat{V}_{en}$) and potential energy of the interaction between the electrons ($\hat{V}_{ee}$) (Eq. 2.2).

$$\widehat{H} = \widehat{T_e} + \hat{V}_{en} + \hat{V}_{ee} \qquad (2.2)$$

The time-independent Schrödinger equation can be only solved exactly for simple systems, such as one-electron systems, the hydrogen atom and cationic dihydrogen.[57] In order to obtain approximate solutions for more complex systems (i.e. many-electron atoms or molecules), further approximations and assumptions must be introduced.

2.2 Hartree-Fock Theory

Hartree-Fock (HF) theory provides a feasible route to create a many-electron wavefunction from one-electron wavefunctions. To satisfy the antisymmetry principle, the many-electron wavefunction is represented as a single Slater determinant of N spin orbitals (Eq. 2.3), Ψ_N. When expanded, the Slater determinant generates all possible permutations of the N electrons among the N spin orbitals.

$$\Psi_N = \frac{1}{\sqrt{N!}} \begin{vmatrix} \psi_{1(x_1)} & \psi_{1(x_2)} & \cdots & \psi_{1(x_N)} \\ \psi_{2(x_1)} & \psi_{2(x_2)} & \cdots & \psi_{2(x_N)} \\ \vdots & \vdots & & \vdots \\ \psi_{N(x_1)} & \psi_{N(x_2)} & \cdots & \psi_{N(x_N)} \end{vmatrix} \qquad (2.3)$$

The best possible Ψ_i is determined by the variation principle, which states that the best wavefunction gives the lowest energy and the energy obtained is greater than or equal to the true ground-state energy E_0,[58] yielding a set of HF equations. These equations include the energy eigenvalue (ε_i) and the Fock operator ($\hat{F}$) (Eq. 2.4-2.5).

$$\hat{F}\Psi_i = \varepsilon_i \Psi_i \qquad \text{i=1, 2… N} \qquad (2.4)$$

$$\hat{F} = \hat{H}^{\text{core}} + \sum_{j=1}^{N} (2\hat{J}_j - \hat{K}_j) \qquad (2.5)$$

The first term in the Fock operator corresponds to the motion of one electron and includes its kinetic energy and the nuclear-electron attraction energy. The second term incorporates the Coulomb ($\hat{J}_j$) and the exchange operators ($\hat{K}_j$) that relate to electron-electron interactions. The $\hat{J}_j$ basically translates to the electron-electron repulsion, while $\hat{K}_j$ arises from the antisymmetry principle and describes the exchange

of any pair of electrons.

The solution to the HF equation yields a set of HF orbitals (Ψ_i) where the Slater determinant constructed from these orbitals is the HF ground-state wavefunction according to the variational method. The square of a given molecular orbital represents the probability distribution of finding an electron, where the attraction to all nuclei and the average repulsion to all the other electrons are included. However, the HF equations are non-linear and therefore must be solved iteratively by following a self-consistent field (SCF) procedure.[59] To solve the HF equations for molecules, it is convenient to express Ψ_i as a linear combination of a finite (basis) set of atomic orbitals (LCAO), which are called basis functions (Eq. 2.6),

$$\Psi_i = \sum_{\mu=1}^{K} C_{\mu i}\varphi_\mu \qquad (2.6)$$

where φ_μ represents the atomic orbitals and $C_{\mu i}$ are the molecular orbital expansion coefficients. Introduction of the LCAO approximation into the HF equations leads to the Roothaan-Hall equations[60,61] (Eq. 2.7), which include the Fock matrix ($F_{\mu\vartheta}$), the energy (ε_i) of the orbital Ψ_i and $S_{\mu\vartheta}$, which is an overlap matrix between basis functions φ_μ and φ_ϑ. The Fock matrix element ($F_{\mu\vartheta}$) includes the core Hamiltonian operator ($H_{\mu\vartheta}$) and the two-electron repulsion integrals (Eq. 2.8). $P_{\lambda\sigma}$ is the matrix element of density matrix $P_{\mu\vartheta}$ (Eq. 2.9).

$$\sum_{\vartheta=1}^{M}(F_{\mu\vartheta} - \varepsilon_i S_{\mu\vartheta})C_{\vartheta i} = 0 \qquad \mu = 1, 2 \ldots K \qquad (2.7)$$

$$F_{\mu\vartheta} = H_{\mu\vartheta} + \sum_{\lambda=1}^{M}\sum_{\sigma=1}^{M} P_{\lambda\sigma}\left[(\mu\upsilon|\lambda\sigma) - \frac{1}{2}(\mu\upsilon|\lambda\sigma)\right] \qquad (2.8)$$

$$P_{\mu\vartheta} = 2\sum_{i=1}^{occ\ MOs} C_{\mu i}\, C_{\vartheta i} \qquad (2.9)$$

Similar to the HF equations, the Roothaan-Hall equations are solved iteratively, and an initial guess for the coefficients is required to begin the SCF procedure. Additionally, the greater the number of basis functions used, the better the description of the molecular orbitals.[57]

2.3 Basis sets

The set of basis functions used in the Roothaan-Hall method is called a "basis set". Since the choice of the basis set may influence the computational accuracy, the type of the basis function, the contraction scheme and the size of the basis set are important for accurate calculations. Two types of basis functions are commonly used in electronic structure calculations: Slater-type orbitals (STO)[62] and Gaussian-type orbitals (GTO).[63] Their equations (Eq. 2.10, Eq. 2.11) are given below, respectively, where

$$\mathrm{STO} = \mathrm{N}Y_{lm}\ (\theta, \varphi) r^{n-1} e^{-\zeta r} \qquad (2.10)$$

$$\mathrm{GTO} = \mathrm{N}Y_{lm}\ (\theta, \varphi) r^{(2n-2-l)} e^{-\zeta r^2} \qquad (2.11)$$

N is a normalization constant and $Y_{lm}(\theta, \varphi)$ are the spherical spherical harmonics. The magnitude of the orbital exponent (ζ) determines the size of the orbital. The exponential depends on the distance between the nucleus and electron (r). Although STOs are

appropriate for describing molecular orbitals, their application is limited because the calculation of three- and four-center two-electron integrals cannot be performed analytically.[57,58] Evaluation of the two-electron repulsion integrals is much easier and faster with a basis set of GTOs due to the Gaussian product theorem: the product of two GTOs on two different centers is a third GTO on a third center. Thus, all three- and four-center two-electron repulsion integrals can be simplified to two-center integrals. However, the r^2 dependence of the exponential leads to the wrong behavior of the GTO near the nucleus since it has a zero derivative and a flat tangent with no cusp. In order to obtain efficiency (GTO) and retain accuracy (STO), the primitive GTOs (g_s) (Eq. 2.12) with their respective contraction coefficients ($d_{\mu s}$) are linearly combined into a small set of functions, referred to as contracted Gaussian basis functions (φ_μ),[64] to reproduce as accurately as possible the exponential behavior of STOs.

$$\varphi_\mu = \sum_s d_{\mu s} g_s \qquad (2.12)$$

In this equation, 's' is the number of Gaussians used in the linear combination and the coefficients ($d_{\mu s}$) are fixed and chosen to optimize the shape of the basis function sum and to ensure normalization.

To achieve more accuracy and flexibility, additional basis functions can be added to form extended basis sets. This may be done by splitting the basis set and by adding polarization and/or diffuse functions. The first way increases the number of basis functions by splitting the valence orbitals into inner and outer valence orbitals.[65] This produces a "split-valence" basis set. Adding polarization functions allows for more

flexibility of the basis sets to model the shape of the orbitals by adding functions that correspond to higher angular momentum quantum numbers. Diffuse functions provide large orbitals when electron density is far from the nucleus, such as in anions, and in molecules with highly excited electronic states and delocalized π systems. Inclusion of polarization and diffuse functions is important for the description of weak interactions in systems containing features such as van der Waals interactions and hydrogen bonds.

Pople split-valence basis sets are the most popular basis sets applied to molecular systems. These basis sets can be described by the formula k-nlmG, where k indicates the number of primitive GTOs (PGTO) used to represent the core orbitals and nlm describes both the number of functions that the valence orbitals are split into, and the number of PGTOs used for each function. The values that appear before the G describe the minimal atomic basis functions, while the added polarization functions are indicated after the G. Diffuse functions are normally s- and p- functions, and are denoted by a plus symbol (+) before the G. For example, 6-311+G(d,p) is a triple split-valence basis, where a contraction of six PGTOs are used for the core orbital and the valence shell is split into three functions, and each function is represented by three, one and one PGTOs, respectively. In this example, a diffuse set of functions (+) and a set of d-type polarization functions are added to the heavy atoms and a set of p-type polarization functions is added to all hydrogen atoms.

Due to the prohibitive computational cost, a complete basis set cannot be used in practice. The absolute errors in energy due to incompleteness of basis sets are quite large

for most systems, possibly up to several atomic units (au). Another source of error from basis sets is basis set superposition error (BSSE). This error illustrates that, for example, when two monomers approach each other, basis functions from one monomer can describe electrons centered on the other monomer, which artificially lowers the energy of the dimer. This is particularly problematic for weak interactions, such as van der Waals interactions and hydrogen bonds. A common solution to correct these errors is the counterpoise (CP) correction, proposed by Boys and Bernardi.[66] In this modification, the single-point energy of one separated fragment (a monomeric unit) is calculated in the presence of 'ghost' basis functions (meaning without the nuclei or electrons) of the next fragment, and vice versa.

2.4 Electron Correlation and Møller-Plesset Perturbation Theory

A lack of electron correlation is one of the drawbacks of HF theory, because the HF orbital model only considers the average electron repulsion instead of treating electron-electron interactions explicitly.[67] In a sufficiently large basis set, the best HF wavefunction yields an energy (E_{HF}) that is still higher than the exact energy, creating the HF limit.[57] The difference between the E_{HF} and the lowest possible energy with a given basis set (E_{exact}), is known as the correlation energy (E_{corr}) (Eq.2.13).[58]

$$E_{corr} = E_{exact} - E_{HF} \tag{2.13}$$

Although this energy difference is typically less than 1% of the total energy, it arises

from the correlated motions of the electrons, which is essential to describe chemical bonds. Therefore, accurate theoretical predictions require the consideration of electron correlation.

Post Hartree-Fock methods are based on HF theory and attempt to improve the HF results by taking into account the effects of electron correlation. Two main methods for calculating electron correlation will be introduced: configuration interaction (CI) and many-body perturbation theory (MBPT). Configuration interaction (CI) is the simplest approach based on the variational principle. This method proposes an approximation by a linear combination of Slater determinants (Ψ_i) with the expansion coefficients (c_i) treated as variational parameters (Eq. 2.14).

$$\Psi = \sum_i c_i \Psi_i \qquad (2.14)$$

Using a mathematically complete basis set CI can yield the exact solution to the N-electron system.[68] However, this is not practical because CI can only handle a finite set of configurations and basis functions.

MBPT is a perturbative approach. The basic principle is to solve the unsolvable but exact equation by dividing it to two parts: an exactly solvable expression, which yields a solution that is only slightly incorrect, and an expression that corrects the incorrect solution to approximate the exact solution of the unsolvable expression.[58] Mathematically, the total Hamiltonian ($\widehat{H}$) (unsolvable) is separated into a zeroth-order or reference Hamiltonian ($\widehat{H}_0$) (solvable but slightly incorrect) plus a perturbation ($\widehat{H}'$). The $\widehat{H}'$ is used to correct $\widehat{H}_0$ and the difference is assumed to be small.[58] Eq. 2.15 and

Eq. 2.16 indicate the perturbed Schrödinger equation, where λ is the parameter determining the strength of the perturbation.

$$\hat{H} = \hat{H}_0 + \lambda\hat{H}' \quad (2.15)$$

$$\hat{H}\Psi = (\hat{H}_0 + \lambda\hat{H}')\Psi = \mathrm{E}\Psi \quad (2.16)$$

This perturbation provides a systematic improvement of the eigenvalue and eigenfunction of the total Hamiltonian by continuously changing the system from unperturbed to perturbed.[69] By increasing the order of perturbation (λ) from zero to a finite value, the corresponding wavefunction, Ψ, and the energies E, will change continuously, which can be expressed as a Taylor series in different powers of λ (Eq. 2.17 and Eq. 2.18). The $\Psi^{(k)}$ and $E^{(k)}$ are the kth-order correction to the wavefunction and energy.[70]

$$\mathrm{E} = E^{(0)} + \lambda E^{(1)} + \lambda^2 E^{(2)} + \cdots + \lambda^k E^k \quad (2.17)$$

$$\Psi = \Psi^{(0)} + \lambda\Psi^{(1)} + \lambda^2\Psi^{(2)} + \cdots + \lambda^k\Psi^k \quad (2.18)$$

Møller-Plesset perturbation theory (MPn) is the most popular MBPT approach, starting from the HF approximation to expand the exact solution of the Schrödinger equation by providing an estimate of the correlation energy. In this method, the unperturbed zero-order Hamiltonian is the HF Hamiltonian and the perturbation $\hat{H}'$ allows for correction of the effects of electron correlation. The 'n' stands for the power or the order of the perturbation. Recall that the perturbation is usually assumed to be small, thus inclusion of the first several orders will be sufficient for most systems.[69] The MP2 method is widely applied in computational chemistry, and its energy is able to account

for 80-90% of E_{corr}.[58] However, the method can lead to overestimation of the electron correlation, which will be discussed more in Chapter 5. Higher-order perturbations account for more electron correlation, but also require more computer power. MPn methods are affordable methods for including electron correlation with reasonable computational expense.

2.5 Density Functional Theory

Density functional theory (DFT) provides a simplified approach to solve the Schrödinger equation which circumvents many problems in HF and post-HF methods. The fundamental principle of DFT is that the ground-state properties of a system can be determined from the electron probability density instead of using a wavefunction.[67] This has been proved by Hobenberg and Kohn[71] through two theorems. First, they proved that the external field potential ($V_{ext}(\vec{r})$) is a unique functional of the electron density ($\rho(\vec{r})$) for its ground state. Therefore, $\rho(\vec{r})$ uniquely defines the full Hamiltonian operator and thus all the ground state molecular properties of the system, such as the energy. Eq. 2.19 demonstrates a direct relationship between the electron density $\rho(\vec{r})$ and the total ground-state electronic energy (E), where E is a functional of $\rho(\vec{r})$.

$$\mathrm{E} = \mathrm{E}[\rho(\vec{r})] \qquad (2.19)$$

Unlike the HF wavefunction, the electron density in DFT is independent of the system size, which means it has a constant number of variables with increasing numbers of

electrons in the system. Second, the density obeys the variational principle.[57] This means the true ground state energy (E_0) can only be delivered when the input electron density is equal to the true ground-state density (Eq. 2.20).

$$E_0 \leq E[\rho] \tag{2.20}$$

Based on the BO-approximation, the total energy functional $E[\rho]$ can be written in three parts (Eq.2.21):

$$E[\rho] = T[\rho] + E_{ne}[\rho] + E_{ee}[\rho] + V_{nn} \tag{2.21}$$

$T[\rho]$ is the kinetic energy, V_{nn} is the potential energy between nulei, $E_{ne}[\rho]$ is the nuclei-electron attraction energy and the electron-electron repulsion energy is represented by $E_{ee}[\rho]$. The $E_{ee}[\rho]$ term can be divided into $\mathrm{J}(\rho)$ and $\mathrm{XC}(\rho)$, the Coulomb and exchange parts, yielding Eq. 2.22.

$$E[\rho] = T[\rho] + E_{ne}[\rho] + J(\rho) + XC(\rho) + V_{nn} \tag{2.22}$$

Since the exact form of $XC(\rho)$ remains unknown, it is difficult to construct the valid energy functional to yield the ground state energy (E_0).[72] To solve this difficulty, Kohn and Sham[73] introduced a non-interacting system of electrons with the same electron density ($\rho(\vec{r})$). It is assumed that it is possible to set up a non-interacting reference system using a Hamiltonian that includes an effective local potential that will yield the exact density of the interacting system. The electron density is first expressed as a linear combination of basis functions of non-interacting electrons called Kohn-Sham (KS) orbitals (Ψ_i^{KS}), yielding a correlation-free Slater determinant (Eq. 2.23), which is similar to a HF orbital in mathematical form.[74] Thus, rather than approximating the true

N-electron wavefunction, as in HF theory, $\rho(\vec{r})$ is written exactly in terms of a set of non-interacting N-electron orbitals,

$$\rho(\vec{r}) = \sum_i^N \left|\Psi_i^{KS}\right|^2 \qquad (2.23)$$

The complexity of a poorly described kinetic energy in DFT is thus improved by creation of a non-interacting reference system. To be specific, the kinetic energy $T[\rho]$ is separated into two parts: 1) the kinetic energy of the non-interacting electrons ($T_s[\rho]$) that can be calculated exactly and 2) the correlation contribution ($T_c[\rho]$), which cannot be exactly calculated, is also a correction term to $T_s[\rho]$.[58] This correction term equals the difference between the exact kinetic energy and $T_s[\rho]$, and is included in the exchange-correlation energy functional ($E_{xc}[\rho]$) (Eq.2.24), which contains all unknowns.

$$E_{xc}[\rho] = (T[\rho] - T_s[\rho]) + (E_{ee}[\rho] - J[\rho]) \qquad (2.24)$$

In this equation, the kinetic energy of correlation is represented in the first term and the potential-energy corrections for the exchange and correlation energies are in the second term. Both $T_s[\rho]$ and $J[\rho]$ are the exact solutions for the non-interacting system, and $E_{xc}[\rho]$ is relatively small. Having defined the important exchange-correlation energy, the electronic energy of DFT can be rewritten as:

$$E_{DFT}[\rho] = E_{ne}[\rho] + T_s[\rho] + J[\rho] + E_{XC}[\rho] + V_{nn} \qquad (2.25)$$

In this way, DFT progresses from approximating the kinetic, exchange and correlation energy functionals to approximating exchange-correlation functionals only.[58] This also means that deriving a suitable $E_{XC}[\rho]$ is the major obstacle for DFT.

The reliability of a DFT functional depends on the accuracy of the

approximated $E_{XC}[\rho]$. This approximation can generally be divided into three functional categories: local density approximation (LDA), generalized gradient approximation (GGA) and the hybrid functionals. Two functionals B3LYP and M06-2X will be briefly introduced due to their application in the current work. B3LYP is a hybrid exchange-correlation energy functional (E_{XC}^{B3LYP}), which contains the B88 exchange functional (E_X^{B88}) and exchange and correlation gradient corrections to the local density approximation (E_X^{LSD} and E_{XC}^{LSD}) paired with the LYP correlation functional (E_C^{LYP}) (Eq. 2.26).[75-77]

$$E_{XC}^{B3LYP} = (1-a)E_X^{LSD} + aE_X^{HF} + bE_X^{B88} + cE_c^{LYP} + (1-c)E_C^{LSD} \quad (2.26)$$

The a, b and c in Eq. 2.26 are determined by fitting them to experimental data. For example, in B3LYP, the value of parameter a is 0.2, which indicates 20% of E_X^{HF} is incorporated into the B3LYP exchange energy.

Although B3LYP has been widely used in most branches of chemistry and the method has been tested extensively in the literature, some deficiencies of the functional have attracted much attention in recent years.[78-81] It is well known that B3LYP gives unsatisfactory results for the energies of weak interactions, for example in the dimerization of large molecules. This is because of a lack of description of dispersion forces, which is also a major drawback of most present DFT approximations. However, this can be partially improved by dispersion corrections, such as the exchange-hole dipole moment (XDM) dispersion correction of Becke and Johnson[82,83] and Grimme's

dispersion correction.[84]

M06-2X, one of the density functionals in the M06 suite of functionals presented by Zhao and Truhlar in 2008, is classified as a hybrid functional.[85] It is a high-nonlocal functional with constraint satisfaction, empirical fits and, as indicated by the 2X, a double amount of nonlocal exchange (54% of HF exchange). It is parameterized for main group thermochemistry and thermochemical kinetics. Although this method was originally recommended for non-metal systems, it is still applied in organometallic chemistry. A recent paper[8] reported that the M06-2X method provided reasonable thermochemistry for organotin-mediated reaction paths.

2.6 Relativistic Effects and Effective Core Potentials

Two major challenges must be overcome when studying heavy-element systems using computational methods. One is that a large number of basis functions are required to describe the large number of electrons in a heavy-element system. Ab initio methods like HF and those including electron correlation are limited in this respect due to the unreasonably long computational time.[86] The other obstacle in performing calculations on heavy-element systems is the effect of relativity. The core theme of this theory is that the speed of light is constant in all coordinate systems that move with respect to each other.[58] When an object travels at a speed comparable to the speed of light, a series of unusual effects arises. The most important effect relevant to a heavy element is the

phenomenon that the mass of an electron will increase significantly as its speed approaches the speed of light. This mass increase has a large influence on the properties of heavy-element containing systems, arising from the strong Coulombic attraction to the inner electrons of a heavy atom created by the large positive nuclear charge. To maintain balance in this strong electrostatic field, the speed of the inner electrons (v) is so large that it is very close to the speed of light (c), which leads to an increase of their mass (m) compared to the stationary mass (m_0) (Eq.2.27).

$$\mathrm{m} = \frac{m_0}{\sqrt{1-\frac{v^2}{c^2}}} \qquad (2.27)$$

Due to this mass increase, the kinetic energy of the electrons (mc^2) increases and the core orbitals will contract for balance. This contraction causes further effects on ionization energy, excitation energy, electronegativity and others.[87] Consequently, relativistic effects must be considered to guarantee the accuracy for the electronic structure calculations of heavy-element systems.

The Schrödinger equation, and thus HF theory, is a non-relativistic description of atoms and molecules. Computational studies on heavy-element systems without the consideration of relativistic effects are known to yield unreliable results with respect to real experiments. For example, non-relativistic calculations of molecules containing heavy elements typically overestimate bond lengths.[88] An effective way to include relativistic effects is to use an effective core potential (ECP), also called a pseudopotential.[86] The ECP method circumvents the relativity problem by replacing the

core electrons with an approximate ECP, and only the valence electrons are treated explicitly in the quantum chemical calculations.[89] In other words, the electronic system is separated into subshells, where the core electrons that are affected by relativistic effects are chemically inert from a computational point of view. Most studies of organotin systems use large-core ECPs which means that 46 core electrons are treated with an ECP and the remaining four valence electrons are included explicitly.[69,86] The LANL2DZdp basis set is employed in the current study to describe the tin atom. The LANL2 ECP was developed by Hay and Wadt[90] at the Los Alamos National Laboratory (LANL2). The four valence electrons were described with a double-zeta basis set (LANL2DZ), and additional diffuse p-type functions and d-type polarization functions, developed by Sunderlin and coworkers,[91] are also included in this basis set (LANL2DZdp).

The use of ECP is beneficial in computational studies on heavy-element systems in three aspects. Except for accounting for the relativistic effects, the primary advantage is reducing computational time. This convenience reduces the N^4 time scale of HF to $(N-Q)^4$, where Q represents the number of orbitals replaced by the ECP. The choice of the size of Q affects the accuracy. In principle, a smaller Q should lead to better results. There are also benefits for methods including the electron correlation. For post-HF methods whose time scales vary from N^5 to N^7, the computational efficiency can be improved to nearly $(N-Q)^5$ to $(N-Q)^7$. Therefore, ECPs can be applied with both DFT and MP2 methods.

2.7 Geometry Optimization

A complete potential energy surface (PES) can provide sufficient predictions of energies with structural changes in a reaction path by defining stationary points (stable minima or transition states) and connecting the pathways between them. Figure 2.1 shows an example PES with three types of stationary points on the reaction coordinate. The lowest energy point between two peaks or ridges on a PES is a local minimum and the lowest energy point for the whole PES is a global minimum. A point which is maximum in one direction and a minimum in the other is called a saddle point (see transition state A and B in Figure 2.1), indicating a transition state (TS).[65]

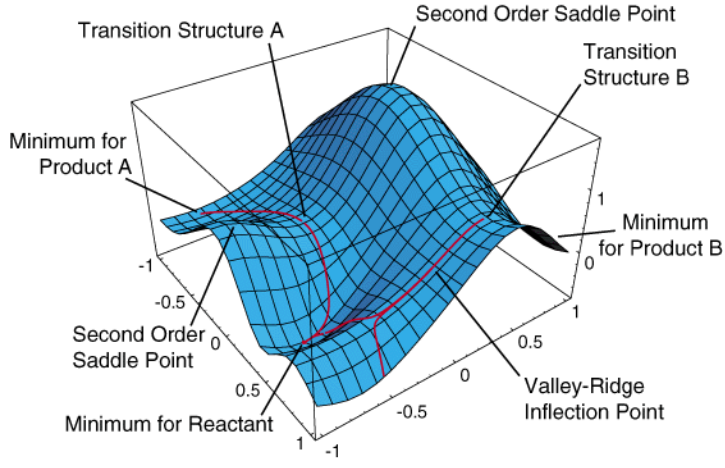

Figure 2. 1: An example of a potential energy surface for reactions of two species A and B. The red lines indicate the reaction pathways.[92]

A vibrational analysis following the optimization can verify the nature of the stationary point via the Hessian index, which is the number of negative eigenvalues of the force-constant matrix. This Hessian index corresponds to the number of imaginary vibrational frequencies. The number is zero for a stable minimum and one for a TS.

These numbers provide additional information that is useful for determining the next step in the optimization process. It is possible that the optimization is trapped in a saddle point, which makes the vibrational analysis necessary to confirm the type of the stationary point for an optimized molecule. Various algorithms for searching on a PES are available in most computational software packages. The Berny optimizer is the most widely used algorithm in the Gaussian program.[93,94] An optimization is completed when it reaches convergence (when the forces are zero). There are some other preset values defined by the algorithm and other conditions to decide the convergence in the Gaussian program.[94] The three major categories of minimization techniques in molecular mechanics are the "search", "gradient" and Newton methods.[58]

The optimization facility can also be applied in locating the TS since the saddle points as well as the minima are stationary points on a PES. It is sometimes difficult to approximate a transition structure directly by specifying a reasonable guess for its geometry. A transition state appears at the highest energy point of a transformation reaction path from one species to another on a PES. The energy of the TS relative to that of the reactants partially determines the reaction rate. This is called transition state theory (TST).[58] On a three-dimensional PES, the TS is a first-order saddle point, which is a maximum energy point in the reaction coordinate direction and a minimum along all other coordinates (Figure 2.1). In the current study, Schlegel's synchronous transit-guided quasi-Newton (STQN) method[93,95] is used to locate transition states. This method takes advantage of a quadratic synchronous transit approach to get closer to the

quadratic region of the TS, followed by a quasi-Newton algorithm to complete the optimization. Given an empirical estimate of the Hessian and suitable starting structures, the method will normally lead to efficient convergence.

Chapter 3: Monoalkylation Reaction of Diols through Fluoridated Dialkylstannylene Acetals

3.1 Introduction

As discussed in Chapter 1, organotin chemistry is an active area for both chemical synthesis and computational modeling. In particular, the extensive application of organotin derivatives as intermediates which facilitate regioselective monosubstitution of diols, polyols and carbohydrates has attracted a great deal of attention from organic chemists. With the aim to better understand the experimental observations, many theoretical studies have been carried out by modeling organotin systems with high-level quantum chemistry methods.[8,11,12,14]

In the following two chapters, the reaction mechanisms of alkylation reactions of diols through dimethylstannylene acetals are explored using computational methods. This chapter mainly shows geometry predictions and outlines several problematic energy profiles found in the calculations. To solve this problem, a small benchmark study is presented in the next chapter on the relevant model organotin systems applying different levels of theory with various Pople basis sets. Additionally, thermochemical results obtained between methods used before and after the benchmarking study and implications for the suggested reaction mechanisms are also shown in these two chapters.

3.1.1 A Reaction Cycle

Dialkylstannylene acetals are the most common kind of tin-containing species employed to obtain regioselective monosubstitution reactions of diols. They are easy to prepare and are obtained in high yields. Alkylation reactions of diols through dialkylstannylene acetals are relatively slow reactions with lower regioselectivity. By means of adding a nucleophile, the reaction rates can be markedly accelerated. However, the reaction mechanism is still under discussion.[8,96] In order to gain insight into the mechanism of these reactions, a cycle of reaction steps was suggested and then examined by theoretical methods (Figure 3.1).

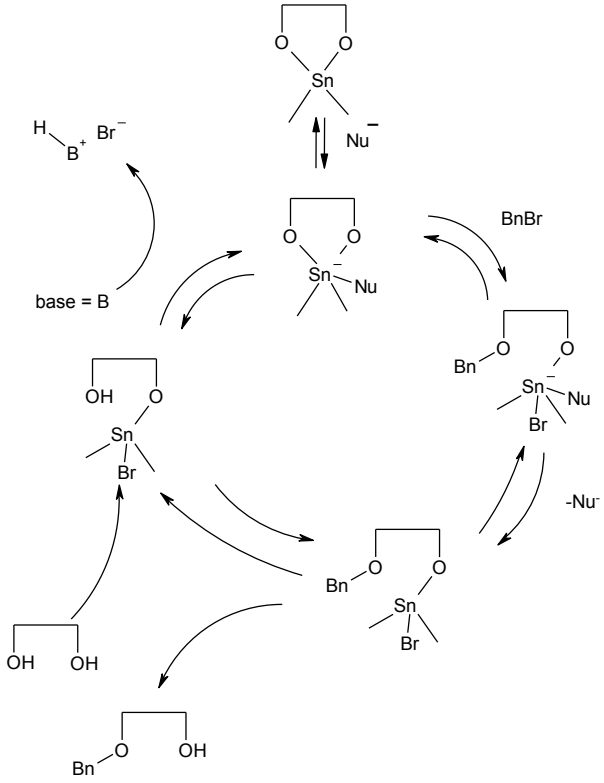

Figure 3. 1: A cyclic sequence of steps occurring in the alkylation reaction of diols through a monomeric dimethylstannylene acetal intermediate, where Bn=benzyl group.

In this reaction cycle, the presence of the nucleophile, for example fluoride, dramatically enhances the reaction rate. It has been suggested that the role of the nucleophile, which coordinates to the tin atom, is to improve the nucleophilicity of the stannylene acetal oxygen atoms.[6,7] Therefore, this attachment makes the reaction with an electrophile more efficient. At the next step, the acetal with an added fluoride reacts with benzyl (Bn) bromide leading to desired benzylation on either oxygen atom, while the leaving group (bromide) binds to the tin atom. During this process, before the second halide (bromide) attaches to the tin atom, it is predicted that there is a bond elongation between the tin atom and the benzylated oxygen due to oxygen's preference for dicoordination. Then the diol part separates from the organotin system because of nucleophilic exchange, which contributes to the achievement of the alkylation. The coordination to the tin atom by the second halide significantly decreases the electron density on the remaining Sn-O bond, which weakens the interaction between the two atoms. Finally, the acetals will be reformed by continuously provided 1, 2-diols participating in the cycle under basic conditions. This proposed cycle combines experimental observations and predictions of the mechanisms. To evaluate the cycle, the first reaction within the cycle, in other words, the alkylation reaction, was explored, using both the monomeric and dimeric form of the dialkylstannylene acetals.

3.1.2 Systems of Interest

When designing the first step of the alkylation cycle, it is important to verify whether the

intermediate exists as a monomer or a dimer. Recall the discussion of oligomeric equilibrium in chapter 1: in the absence of added nucleophiles, many experimental results support that the dimeric form of dialkylstannylene acetals is the dominant species in solution. In the instance of monocoordination of nucleophiles to monomers, it is unlikely for the acetals in solution to aggregate to form dimers or higher oligomers. Although there is evidence that dimers are the most likely intermediates in this reaction, the reaction mechanisms are often considered to involve monomers. This is justified because monomers are not much less stable than dimers. Particularly for alkylation, the reactions are conducted at elevated temperatures and it is known that the equilibria increasingly favor monomers as the temperature is raised.[8,11,20] In this study, monomeric and dimeric dimethylstannylene acetals were studied as starting models for relevant alkylation reactions with methyl bromide (Scheme 3.1). Computational methods were employed for the evaluation of thermodynamics, which involves locating transition states and calculating corresponding activation energy for each reaction.

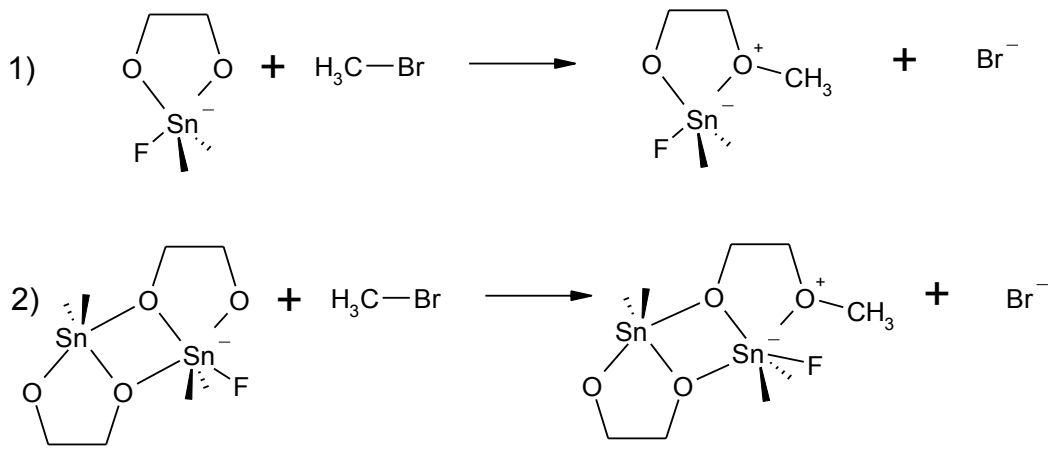

Scheme 3. 1: Proposed alkylation reactions of diols through monomeric and dimeric organotin intermediates.

In the monomeric intermediate, the formation of two O-Sn bonds between an ethane-1, 2-diol and the tin atom substituted with two methyl groups results in a five-membered ring. The choice of a simple diol and small substituents on tin is to avoid steric effects of the intermediate structures and to reduce calculation time. In section 1.4, it was stated that steric effects are the most important factor that affects the population of dimeric species and the regioselectivity of monosubstitutions. For the purpose of focusing on the analysis of reaction mechanisms, it is appropriate to start the theoretical modeling from relatively simple molecules. To the five-membered ring is added a fluoride ion as the nucleophile, in which the coordination number on tin changes from four to five. This fluoridated monomer intermediate reacts with CH_3Br, giving the product which has a methyl group attached to one stannylene acetal oxygen plus a bromide ion. For the second reaction, the dimeric form of the dimethylstannylene acetal

with an added fluoride undergoes methylation on an oxygen atom by reacting with CH_3Br. In this dimer structure, the oxygen atoms on the inner side are tricoordinate with an additional bond to the tin atom from the next monomeric unit. It is known that dicoordinate oxygens are electronically and sterically more reactive with electrophiles than tricoordinate oxygen atoms. At the same time, the presence of an added nucleophile on the tin atom enhances the nucleophilicity on the adjacent oxygen atom so that the dicoordinate oxygen at the right hand side of the complex (Scheme 3.1) tends to react with the incoming CH_3Br. It should be noted that the two tin centers in the dimer complex are pentacoordinate and hexacoordinate for the leaving and added nucleophile.

There are two reactive dicoordinate oxygen atoms in both monomeric and dimeric dimethylstannylene acetals. If the parent diols have a C_2-symmetry axis relating the oxygen atoms, both forms of the stannylene acetals will also have this axis. When a nucleophile is added to the tin atom, it assumes trigonal bipyramidal geometry with both oxygen atoms, the tin atom, and the nucleophile in a plane. In the monomeric adduct, one oxygen atom is syn to the nucleophile while the other is anti and as a result at least two pathways must be evaluated. Both of the O-Sn bonds are weakened by the presence of the added nucleophile. Thus, considering the direction of the incoming CH_3Br, two reaction pathways are suggested (Scheme 3.2). For the first reaction pathway, the alkylation reaction occurs on the oxygen on the side of the two methyl groups (pathway 1). For the other reaction pathway, CH_3Br reacts with the stannylene acetal oxygen on the side of the added nucleophile (pathway 2).

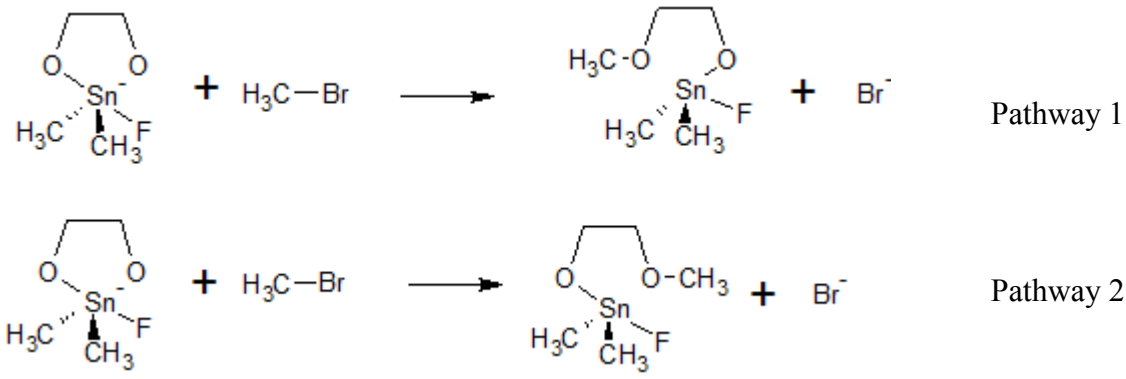

Scheme 3. 2: Two possible pathways for alkylation reactions of the monomer of dimethylstannylene acetal.

Only one pathway was analyzed for the dimeric intermediate. This is because the nucleophilicity of the dicoordinate oxygen atom of the monomeric unit containing added fluoride is markedly enhanced compared to the other dicoordinate oxygen from the monomeric unit without an added nucleophile.

3.2 Computational Methods

Gas-phase calculations were carried out with the Gaussian 09 software package in this study.[94] The popular B3LYP density functional, with Becke's three-parameter hybrid exchange functional (B3)[75,76] and the correlation functional of Lee, Yang and Parr,[77] was used for geometry optimizations and frequency calculations. According to a previous study, this level of theory provides reasonable geometries for organotin systems.[13] However, Wakamatsu *et al.*[14] discovered that the B3LYP functional is not

reliable for thermochemical estimates of organotin compounds and others agree.[98] Previous work in our group[11] used single-point energy calculations at the MP2[99-103] level with a larger basis set on the B3LYP-optimized geometries in order to pursue the thermochemical results. Thus, this level of theory, denoted as MP2/6-311G(2d,p)//B3LYP/6-31G(d,p), was chosen for this study. Transition states were found by Schlegel's synchronous transit-guided quasi-Newton (STQN) method[93,95] and the reaction path was followed by using intrinsic reaction coordinate (IRC)[104,105] calculations.

In view of the significant relativistic effects present and the unavailability of a complete basis set for heavy atoms, the tin atom was treated with an effective core potential (ECP). The Los Alamos National Laboratory double-zeta basis set (LANL2DZdp) with diffuse and polarization functions[91] was selected for the tin atom. It is known that the addition of diffuse and polarization functions improves the accuracy of thermochemical predictions for some tin complexes.[106] All non-tin atoms in this study (C, H, O, F and Br) were treated at the MP2/6-311G(2d,p)//B3LYP/6-31G(d,p). In the previous benchmark study,[13] the B3LYP method with the LANL2DZdp ECP on tin together with the 6-31G(d,p) was recommended for the predictions of the geometries of organotin systems. On the other hand, an examination of the B3LYP and MP2 methods in the dimerization reaction of dimethyltin dimethoxide carried out by the Wakamatsu group indicated that it is necessary to include electron correlation at the MP2 level in order to obtain reliable thermochemical results.[10] All relative energies shown in the

following figures and charts include the zero-point energy (ZPE) corrections.

3.3 Results and Discussion

3.3.1 Geometry Prediction

The starting guesses for the geometry optimizations were based on the experimental studies summarized in Chapter 1 and the optimized structures of dialkylstannylene acetals with added nucleophiles from the previous study.[107]

3.3.1.1 Monomer Organotin Intermediate

Figure 3.2 exhibits optimized structures for pathway 1 in which the CH_3Br reacts with the stannylene acetal oxygen on the side with two methyl groups attached to the tin atom.

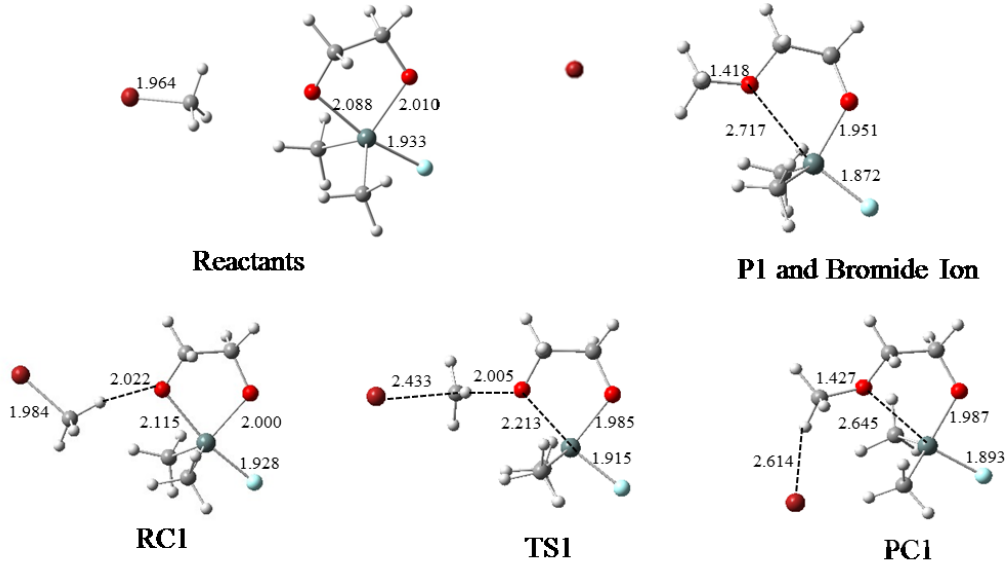

Figure 3. 2: Optimized structures for pathway 1 of the alkylation reactions through the monomer intermediate.

For the fluoridated monomer intermediate, the two oxygen atoms from a 1, 2-diol coordinate to the same tin atom to form a five-membered ring. If the oxygen atoms and the tin atom are placed in a plane, one of the carbon atoms in the ring is above the plane and the other carbon is below the plane (twist conformation). In the absence of the added nucleophile, the methyl groups are located symmetric to the O_2Sn plane. In the presence of the added nucleophile, the fluorine is axial and the methyl groups are equatorial about the trigonal bipyramidal tin atom. The nucleophilicity of the oxygen atoms is enhanced by the added fluoride, which leads to great attraction to the CH_3Br. In this process, a reactant complex (RC1) is formed and the system is stabilized by a hydrogen bond (2.022 Å) generated between the nucleophilic oxygen and the hydrogen atom of the methyl group of CH_3Br. Both the distance of the C-Br bond and the O-Sn bond are elongated due to the presence of the hydrogen bond. Another reaction complex without a hydrogen bond was found, which is 0.63 kcal/mol higher than the former one. The structure of the former complex (RC1) was confirmed by a scan job that starts from the transition state (TS1) with a gradual elongation of the distance between the oxygen atom and the carbon atom of the methyl group. This TS1 was located for pathway 1 of the alkylation reaction and the optimized geometry is the well-known transition state structure of the S_N2 reaction. It has a five-coordinate carbon because of a partially cleaved C-LG (Br^-) bond and a partially formed C-Nu (F^-) bond. The remaining three substituents (hydrogen atoms) are in a trigonal planar arrangement around the carbon center. It should be noted that there is an unexpected weakening of the O-Sn interaction

with the interatomic distances increasing from 2.115 Å to 2.213 Å. This can be explained firstly because the normal coordination number of the oxygen atom is two, and secondly because the C-O bond is much stronger than the O-Sn interaction. The latter explanation can be understood by the fact that C is more electronegative than Sn, thus larger electronegative difference between two atoms makes the bond stronger. As in RC1, formation of a hydrogen bond between the bromide ion and the hydrogen of the methyl group contributes to the stabilization of the product complex (PC1). Compared to the TS1 structure, the O-Sn bond becomes even longer (2.645 Å) and the bond distance between tin and the fluorine atom becomes shorter (1.893 Å). Furthermore, in the geometry comparison between the product complex (PC1) and the product (P1), without the stabilization by the hydrogen bond, the O-Sn bond length gets even larger which results in a complete distortion of the ring system. Simultaneously, the alkylation reaction completes and the bromide ion leaves the system. Actually, the predicted geometry of PC1 favors the next step following the alkylation reaction in the reaction cycle: the nucleophilic exchange. The bromide ion could further coordinate to the tin atom, which expands the coordination on the tin atom from four to five.

When exploring the structure of the product (P1), a variety of the initial geometries with different dihedral angles for the methyl group to the C-O-Sn plane of the stannylene ring were tested (Table 3.1). According to the results, similar structures were optimized with different starting dihedral angles, and the conformation with 136° dihedral angle has the lowest energy geometry.

Table 3. 1: The initial orientation of the methyl group relative to the C-O-Sn plane of the stannyl ring system for the geometry optimization of the monomer intermediate. Numbers indicated in the input columns were the angles set for the initial geometries, and numbers shown in the output columns were the angles predicted from optimizations.

	Dihedral Angle(°) (Input)	Dihedral Angle(°) (Output)	Relative Energy (kcal/mol)		Dihedral Angle(°) (Input)	Dihedral Angle(°) (Output)	Relative Energy (kcal/mol)
P1	180	136	0.00	P2	180	125	0.00
	150	136	0.00		150	125	0.00
	126	132	+2.00		126	125	0.00
					90	136	+3.01

The optimized structures of pathway 2 with the methylation occurring on the oxygen on the side with the fluoride added on the tin atom are shown in Figure 3.3.

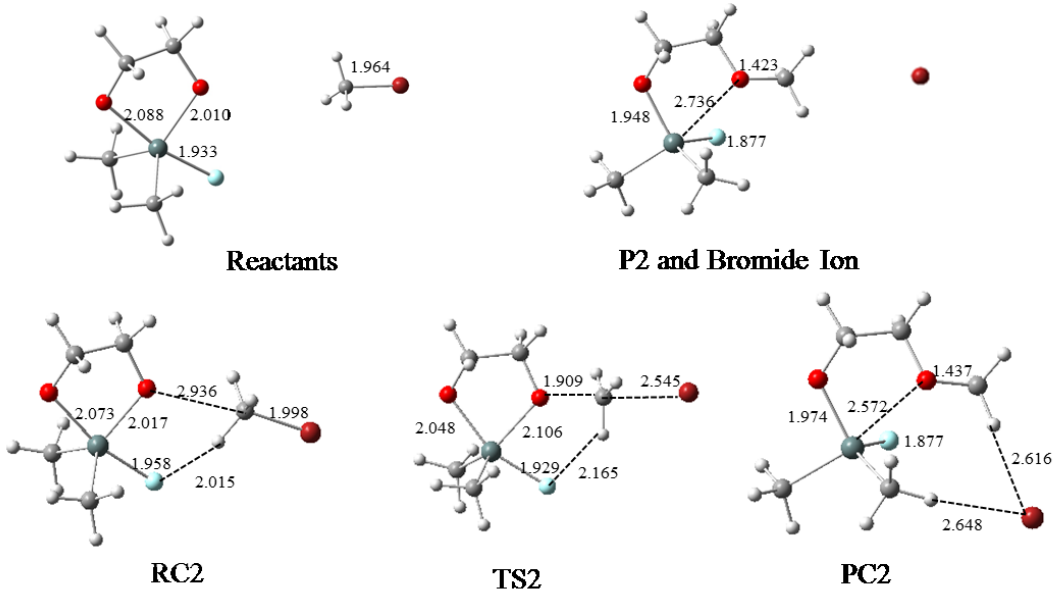

Figure 3. 3: Optimized structures for pathway 2 of the alkylation reaction through the monomeric intermediate.

There are several differences in the geometry structures in contrast to those in the pathway 1. First of all, for the reactant complex (RC2), the CH_3Br was placed in a different orientation because a hydrogen bond (2.015 Å) was created between the fluorine atom and a hydrogen atom of the methyl group from CH_3Br. The O-Sn bond length did not change appreciably, while the C-Br and Sn-F bonds were elongated significantly. For the transition state (TS2) structure, the methyl group maintains its placement in the hydrogen bond of the reactant complex, which is also an important stabilizing factor of the structure. The O-Sn bond on the right hand side only elongates slightly, which helps retain the ring structure in the formation of the stronger C-O bond (alkylation). There were two product complexes (PC2 and PC2b) found in this case (Figure 3.4). The structure of PC2 is very similar to that of PC1, in which the bromide ion moves to the lower part of the system and two hydrogen bonds are established between the bromide ion and the hydrogen atoms from two different methyl groups. On the other hand, in the structure of PC2b, the bromide migrates to the upper part of the system and also two hydrogen bonds are formed between the bromide and a methyl group and a methylene group, respectively. Although the latter one is more stable in energy (-1.63 kcal/mol), the former structure is more relevant to the next step of the reaction cycle. The most stable product structure (P2) was searched by changing the dihedral angles between the methyl group and the C-O-Sn plane of the stannyl ring system for different starting geometries (Table 3.1). It was found that initial geometries with different dihedral angles result in the same lowest-energy structure, which has the

conformation with a 125°dihedral angle.

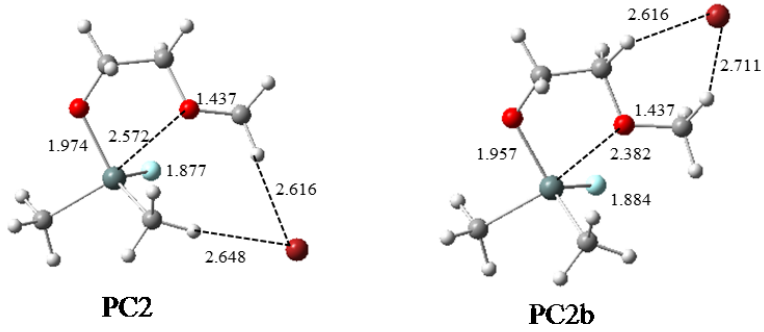

Figure 3. 4: Two possible product complexes PC2 and PC2b optimized for pathway 2 of the alkylation reaction.

Transition states for both pathways were confirmed by IRC calculations, which indicate that alkylation together with the same side Sn-O bond cleavage is a one-step process.

3.3.1.2 Dimer Organotin Intermediate

The only pathway investigated via the dimeric intermediate is similar to pathway 2 of the alkylation reaction through the monomeric intermediate (Figure 3.5). Comparing the dimer structure with an added nucleophile to that without an added nucleophile (Figure 1.2), the well-arranged staggered configuration is distorted to some extent. One of the two O-Sn bond distances between the two monomeric units contracts from 2.202 Å to 2.156 Å, while the other elongates to 3.436 Å. In the presence of the added fluoride, one of the two O-Sn bonds on the right hand side of the dimeric reactant cleaves, which is a result of oxygen's preference for dicoordination (Figure 3.5). In the structure of the reactant complex (RCd), the two interaction distances (O-Sn) between the monomeric

units are even longer. With the formation of a hydrogen bond between the fluorine atom and a hydrogen atom of the methyl group, both the O-Sn bond and the C-Br bond are elongated, which indicates that the O-Sn bond is slightly weakened by the generation of the hydrogen bond. The distances between the two units (O-Sn interaction) return to 2.152 Å and 2.540 Å in the structure of the transition state (TSd). At the same time, one of the O-Sn bonds of the right hand side monomeric units decreases to 2.225 Å, while the other bond increases to 2.111 Å. The methyl group maintains the placement of its substituents from the reactant complex. In the product complex, both of the O-Sn bonds are broken once the alkylation substitution finishes. However, O-Sn interaction distances between the two monomeric units are greatly shortened. The bromide leaving group travels to the upper part of the system, creating two hydrogen bonds with the methyl group and the methylene group.

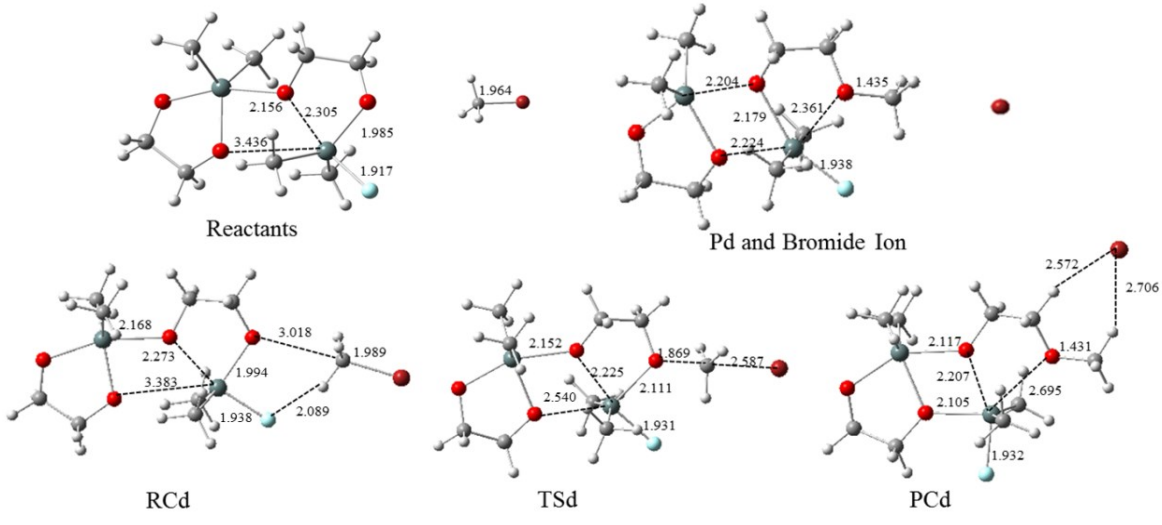

Figure 3. 5: Optimized structures for the alkylation reaction through the dimeric

intermediate.

In order to search for the lowest energy product (Pd) structure, various incoming directions for the methyl group to the C-O-Sn plane were calculated (Table 3.2). Most of the calculations with different starting geometries give similar results for the dihedral angle between the methyl group and the C-O-Sn plane which is -143.5°, except for one that gives a different angle which is 9.9 kcal/mol higher in energy.

Table 3. 2: The initial orientation of the methyl group relative to the C-O-Sn plane of the stannyl ring system for the geometry optimization of the monomer intermediate. Numbers indicated in the input column were angles set for the initial geometries, and numbers shown in the output column were angles predicted from optimizations.

Dihedral Angle (Input)(°)	Dihedral Angle (Output)(°)	Relative Energy (kcal/mol)
54	-	-
30	-143.5	0.0
0	-143.5	0.0
-54	-115.0	+9.9
-30	-143.5	0.0

3.3.2 Unexpected Thermochemical Results

The way to verify the most probable intermediate for promoting the alkylation reaction of diols using theoretical methods is to identify the transition states of each reaction and then compare their activation energies. In a common S_N2 reaction calculated in the gas-phase, the potential energy profile is of a double-well type,[108-110] which includes

three steps (Figure 3.6). The reaction starts from the formation of the reactant ion-molecule complex (RC), then RC converts to the product ion-molecule complex (PC) through the transition state (TS). The final step involves relaxation of RC to yield the products. For example, Figure 3.6 displays a S_N2 reaction of CH_3CH_2Cl with various nucleophiles (shown as X^-), therein $X^-\cdots HCH_2CH_2Cl$ and $Cl^-\cdots CH_2CH_2X$ separately represent the RC and the PC, while $[X\cdots CH_3CH_2\cdots Cl]^{-\ddagger}$ indicates the TS between the RC and the PC.

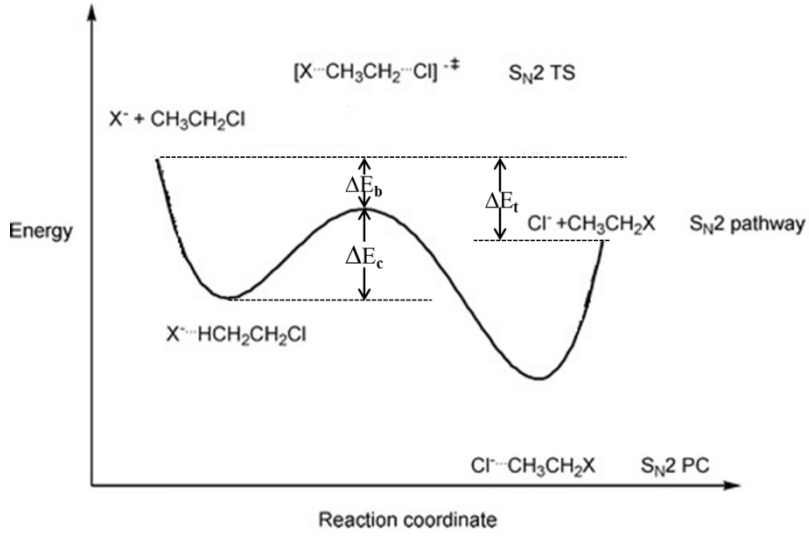

Figure 3. 6: Schematic energy profile of a gas-phase S_N2 reaction.

The energies shown in Figure 3.6 are defined in Equations 3.1 to 3.3.

$$\Delta E_c = E(X^-\cdots HCH_2CH_2Cl) - E([X\cdots CH_3CH_2\cdots Cl]^{-\ddagger}) \qquad (3.1)$$

$\Delta E_{\mathbf{c}}$ (Eq. 3.1) is the energy barrier for the second step of the S_N2 reaction.

$$\Delta E_{\mathbf{b}} = E([X\cdots CH_3CH_2\cdots Cl]^{-\ddagger}) - E(X^- + CH_3CH_2Cl) \qquad (3.2)$$

$\Delta E_{\mathbf{b}}$ (Eq. 3.2) is the energy barriers for the entire reaction. It is possible that $\Delta E_{\mathbf{b}}$ is a negative value, which means the transition state is in lower energy than the reactants.

$$\Delta E_{\mathbf{t}} = E(X^- + CH_3CH_2Cl) - E(Cl^- + CH_3CH_2X) \qquad (3.3)$$

$\Delta E_{\mathbf{t}}$ (Eq. 3.3) is the energy change for the gas-phase S_N2 reaction.

For the alkylation reaction of the dimethylstannylene acetal and CH_3Br, there were several unexpected thermochemical results found when the reaction profiles were plotted. Figure 3.7 gives a view of the thermochemistry of both pathways for the alkylation reaction calculated by B3LYP/6-31G(d,p), which gave poor thermochemical results. In particular, the energy difference between reactants and reactant complexes and the products and product complexes were unrealistically large.

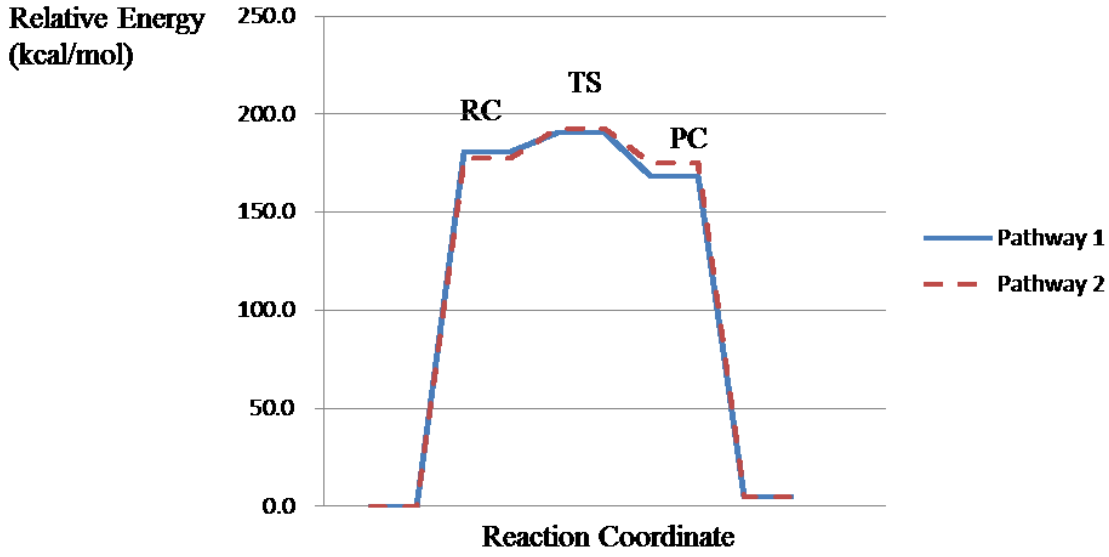

Figure 3. 7: Reaction profiles of two pathways for the alkylation reaction via monomeric intermediates calculated by B3LYP/6-31G(d,p). The blue solid line indicates the reaction path of pathway 1, and the red dash line indicates pathway 2.

The energy of RC1 is 180.5 kcal/mol higher than the sum of the energies for separated reactants, and the relative energy difference between RC2 and the reactants is 177.5 kcal/mol, which is unreasonably large for the formation energy of a reactant complex. Another important consideration is that the energy of the reactant complex should be slightly lower than the reactants, while in this reaction profile, the thermochemical data for the reactant complexes are much higher than that of the separated reactants. The reaction barriers of the second step or ΔE_c are 9.9 kcal/mol and 15.1 kcal/mol, yet the activation energies for the whole reactions, ΔE_b, are 190.4 kcal/mol and 192.6 kcal/mol. These extremely high reaction barriers result from the huge energy gap generated by the formation of reactant complexes. The overall energy

changes ΔE_t, are 4.8 kcal/mol and 4.6 kcal/mol for the two pathways. Since the energy of the products is higher than that of the reactants, these reactions are calculated to be unfavorable, which is not expected based on the experimental results. These unreasonable B3LYP/6-31G(d,p) thermochemical results prove the unreliability of this method.

MP2 single-point energy calculations were applied based on the B3LYP optimized geometries in order to yield more reliable thermochemical results (Figure 3.8). In this reaction profile, the energies of reactant complexes and product complexes are in the correct direction, which displays the expected double-well shape. Nevertheless, in the comparison of energies between reactant complexes and the separated reactant (-110.0 kcal/mol and -112.0 kcal/mol), also the energies between product complexes and the separated products (-134.0 kcal/mol and -125.2 kcal/mol), the values of energies are still unreasonably huge. The barriers of the second step of the reaction ΔE_c are 11.6 kcal/mol and 16.2 kcal/mol. In these cases, the energies of the transition states are much lower than the reactants, in other words, the values of the activation energy of the whole reaction are fairly large numbers. ΔE_b represents the reaction barriers for the whole reactions between the transition states and reactant complexes are -98.4 kcal/mol and -95.8 kcal/mol. The total thermochemical changes for the two pathways ΔE_t give -8.0 kcal/mol and -6.0 kcal/mol. These results indicate that the products are relatively more stable than the reactants.

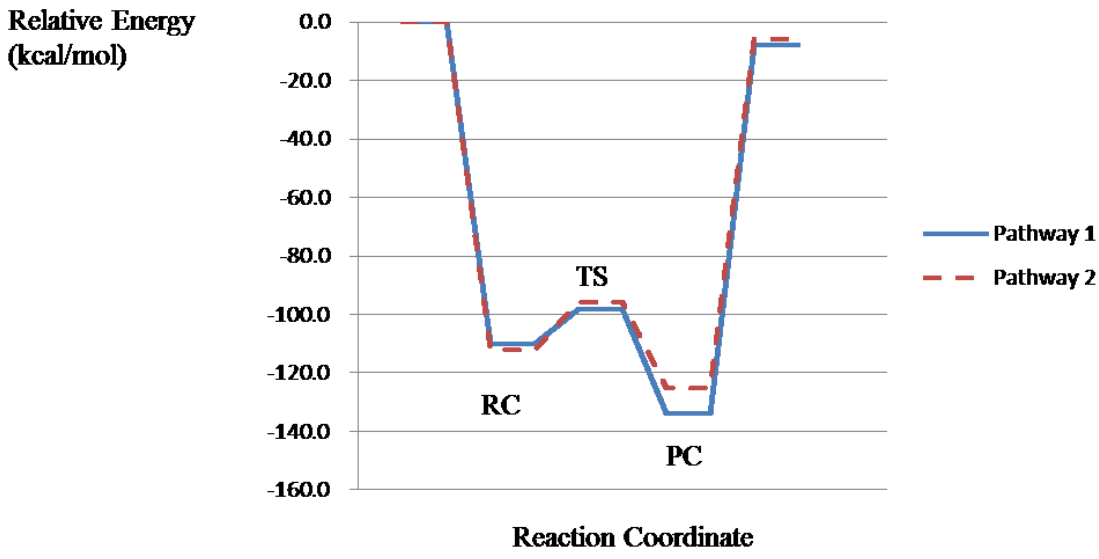

Figure 3. 8: Reaction profile for the two pathways for the alkylation reaction via monomeric intermediates calculated by MP2/6-311G(2d,p)//B3LYP/6-31G(d,p). The blue solid line indicates the reaction path of pathway 1, and the red dash line indicates pathway 2.

According to the B3LYP results obtained by modeling the reaction pathway through the dimeric intermediate, the potential energy profile indicates a similar thermochemical problem (Figure 3.9). The energy difference between the separated reactants and reactant complex is 180.4 kcal/mol, which is an unreasonable number for the formation of the reactant complex in the gas phase. Also, the direction of the energy difference is wrong in the comparison of the double-well potential energy surface. The barrier, ΔE_c, for the second step of the profile is approximately 20.0 kcal/mol, which is higher than the value shown in the reactions via monomeric intermediates.

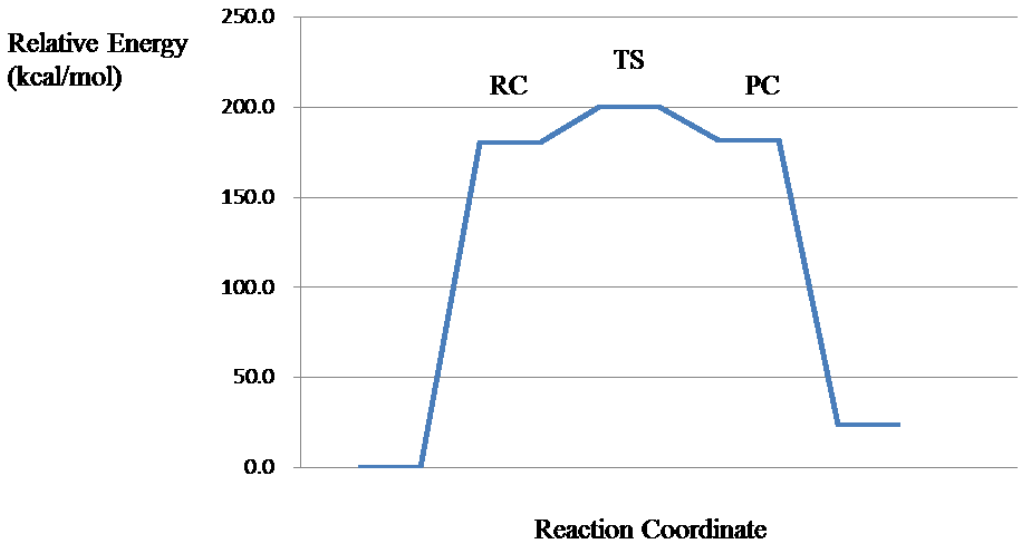

Figure 3. 9: Reaction profile for the alkylation reaction via the dimeric intermediate calculated by B3LYP/6-31G(d, p).

A reaction profile calculated at the MP2 level is also shown (Figure 3.10). Compared to the one of the monomer, the shape of the potential energy surface gives an expected double-well trend. Nevertheless, the large energy difference (-109.5 kcal/mol) between the reactants and the reactant complex still results in a huge reaction barrier. The activation energy for the whole reaction is ΔE_b= -90.1 kcal/mol, and the barrier for the second step from the reaction complex to the transition state is 19.4 kcal/mol, which is higher than the monomer reaction pathways. Although this result favors the alkylation reaction through the monomeric intermediate, unreliable thermochemical results occur in these reaction profiles. A large energy gap was also found between the products and the product complex, which reaches to124.0 kcal/mol. In addition, the energy of the products is 8.5 kcal/mol higher than those of the reactants, which is contrary to the experimental results.

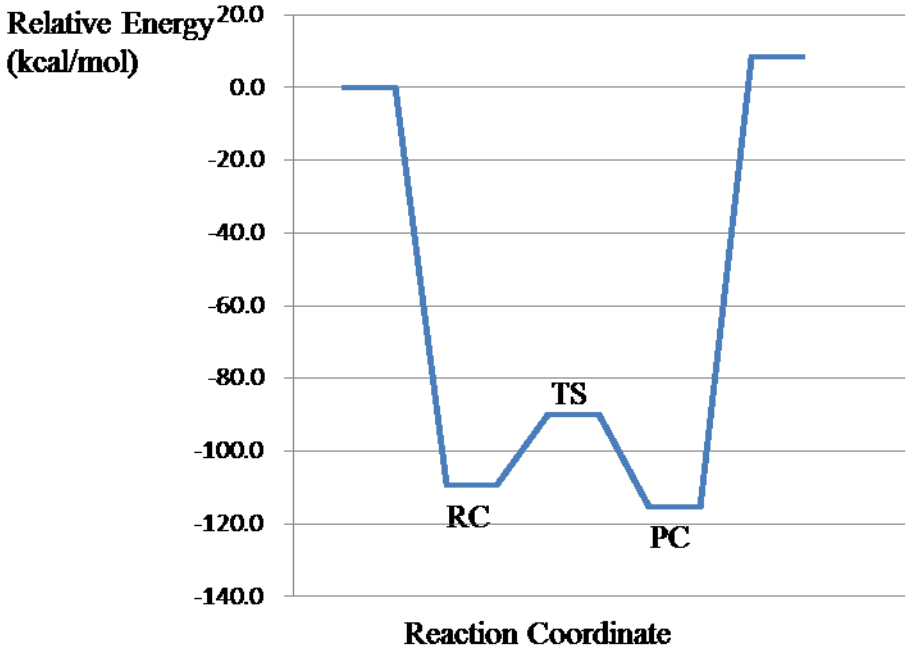

Figure 3. 10: Reaction profile for the alkylation reaction via the dimeric intermediate calculated by MP2-6-311G(2d, p)//B3LYP/6-31G(d,p).

Table 3. 3: Summary of activation energies of all reaction pathways calculated with two methods.

ΔE_c (kcal/mol)	B3LYP/6-31G(d,p)		MP2-6-311G(2d,p)//B3LYP/6-31G(d,p)	
	Monomer	Dimer	Monomer	Dimer
Pathway 1	9.9	-	11.6	-
Pathway 2	15.1	20.0	16.2	19.4

Table 3.3 summarizes the activation energies of reaction pathways through the monomeric and dimeric intermediates. In the reactions of monomers, pathway 1 is slightly favored because of a lower reaction barrier. The dimeric intermediate appears to

be not as reactive as expected based on the higher energy barrier, and both of the methods provide similar conclusions. Although MP2 single-point energy calculations provide more reasonable thermochemical data for the alkylation reaction, the values for the energy difference between separated reactants or products and the complexes are still unacceptable. B3LYP provides unreliable thermochemical results as expected owing to the unexpectedly large energy gap and the incorrect relative energy direction of the complexes with respect to the starting and finishing species. Both levels of theory suggest unfavorable reaction pathways due to the higher energy of the products, which is contrary to experimental observations. To solve this problem, it was essential to understand the causes of the unacceptable thermochemical results, which is the subject of Chapter 4.

3.4 Summary

The monoalkylation reactions of diols via the monomeric and dimeric organotin intermediates have been investigated. Theoretical methods were employed and geometry data and thermochemical results were reported. The mechanism of the alkylation reaction is an one-step reaction involving alkylation and the selective Sn-O bond cleavge. Odd thermochemical results were found in the B3LYP thermochemical calculations which predict that there was a huge energy gap between the separated reactants and the reactant complexes that leads to extremely high activation energies for the reactions. In

addition, the direction of the energy difference must be incorrect according to previous studies of S_N2 reactions in the gas phase. On the other hand, MP2 single-point energy calculations provided more reasonable thermochemistry with the correct direction of the energy difference; however, the values of the energy gap are unrealistically high. Thus, it can be concluded that B3LYP/6-31G(d,p) can be applied for the geometry predictions of the organotin compounds, but is unreliable for thermochemical predictions. MP2/6-311G(2d,p)//B3LYP/6-31G(d,p) also yields unreliable thermochemical results, which indicates the MP2 single-point energy calculations are unsuitable for the thermochemistry of the organotin systems. Therefore, this method cannot be used to compare the energy barriers of the reactions through monomeric and dimeric intermediates.

Chapter 4: Benchmarking of Basis Sets for Thermochemistry of Organotin-Mediated Alkylation Reactions of Fluoridated Diols

Although the B3LYP/6-31G(d,p) level of theory provides reasonable geometries for the reaction paths of organotin compounds, unexpected thermochemistry was observed. In this chapter, possible explanations for this problem are summarized. To do this, the relative energies of the reactants and the corresponding complexes which cause results that were very far from expectation were tested by using different levels of theory applied to a series of organotin systems. Then, a reasonable solution to improve the thermochemistry is offered according to a benchmarking study of an appropriate basis set.

4.1 Motivation

Interest in studying organometallic systems by theoretical methods focuses on chemical problems related to the heavy-metal systems and complexation that are difficult to elucidate experimentally. An important precondition is to choose the most appropriate level of theory[58] based upon the type of chemical system and the chemical properties of interest. Since numerous methods have been developed and are available for use, a benchmarking study is necessary to guide specific directions for computational choices. A previous benchmarking study carried out by Whittleton in 2006[13] recommended that the B3LYP method with the LANL2DZdp basis set and LANL2[112] effective core

potential on tin, together with the 6-31G(d,p) basis set for the other atoms, be employed for geometry predictions of organotin compounds. Later in 2008, the Wakamatsu group[10] studied dimerization reactions of organotin alkoxides and reported unsatisfactory thermochemical results with the B3LYP functional. The explanation for this result was that the dispersion which is important in dimer structures was poorly reproduced. Additionally, MP2 was found to overestimate the effect of electron correlation but this could be improved by inclusion of higher orders of perturbation. However, the dimerization energy calculated with the MP2, MP3[113,114] and MP4[115] (SDQ) methods has been found to be nearly constant. Another paper published by Whittleton in 2010[11] found that the inclusion of diffuse and polarization functions in the LANL2DZdp effective core potential was important for the treatment of the tin atom in both geometry and thermochemical explorations. Simultaneously, in order to improve the accuracy of thermochemical results, MP2 single-point energy calculations were applied based on the B3LYP optimized species. In the same year, the Wakamatsu group[14] confirmed the validity of the M05-2X[116]/6-311+G(d)-LANL2DZ (Sn) method for reliable thermochemical predictions.

The unexpected thermochemical results were observed both in the monomer and dimer pathways. The effect of dispersion is essential in the dimer structures, while it has less impact on the monomers. Thus, there should be other possible causes involved besides the missing dispersion. The drawbacks of standard B3LYP/6-31G(d) for predictions of molecular thermochemistry have been described.[98,117] The main problems

associated with this method are: lack of London dispersion and the incompleteness of the basis set. It has been shown that the B3LYP method shows unsatisfactory performance for the evaluation of the enthalpies of formation of large molecules. This result is caused by the lack of long-range interactions (missing dispersion), which become large as the molecular size increases. The basis set incompleteness error (BSIE) is the inherent basis set problem, which gives insufficient description of physical effects, such as electrostatics and induction (polarization). On the other hand, the use of a small basis set conducted in the calculation of interaction energies usually leads to an unbalanced description of the reactant and complex wavefunctions. Since in a complex structure, each reactant unit tends to borrow the basis functions from other units, an artificially low energy is obtained. The error related to this phenomenon is termed as intermolecular basis set superposition error (BSSE). Most benchmark studies were conducted with very large basis sets to minimize this error.

Unreasonably large relative energies were observed between separated reactants and reaction complexes, thus an examination of the formation energy of the monomeric reactant complexes was performed to identify the source of the huge energy gap. In this formation reaction, three types of dimethylstannylene acetals were considered to react with three different methyl halides. Scheme 4.1 reveals two pathways of this formation that a hydrogen bond generated between two reactant individuals, where X represents a halide as a nucleophile and Y stands for the halogen atom in the incoming electrophile.

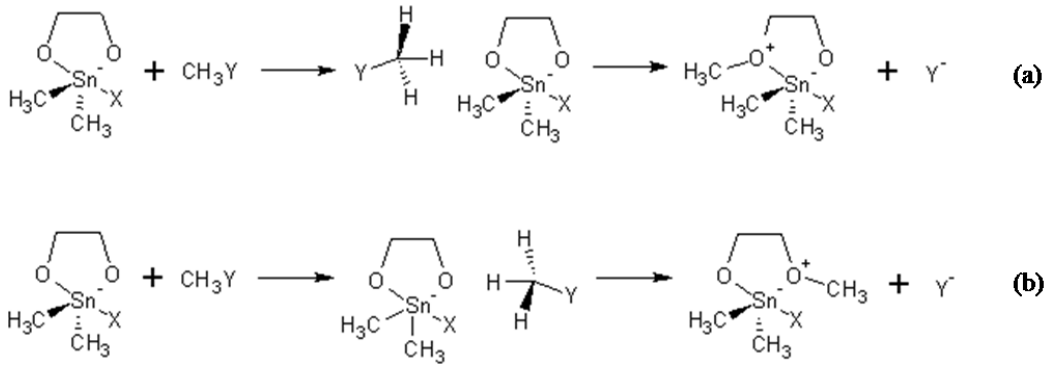

Scheme 4. 1: The formation of reactant complexes in (a) pathway 1 and (b) pathway 2 for the monomeric intermediate, where X = F, Cl, Br; Y = F, Cl, Br.

4.2 Computational Methods

All geometry optimizations and frequency calculations were performed using the B3LYP functional in the Gaussian 09 program package.[94] The Los Alamos National Laboratory double-zeta basis set (LANL2DZdp) effective core potential with diffuse and polarization functions was used to describe the tin atoms. Other atoms including halogen atoms were treated with the 6-31G(d,p) basis set. Single-point energies were calculated at the MP2 level of theory with the 6-311G(2d,p) basis set on the B3LYP-optimized geometries. Also, the B3LYP/6-311G(2d,p) single-point energy calculations were included for the energy comparisons. All thermochemical results include the zero-point energy corrections. Frequency analysis confirmed that all of the structures are minima on the potential energy surfaces.

4.3 Results and Discussion

A series of unacceptable energy differences for the formation of reactant complexes were discovered both in the B3LYP optimizations and the MP2 single-point calculations (Figure 4.1). From the B3LYP results, the huge energy gaps were only observed in reactions with CH_3Br, additionally, the directions of these relative energies were incorrect based on the standard double-well S_N2 potential energy profile in gas phase. By contrast, MP2 single-point energy calculations indicate that the large energy differences were present both in reactions with CH_3Cl and CH_3Br. Although the relative energies this time were negative, the values are still unreasonably large, especially for the reactant complex formation with CH_3Br. These outcomes can be seen as evidence that MP2 overestimates the stability of the complex structures which include intermolecular non-covalent interactions. With the increasing number of electrons encountered in the reaction, the overestimation of the stabilization of reactant complexes increases as well. This is probably related to the overestimation of the electron correlation by MP2 method. Therefore, this level of theory was unable to afford reasonable energy differences of the reactant complexes although a larger basis set was involved.

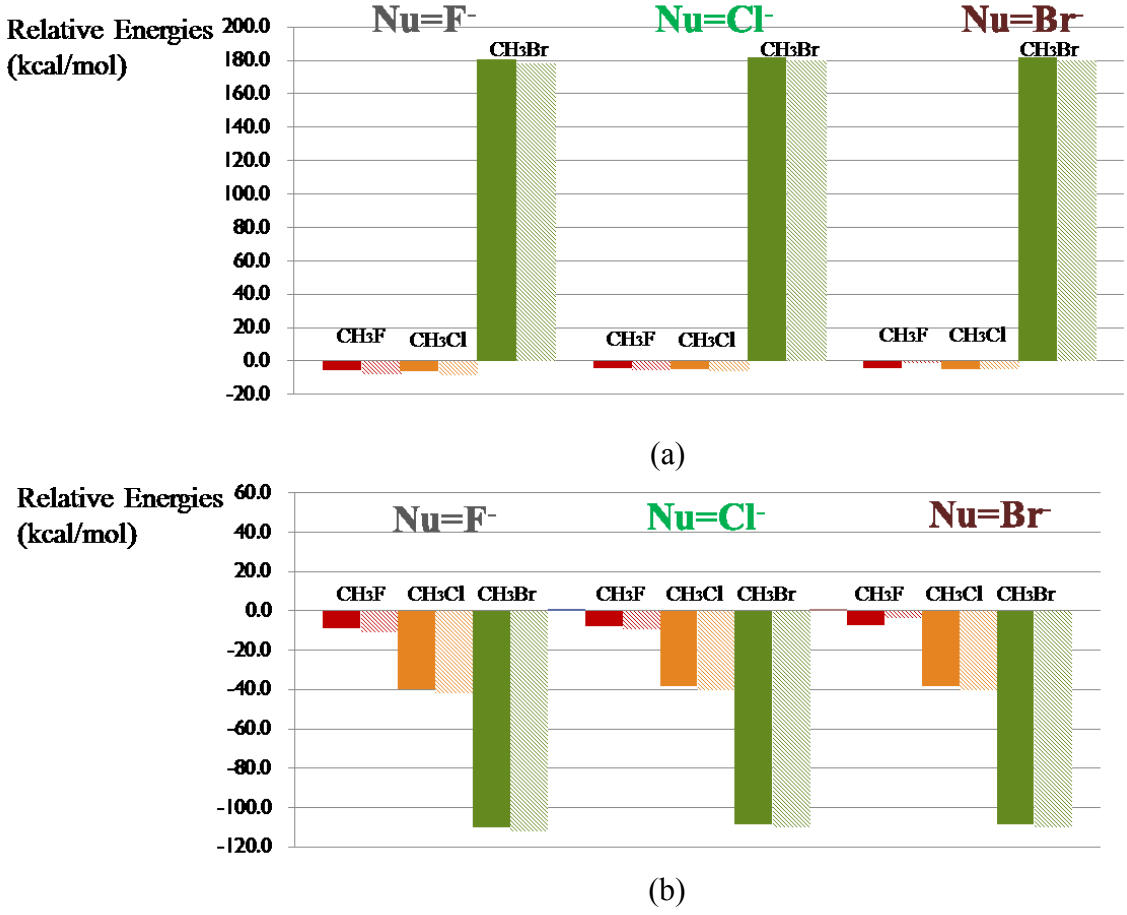

Figure 4. 1: Relative energies between separated molecules and corresponding complexes calculated by using (a) B3LYP/6-31G(d,p) method; (b) MP2/6-311G(2d,p)//B3LYP/6-31G(d,p). C1 = reactant complex from the first reaction pathway, C2= reactant complex from the second reaction pathway; Nu means a nucleophile attached to the tin atom which could be F^-, Cl^-, and Br^-; CH_3F (red), CH_3Cl(orange) and CH_3Br(green) are the incoming electrophiles involved in the alkylation reactions. Solid bars are the reactions through pathway 1 and dash bars through pathway 2.

It is noteworthy that the unexpected thermochemical results appear for reactions with CH_3Br even under circumstances when the bromide ion acts as the nucleophile attached to the tin atom. It is highly possible that this problematic outcome is relevant to

construction of the reactant complex with the CH_3Br encountered in a reaction path, especially the description of hydrogen bonds in the system. The difference in thermochemical evaluation between B3LYP and MP2 probably arises from the difference in electron correlation. With an increasing number of electrons (from 18 in CH_3F to 44 in CH_3Br), the effect of electron correlation will be stronger. Therefore, an increasing energy difference or stabilization of the reactant complexes was shown from MP2 single-point calculations (Figure 4.1 (b)). On the other hand, it was mentioned that the small basis set causes the problem of BSIE, especially for the complex structures. With increasing size of the basis set, it is expected that this situation could be relatively improved. BSSE is a small part of the total energy in this case which cannot be the factor that significantly affects the formation energy.

Since MP2 failed to yield reasonable thermochemistry, B3LYP/6-311(2d,p) single-point energy calculations were carried out. The extension of the basis set may reduce the BSSE to some extent. Figure 4.2 summarizes the results from this level of theory, all of the unexpected energies disappear (reduced to less than -10 kcal/mol), which meets the requirement of a reactant complex that is slightly lower in energy than the reactant in the standard double-well potential energy surface. Consequently, this supports the idea that the BSIE plays an essential role in predicting the formation energy of the reactant complexes.

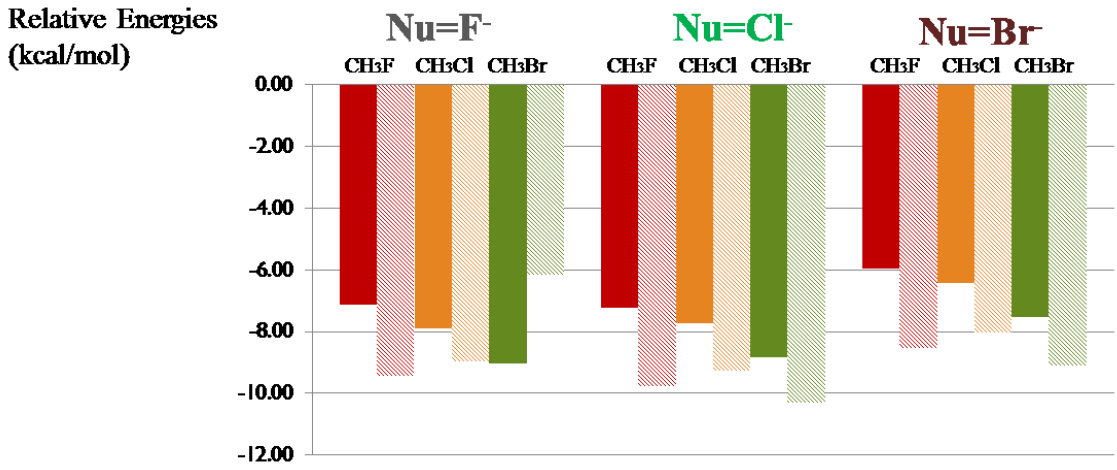

Figure 4. 2: Relative energies between separated molecules and corresponding complexes calculated by using B3LYP/6-311G(2d,p) single-point energy job type based on B3LYP/6-31G(d,p) optimization. C1 = reactant complex from the first reaction pathway, C2= reactant complex from the second reaction pathway; Nu means a nucleophile attached to the tin atom which could be F^-, Cl^-, and Br^-; CH_3F (red), CH_3Cl(orange) and CH_3Br(green) are the incoming electrophiles involved in the alkylation reactions. Solid bars are the reactions through pathway 1 and dash bars through pathway 2.

4.3.1 Choice of an Appropriate Basis Set

To select an appropriate basis set to be used in the future research, a small benchmark study was carried out to check the combination of different levels of theory with a variety of Pople basis sets (Figure 4.3). The reason to consider Truhlar's functional is that several papers[8,14] that employed the M0 series of functionals, which include London dispersion, have yielded good results for thermochemistry and noncovalent interaction at a reasonable computational cost. The relative energies calculated at the B3LYP level do not differ significantly from those obtained at the M06-2X level,[118] the difference being approximately 1 kcal/mol. Although results obtained from different levels of theory combined with double split-valence basis sets

were unrealistically far from the expected range, the difference of these energies is not much. In contrast, with triple split-valence basis sets, MP2 overestimates the stability of the reactant complexes.

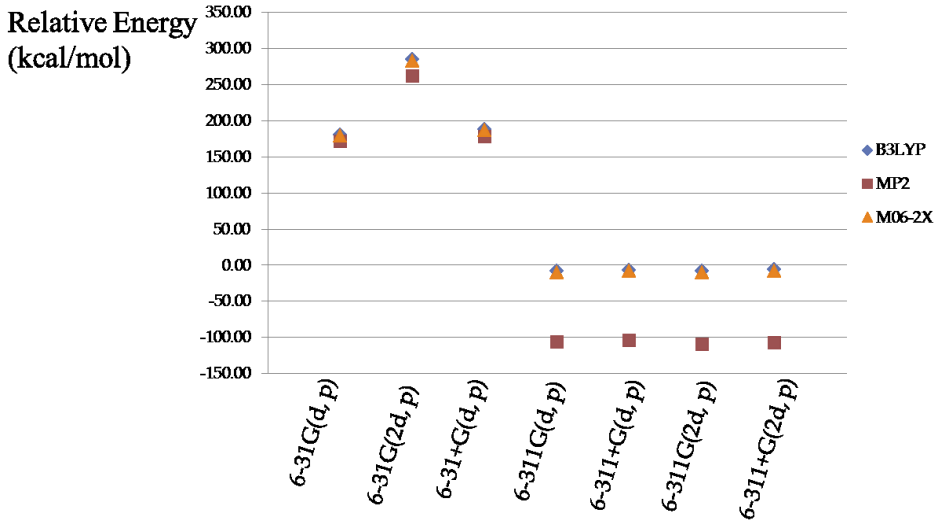

Figure 4. 3: Relative energy between separated reactants and complexes from pathway 1 via the monomeric intermediate calculated with the B3LYP, MP2 and M06-2X methods and various basis sets.

On the basis of these thermochemical results, the 6-311+G(d,p) basis set was chosen for use in further calculations. The inclusion of the diffuse functions is based on consideration of the negative charge introduced by the added nucleophile to most of the systems. Among the four triple split-valence basis sets, the thermal energies predicted from the basis sets without diffuse functions are ~2 kcal/mol larger than those with diffuse functions. In other words, 6-311+G(d,p) and 6-311+G(2d,p) give smaller energy differences between the reactants and the reactant complexes. The former basis set was selected in order to reduce the computational costs.

4.3.2 Implications for Suggested Mechanisms

A new computational method is proposed through the evaluation of the benchmark: B3LYP/6-311+G(d,p)-LANL2DZdp (Sn). The combination of Truhlar's functional M06-2X with 6-311+G(d,p) is also employed for energy comparisons.

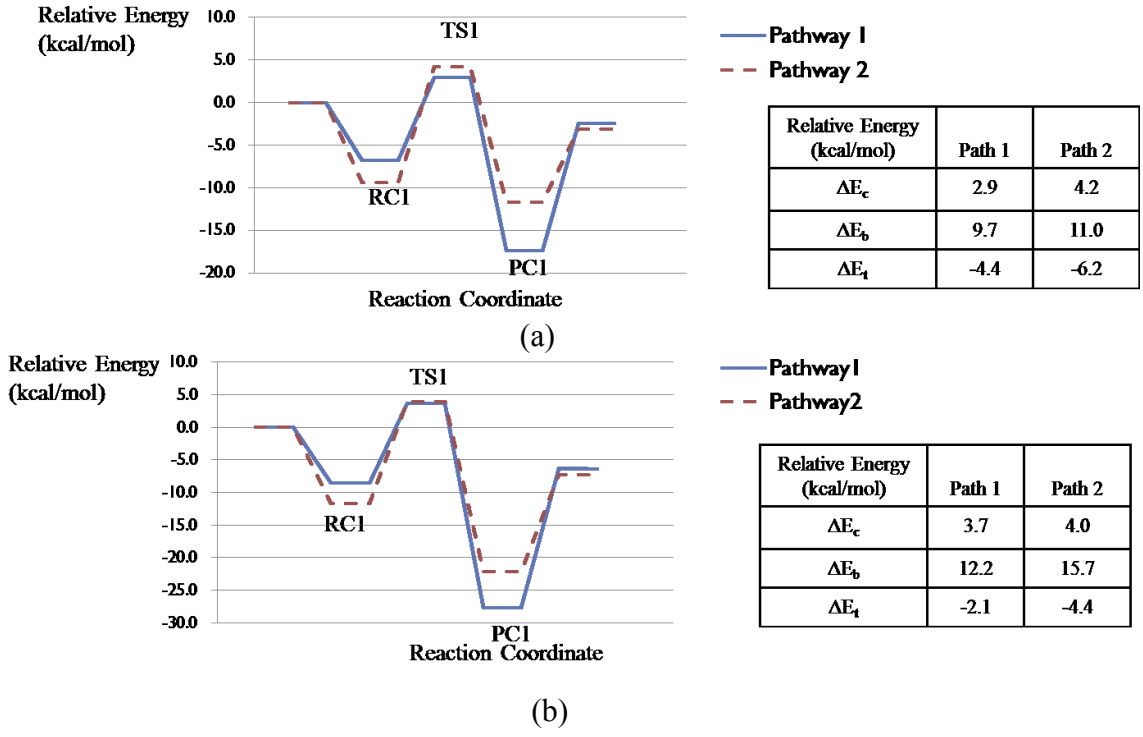

Relative Energy (kcal/mol)	Path 1	Path 2
ΔE_c	2.9	4.2
ΔE_b	9.7	11.0
ΔE_t	-4.4	-6.2

Relative Energy (kcal/mol)	Path 1	Path 2
ΔE_c	3.7	4.0
ΔE_b	12.2	15.7
ΔE_t	-2.1	-4.4

Figure 4. 4: Reaction profiles of two pathways via the monomeric intermediate for the alkylation reaction calculated by (a) B3LYP/6-311+G(d,p); (b) M06-2X/6-311+G(d,p).

These two reaction profiles (Figure 4.5) display the expected double-well shape. From the B3LYP results, pathway 1 is slightly favored over pathway 2 due to a lower reaction barrier for the second step in the energy surface (energy difference between the transition state and the reactant complex ΔE_b). Nonetheless, the products generated from pathway 2 are more stable by 1.8 kcal/mol. The predictions obtained with M06-2X are

consistent with those from B3LYP. Pathway 1 is kinetically more stable which overcomes a lower reaction barrier, however, pathway 2 is thermodynamically more stable with products having a lower energy.

Two mechanisms have been proposed for the monoalkylation reactions of diols through the monomeric organotin intermediate on the basis of the geometries presented in Chapter 3. Moreover, reasonable thermochemistry is obtained using the new methods. Both of the mechanisms were confirmed by IRC calculations which examine the reaction paths leading down from two transition structures on their potential energy surfaces. The first step of the alkylation reaction includes the formation of the reactant complex, which is slightly lower in energy than the separated reactants. This complex then goes over a high reaction barrier leading to the product complex. In this process, the leaving group bromide ion moves apart once the C-O bond forms, then travels to the lower part of the system leading to the formation of the production complex (PC1), which is prepared for the next step in the reaction cycle: the nucleophilic exchange. The alkylation process is actually a one-step reaction, which involves Sn-O bond cleavage occurring on the same side of tin as the O-C bond is formed.

4.4 Summary

The unsatisfactory thermochemical results obtained with the B3LYP/6-31G(d,p) method were attributed to a lack of the London dispersion and the significant BSSE associated

with the relatively small basis set. MP2 single-point energy calculations were carried out to improve the thermochemistry. However, MP2 often overestimates the effect of electron correlation, and thus leads to overestimation of the stability of the complex. A small benchmark study was performed to evaluate the effect of increasing the size of the basis set and hence reduce the BSSE. The 6-311+G(d,p) with triple split-valence basis set with diffuse functions was selected to compare the B3LYP and M06-2X functionals. These methods led to standard double-well potential energy profiles and the proposed reaction mechanisms.

Chapter 5: Computational Models of Organotin-Mediated Alkylation Reactions of Diols in the Presence of Various Nucleophiles

Since the presence of added nucleophiles plays a key role in facilitating alkylation reactions, it is necessary to understand the nucleophilic effects on the organotin intermediates both in monomeric and dimeric forms. In this chapter, the reactivity trends for various added nucleophiles to the dimethylstannylene acetals involved in the alkylation reactions in diol substrates is examined.

5.1 Introduction

Organotin compounds have been widely known as catalytic agents since the discovery of their various applications in organic synthesis, which has been a major field of organometallic chemistry during the last few decades.[119] Tin-hydrogen, tin-oxygen and tin-carbon bonds are strong enough to afford stable reagents but labile enough to allow high reactivity under mild conditions, providing valuable and versatile uses in organic chemistry. These tin-containing species play important roles as intermediates to facilitate regioselective monosubstitutions of hydroxyl groups in diol or polyol substrates with a variety of electrophiles. Many papers described the use of dialkylstannyl ethers and dialkylstannylene acetals to effect alkylation,[41,43] acylation,[37,120] and sulfonylation.[121,122] Although stoichiometric amounts of potentially toxic di- or trialkyltin (IV) derivatives are employed, these derivatives have continued to be used heavily because they give

products in high-yields with much better regioselectivity that is unobtainable by other methods.[97,123,124] The complexation that occurs between organotin intermediates and diol moieties is exploited in processes such as the monofunctionalizations of diol substrates (Scheme 5.1).[120,122,125] More recently, these reactions have been the subject of renewed interest because of utilization of advanced computational techniques to better understand the complex structures and reaction mechanisms.[8,10,11,14]

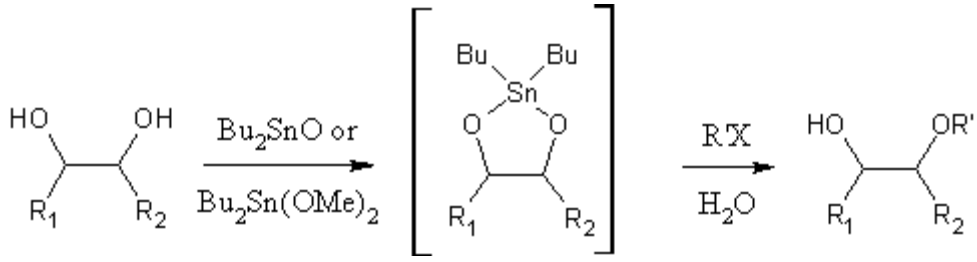

Scheme 5. 1: Proposed reactivity of dialkyltin oxide activation of *cis*-diol.

The desirable development of methods to allow reactions to occur under conditions that are catalytic in toxic tin reagents would be aided by a better understanding of the mechanism of the reaction.[9,19] An important factor that could influence the reaction mechanism is the population of the monomeric or oligomeric form of the acetal and their corresponding reactivity involved in the process under reaction conditions. Relevant experimental studies using ^{119}Sn NMR showed that dimeric species possess the greatest populations in solution.[27,30,31] Nevertheless, monomers have been considered as intermediates for oligomer and dimer interconversion[19,45] and also as the reaction

intermediates in the literature.[8,19,45,50] In addition, the mechanistic understanding of these reactions, especially those at the molecular level, have not yet been fully obtained. Previous publications by Nagashima *et al.*[41] proposed the main features of the monoalkylation reaction mechanism, while recent evidence discussed controversial results through both experimental and theoretical studies.[8,9,96] One theory[4,6,7] indicates that regioselective products from organotin-mediated reactions are related to the complex stannylene structures, which are difficult to elucidate experimentally. Dong *et al*.[8,96] suggested that the regioselectivity of the organotin-mediated protection was controlled by the stereoelectronic structures of parent carbohydrates or diols and polyols. They proposed that the reaction mechanism proceeded via selective Sn-O bond cleavage, which has also been found in the current computational research. To gain insight into the most probable reaction pathway and implications for the mechanism in the presence of added nucleophiles, a systematic theoretical study using the DFT has been carried out.

Another complicating factor is that these reactions are usually performed in the presence of nucleophiles or bases that further advance the reaction rates.[42,43,47] For example, alkylation usually requires more vigorous conditions. Some early work presented these reactions on the stannylene acetal with the most active alkylating reagents (e.g. methyl iodide or benzyl bromide) in DMF at elevated temperature.[126] Several reports then discovered that the addition of nucleophiles to the acetals, such as halides,[43] markedly accelerates monoalkylation to the diol substrates. However, a series of questions and uncertainties that concerns this improvement were unsolved even

though the assistance of halides in the regioselective alkylation was described many times.[6,49,96,127] These problems include the choice of a halide, the amount of halide salt used, and the production of the specific alkylated diols. Because of a lack of experimental observation and systematic studies on the nature of its effect, the role of a nucleophile coordinated to the tin has not been fully examined. A commonly accepted interpretation is that the added nucleophile activates the acetal structure and enhances the nucleophilicity for both oxygen atoms on the five-membered ring structure.[6] It was also suggested by the Dong group[8] that the improvement by the coordination of the nucleophile to the tetracoordinate tin atom is also related to the selective Sn-O bond cleavage because the stronger Sn-X (halide) bond would lead to more reactive oxygen anions, which dramatically increases the rate of reaction with the electrophiles. However, there was no strong evidence to support these statements. In the present study, an examination of the activation ability of different nucleophiles and the origin of the activation mechanism has been investigated. Also, the computational results will be compared with Dong's experimental observations.[96]

Usually, the interest in the gas-phase chemistry of dialkylstannylene acetals has prompted studies related to S_N2-type reactions involving geometries exploration, thermochemistry and reaction mechanisms.[16] By comparison, few studies have addressed gas-phase chemistry that can be relevant both to understanding the mechanisms and intrinsic reactivity of monomeric and dimeric acetals with various added nucleophiles. To elucidate the mechanism of the gas-phase reaction, an overall alkylation of ethylene

glycol through nucleophilic dimethylstannylene acetals were described with optimized intermediate complexes and transition states. For simplicity and cost-effectiveness, systems without sterically bulky alkyl groups attached were modeled in order to minimize the regioselective effects and focus on the analysis of reaction mechanisms. Potential energy surfaces for both monomeric and dimeric tin containing intermediates were explored with emphasis on comparison of the activation energies. A particular interest is the effect of adding different nucleophiles on the reactivity of these complex systems. Theoretical studies of reaction pathways for alkylations with the monomeric intermediates with the added nucleophiles F^-, Cl^-, Br^-, $N(CH_3)_3$, $P(CH_3)_3$, and dimeric intermediates with F^- and Br^- addition were built, leading to an establishment of the relationship between the presence of nucleophiles and the activity of the intermediates.

5.2 Computational Details

The basic reactions are shown in formulas from (1) to (3) in Scheme 5.2. The alkylation reaction of 1, 2-diol with methyl bromide through the monomeric dialkylstannylene acetal was described in two pathways. Because both of the acetal oxygen atoms are activated by the added nucleophile, there are two possibilities for the intermediate complex to attack the methyl group. In the trigonal bipyramidal complex formed by addition of the nucleophile, either the oxygen atom syn to the added nucleophile or anti to the added nucleophiles could react. Formation of the dimer creates two kinds of oxygen atoms: tricoordinate and dicoordinate. The former one interacts with two tin

atoms from two monomeric units, resulting in steric effects from the four alkyl groups on the two tin atoms that hinder the approach of electrophiles. The apical position in the trigonal bipyramid of the tin geometry for the dicoordinate oxygen atom is usually considered to be more reactive.[4] In the presence of the nucleophile, the dicoordinate oxygen atom from the right hand side unit is the most nucleophilic site to undergo the alkylation reaction. In Scheme 5.2, (1) and (2) describe two pathways through the monomeric intermediate, where X represents F^-, Cl^-, Br^-, $N(CH_3)_3$, and $P(CH_3)_3$, while (3) presents the alkylation reaction in the aid of the dimer, where X' means F^- or Br^-.

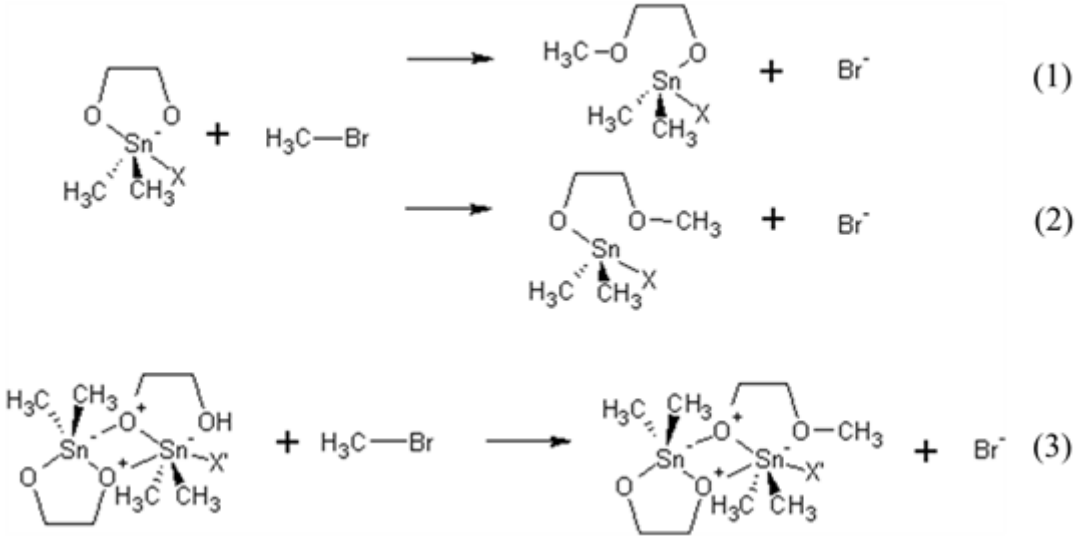

Scheme 5. 2: Monoalkylation of diols through monomeric and dimeric dimethylstannylene acetals with various added nucleophiles.

Theoretical calculations were carried out with the Gaussian 09 suite of programs.[94] The gas-phase geometry optimizations were conducted using the B3LYP hybrid functional combined with 6-311+G(d,p) for the non-tin atoms. The inclusion of the

diffuse functions is important due to one negative charge carried by the nucleophile in the computed systems. The choice of a relatively large size of the basis set improves the reliability of the thermochemical predictions. The Los Alamos National Laboratory double-zeta basis set (LANL2DZdp) with diffuse and polarization functions and its effective core potential developed by Hay and Wadt were used to treat the tin atom in the account of the relativistic effect and in order to increase the computational efficiency. Transition states were found by Schlegel's synchronous transit-guided quasi-Newton (STQN) method[93,95] and the reaction path was followed by using intrinsic reaction coordinate (IRC)[104,105] calculations.

Thermochemistry is the most problematic issue in theoretical studies related to tin chemistry, especially for the implications of the reaction pathways, due to insufficient experimental results for comparison. B3LYP was reported to be unreliable for thermochemical estimates,[10] thus single-point energy calculations at the MP2 level (MP2/6-311+G(d,p)//B3LYP-6-311+G(d,p)) were performed on the optimized species. In addition, recent literature[8,14] indicated Truhlar's functionals were suitable for thermochemistry and noncovalent interaction at reasonable computational costs in this case. Herein, M06-2X was selected as the supplementary method to reinforce the accuracy of the thermochemical predictions. This method was also validated in the benchmark study in Chapter 4.

Vibrational frequency calculations were carried out to characterize stationary points and confirm the minima for all structures on the potential energy surfaces (no imaginary

frequencies for a local minimum and one for a transition state). All the thermochemical parameters were evaluated at default conditions (298.15 K and 1 atm). Selected Mülliken charges were used for the data analysis. All of the relative energies displayed from the thermochemical results include zero-point energy (ZPE) corrections.

5.3 Results and Discussion

5.3.1 Geometry Predictions

5.3.1.1 Monomeric Intermediate

Table 5.1 reports the structural characteristics of models of reactant complexes, transition states and product complexes involved in both of the reaction pathways via the monomeric intermediates. Here DA represents dimethylstannylene acetal, the groups indicated in the brackets express different added nucleophiles to the tin atom, and the numbers 1 and 2 denote geometries optimized following pathway 1 and 2, respectively. In all cases, the arrangements of the hydrogen bonds in complexes and the trigonal bipyramidal geometries around the carbon of the transition states are similar, indicating the corresponding reaction mechanisms (Figures 5.1 and 5.2). On adding different nucleophiles, small changes in the geometry around the pentacoordinate tin atom were found. Compared to the added halides, nucleophiles $N(CH_3)_3$ and $P(CH_3)_3$ had more effects on the five-membered ring and on the connection to the methyl bromide or the bromide ion in the complexes, owing to the relatively bulky substitution of the tin atom.

Also, this steric effect makes the approach of the methyl bromide in the pathway 2 more difficult, and the corresponding structures of the complexes were hard to locate. In the pathway 1, for example, in the presence of added fluoride, the r(Sn,O)l was elongated from 2.123 Å to 2.643 Å during the process of the alkylation or during the approach of the electrophile. The other Sn-O bond did not change much. With the gradual shortening of the C-O bond, the distance between the carbon atom and the bromide atom separated step by step, indicating the structural alteration of the alkylation reaction. The Sn-X bond lengths in the complex structures with added trimethylamine were surprisingly equivalent to the bond length in the system with an added chloride. For the geometry around the tin center, the O-Sn-O angle closed from 80.3 to 70.4°, while the angle between two methyl groups through the tin atom opened by 8.6° due to the insertion of the leaving group bromide ion. In the pathway 2, similar changes of the bond lengths and bond angles were found; however, in this case the hydrogen bonds were arranged in a different way. In the reactant complexes 2, hydrogen bonds, or some type interaction between a hydrogen atom from the methyl bromide and the halides, were formed, while in the product complexes 2, two hydrogen bonds were observed.

Table 5. 1: Selected geometric parameters for the reactant complexes, transition states and product complexes using B3LYP/6-311+G(d,p) (r in Å, < in degrees).[a]

Reactant Complex 1

	DA(F)	DA(Cl)	DA(Br)	DA(NMe_3)	DA(PMe_3)
r(Sn,O)l	2.123	2.105	2.097	2.019	2.014
r(Sn,O)r	2.014	2.009	2.008	1.995	2.002
r(Sn,X)	2.004	2.564	2.757	2.593	2.990
r(O,H)	2.040	2.076	2.082	2.225	2.227
r(C,Br)	1.985	1.984	1.983	1.974	1.974
<(O,Sn,O)	80.3	81.0	81.3	83.8	83.8
<(O,Sn,X)	88.2	88.0	87.8	75.9	69.6
<(C,Sn,C)	119.2	120.0	120.2	119.1	118.7

Reactant Complex 2

	DA(F)	DA(Cl)	DA(Br)	DA(NMe_3)	DA(PMe_3)
r(Sn,O)l	2.092	2.078	2.072	-	-
r(Sn,O)r	2.027	2.019	2.019	-	-
r(Sn,X)	2.024	2.592	2.788	-	-
r(X,H)	2.100	2.804	2.988	-	-
r(C,Br)	2.001	1.996	1.995	-	-
<(O,Sn,O)	80.7	81.3	81.6	-	-
<(O,Sn,X)	85.3	86.1	86.3	-	-
<(C,Sn,C)	119.5	120.2	120.5	-	-

Transition State 1

	DA(F)	DA(Cl)	DA(Br)	DA(NMe_3)	DA(PMe_3)
r(Sn,O)l	2.215	2.199	2.192	2.126	2.125
r(Sn,O)r	1.998	1.996	1.997	1.983	1.994
r(Sn,X)	1.984	2.509	2.685	2.461	2.820
r(O,C)	2.028	2.006	1.998	1.803	1.805
r(C,Br)	2.437	2.456	2.464	2.631	2.630
<(O,Sn,O)	78.3	78.6	78.6	80.3	80.0
<(O,Sn,X)	90.0	89.6	89.4	79.1	74.1
<(C,Sn,C)	121.8	121.7	121.9	122.3	121.2

Transition State 2

	DA(F)	DA(Cl)	DA(Br)	DA(NMe_3)	DA(PMe_3)
r(Sn,O)l	2.069	2.059	2.056	-	-
r(Sn,O)r	2.095	2.108	2.113	-	-
r(Sn,X)	1.994	2.524	2.704	-	-
r(O,C)	1.948	1.914	1.906	-	-
r(C,Br)	2.537	2.581	2.588	-	-
<(O,Sn,O)	78.2	78.6	78.6	-	-
<(O,Sn,X)	82.0	85.8	87.1	-	-
<(C,Sn,C)	121.4	123.2	123.6	-	-

Product Complex 1

	DA(F)	DA(Cl)	DA(Br)	DA(NMe_3)	DA(PMe_3)
r(Sn,O)l	2.643	2.614	2.629	2.434	3.077
r(Sn,O)r	1.995	1.994	1.995	2.062	2.071
r(Sn,X)	1.952	2.437	2.597	2.407	2.676
r(O,C)	1.431	1.432	1.432	1.431	1.416
r(H,Br)	2.655	2.625	2.627	3.356	5.890
<(O,Sn,O)	70.4	70.7	70.4	73.9	64.4
<(O,Sn,X)	94.4	94.2	94.2	84.7	71.7
<(C,Sn,C)	127.8	126.9	126.5	167.9	133.2

Product Complex 2

	DA(F)	DA(Cl)	DA(Br)	DA(NMe_3)	DA(PMe_3)
r(Sn,O)l	1.983	1.979	1.978	-	-
r(Sn,O)r	2.583	2.645	2.681	-	-
r(Sn,X)	1.933	2.402	2.554	-	-
r(O,C)	1.438	1.437	1.436	-	-
r(H,Br)	2.728	2.713	2.710	-	-
r(H',Br)	2.827	2.852	2.817	-	-
<(O,Sn,O)	71.5	70.2	69.7	-	-
<(O,Sn,X)	76.7	81.2	82.6	-	-
<(C,Sn,C)	113.5	112.7	112.6	-	-

[a] The r(Sn,O)l and r(Sn,O)r, respectively, refer to the intramolecular bonds between tin and dicoordinate oxygen atoms placed on the left and right (see Figure 5.1 and 5.2). The r(H, Br) and r(H', Br) in the product complex 2 table refer to the hydrogen bond between the bromide atom and the hydrogen atoms on its top and on its left, separately. X indicates different nucleophilic ions or groups.

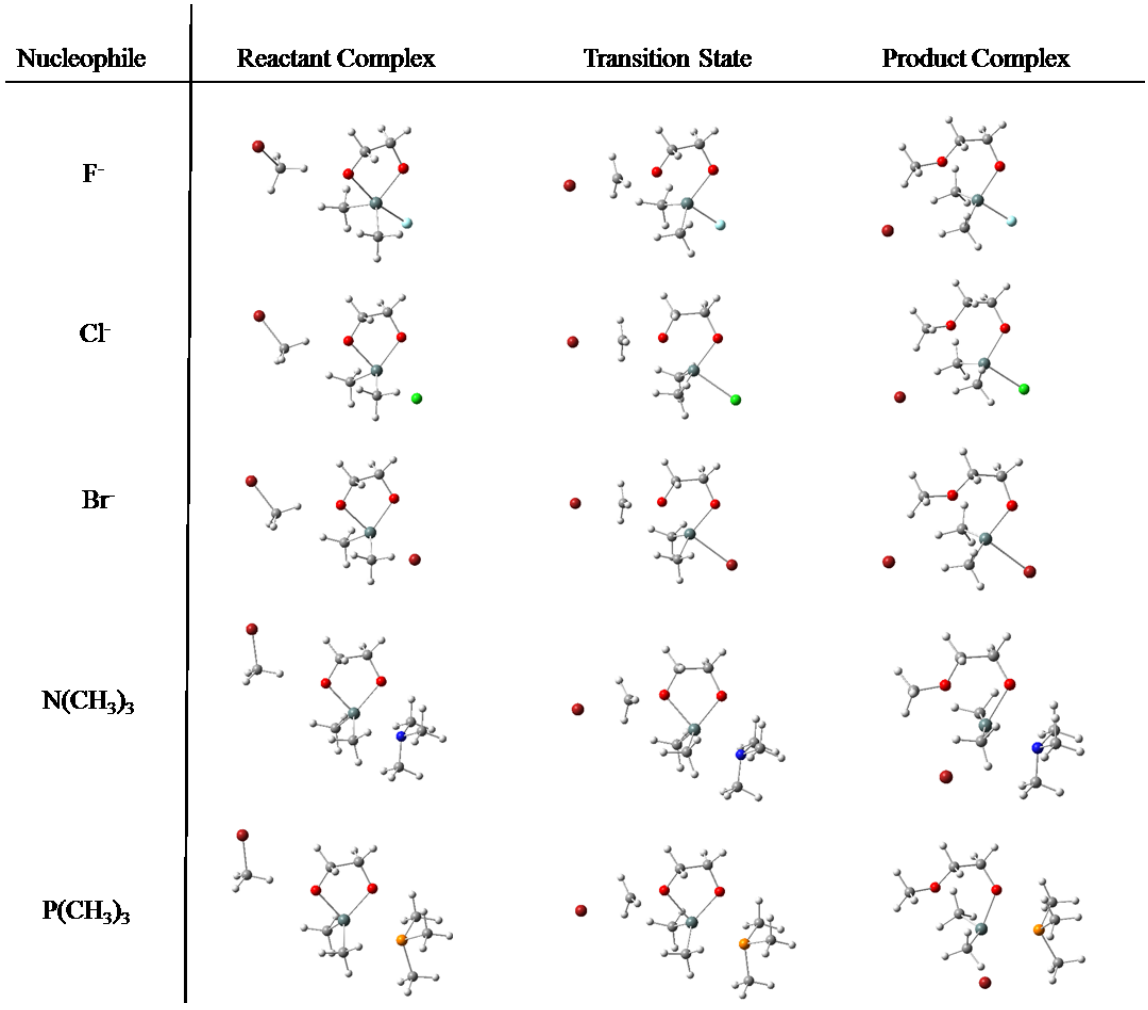

Figure 5. 1: Geometry structures along the reaction pathway 1 via monomeric intermediates with various added nucleophiles.

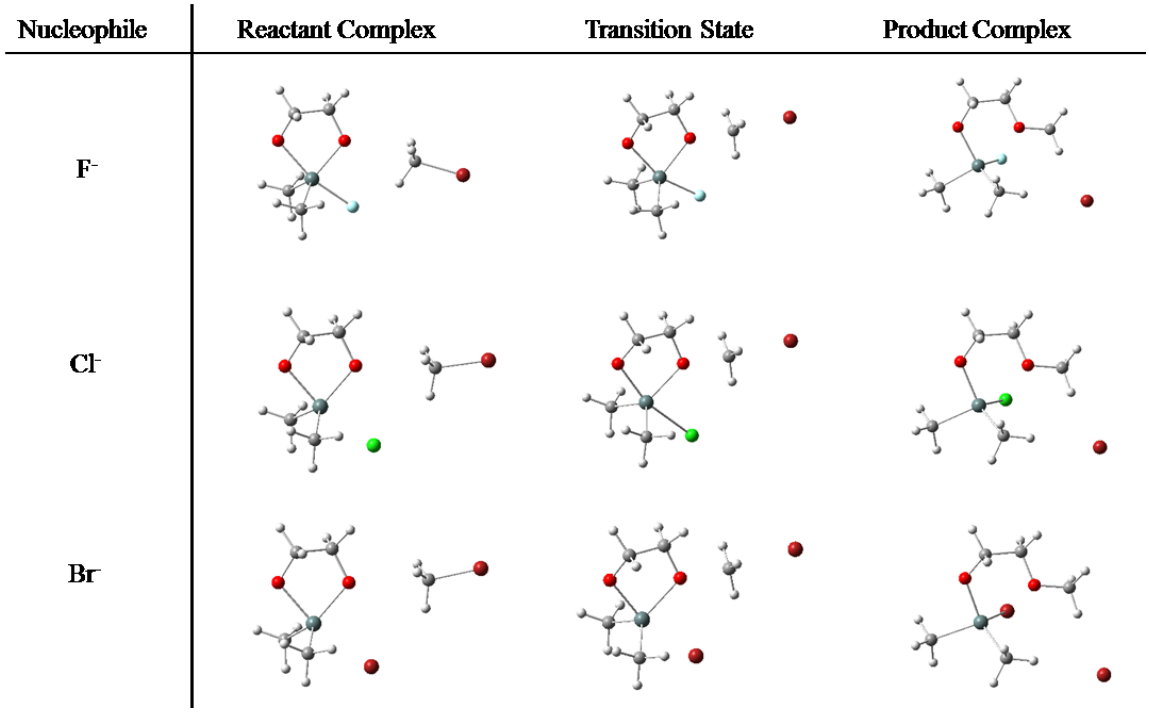

Figure 5. 2: Geometry structures along the reaction pathway 2 via monomeric intermediates with various added nucleophiles.

Optimized structures calculated with B3LYP/6-311+G(d,p) along both of the pathways through the monomeric intermediates are shown in Figure 5.1 and 5.2. In the approach of the methyl bromide in pathway 1 (Figure 5.1), a hydrogen bond was formed between the nucleophilic oxygen atom and one of the hydrogen atoms from the methyl group. In the comparison of the reactant complexes with different added nucleophiles, the orientations of the incoming methyl bromide were different. This difference in the placement of the methyl bromide can be described by considering the angle between the C-Br bond and the closest oxygen atom. It was observed that this angle in the systems with added halides (e.g. 119.3° for the complex with an added fluoride) were slightly larger than those with added trimethylamine or trimethylphosphine (e.g. 108.7° for the

complex with an added trimethylamine). In the system with an added fluoride, the C-Br bond was more perpendicular to the plane defined by the O-Sn-O unit in contrast with other geometries, while for the systems with added trimethylamine and trimethylphosphine, the C-Br bond was more in the O-Sn-O plane compared to the systems with added halides. For the transition states in the pathway 1, the structures had standard transition state geometries in the S_N2 reactions with a partially pentacoordinate carbon having trigonal bipyramidal geometry. The arrangement of the three C-H bonds were distinguishable in the systems with different nucleophiles. The three C-H bonds were not exactly in the same plane of the structures with added trimethylamine and trimethylphosphine. In other words, the geometries around the carbon in these systems were slightly distorted trigonal bipyramidals. An unexpected bond cleavage of Sn-O was found in the transition states, while for the systems with added trimethylamine and trimethylphosphine, the Sn-O bond still exists at this point. This difference could be interpreted as being due to the neutral nucleophiles the trimethylamine and trimethylphosphine in the contrast to negative charged halides have less effect to weaken the Sn-O bond. The degree of the weakness could be presented by the competition of the bond strength between the Sn-X bond and the Sn-O bond. For example, the strongest nucleophile F^- can form a stronger bond with Sn than a Sn-O bond, which should lead to more cleavage of the Sn-O bond, providing the most convenience for the addition of the electrophile. It was predictable that a weaker added nucleophile leads to lower cleavage of the Sn-O bond, indicating less activation ability of the nucleophile. On the other hand,

a stronger nucleophile could provide more nucleophilic oxygen, which will be discussed in section 5.4. There was a formation of one hydrogen bond in the product complexes with bromide ion, which contributes to the stabilization of the systems. The five-membered ring structure was distorted at this point due a significant elongation of the Sn-O interaction distance. For the systems with added trimethylamine and trimethylphosphine, no transitional structures between the transition state and these product complexes were observed. A couple of trial initial geometries with various possible positions of the bromide were attempted, however, all the explorations on the PES from different starting points converge to the same geometries which are shown in Figure 5.1. In fact, another optimized structure of the product complex was found. For example, in the system with added halides (Figure 5.3), there were no hydrogen bonds formed in these cases. These structures were more like an intermediate step between the transition states and the first types of product complexes (with occurrence of hydrogen bonds). In contrast, the geometry structures shown in Figure 5.1 were closer to the intermediate status to the next nucleophilic exchange step of the reaction cycle.

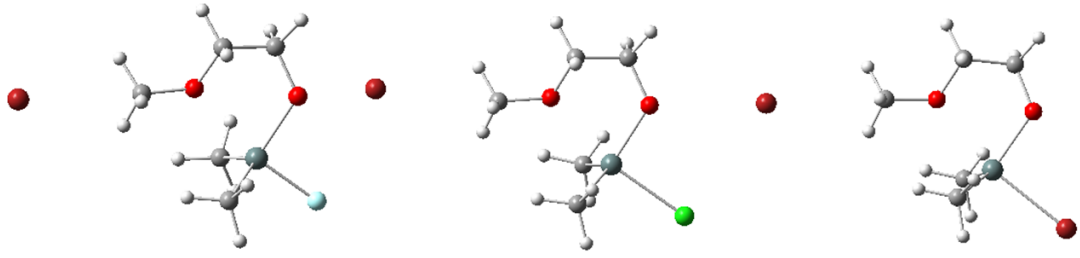

Figure 5. 3: Optimized product complexes with added halides along the pathway 1 without formation of hydrogen bonds.

Figure 5.2 displays the optimized geometries along pathway 2 through the

monomeric intermediate: it was observed that a hydrogen bond formed between the halides and one of the hydrogen atoms of the methyl group in the reactant complex 2. The distance of the H…X interaction was dramatically longer in the systems with added chloride and bromide in the comparison with the one with an added fluoride. Through these transition states, the methyl group maintains its arrangement from the reactant complexes 2, and at the same time, a trigonal planar configuration around the partially pentacoordinate carbon was organized. Furthermore, the ring forms in the product complexes 2 were destroyed by the attachment of the alkylated reagent and the dramatic stretching of the Sn-O connection. These distorted complexes are stabilized by two hydrogen bonds.

5.3.1.2 Dimeric Intermediates

As explained in the beginning, only one pathway was described for the dimeric intermediate. Two halides (F^- and Br^-) as nucleophiles were attached to the tin atom of one unit of a dimer (Figure 5.5). The reaction paths are similar to the pathway 2 of monomeric intermediates.

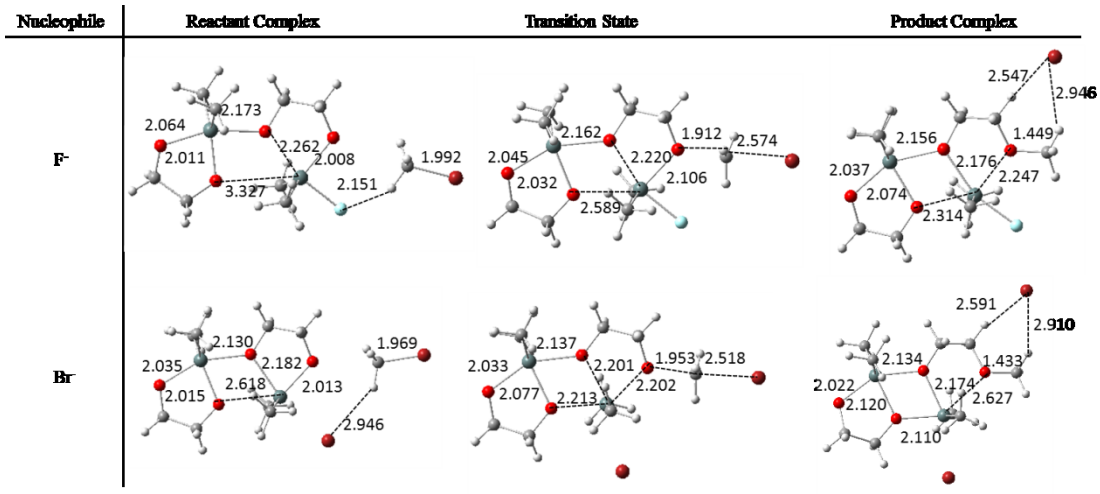

Figure 5. 4: Geometry structures along the reaction pathway via the dimeric intermediates with two different added halides by using B3LYP/6-311+G(d,p), and the geometry paramters were shown in the figure, where bond length in Å.

In the presence of the added halides, the symmetry of the dimer structure was ruined by weakening the Sn-O bond of the right hand side unit, leading to a significant bond extension of the bottom Sn-O interaction between two monomeric units. In this case, the original tricoordinate oxygen atom turns back to dicoordinate due to this bond cleavage. A hydrogen bond formed between the halide and the hydrogen atom that was present in the reactant complex contributes to the stabilization of the system. In the transition states, the bottom Sn-O bonds were shortened, which gave better symmetry of the dimer structures. The methyl group kept its arrangement from the reactant complex, and the carbon center became partially pentacoordinate with regular trigonal planar geometry. For the system with an added bromide, both of the Sn-O bonds were cleaved in the right hand side unit. In addition, with the movement of the bromide to the very bottom of the system, the angle between two methyl groups connected through the tin atom were

opened from 142.7° to 173.1°. The left Sn-O bond in the right hand side unit was shortened, while the right Sn-O bond was elongated. With the completion of the alkylation, the bottom Sn-O bond (2.314Å and 2.110Å) length returned to normal compared to the top Sn-O bond (2.156Å and 2.134Å). The right Sn-O bond from the right hand side unit was dramatically stretched due to the attachment of the alkylating agent to the nucleophilic oxygen. Two hydrogen bonds were observed, which strengthen the stabilization of the complex systems. However, such system organizations were hardly to be observed in the real experiments. In the account of the one negative charge carried by the halide ion and solvent effect, these systems will be stabilized by the intermolecular interactions with the polar solvent molecules (e.g. DMF).

5.3.1.3 Geometry Comparisons

In the comparison of optimized structures between B3LYP and M06-2X functionals, small differences of the geometric parameters were discovered. For example, Table 5.2 displayed the geometric parameters of the reactant complexes with various added nucleophiles along reaction pathway 1 via the monomeric intermediate. The largest differences are in the calculated lengths of the hydrogen bonds. For the systems with added halides, M06-2X implied slightly longer distances between the nucleophilic oxygen atoms and the hydrogen atoms. Nevertheless, in the structures with the addition of trimethylamine and trimethylphosphine, M06-2X providedlengths of hydrogen bonds that were close for the systems with added halides (2.099Å~2.147Å), while B3LYP

showed bond lengths extended to 2.227Å. Although it is well known that B3LYP fails in estimating London dispersion, this method still predicts reasonable numbers for hydrogen bond lengths. For the systems with added trimethylamine and trimethylphosphine, the deviation of Sn-X bond lengths between the two methods is close to 0.1 Å. Therefore, the big difference in prediction of the hydrogen bonds for these two systems can be explained through the disagreement of the estimate of the Sn-X bonds. If the results obtained from M06-2X were close the actual values of these bonds lengths, B3LYP underestimated the activation abilities of trimethylamine and trimethylphosphine, namely: longer Sn-X bond lengths, less nucleophilicity on the stannylene acetal oxygen atom, and of course poorer interaction of the hydrogen bonds, i.e. longer O-H interaction distances. If the results obtained from B3LYP were closer to the experimental data, then M06-2X overestimates their activation ability. It is also possible that neither of the methods provide comparable results to experiment. Unfortunately, no experimental studies have been carried out by using trimethylamine and trimethylphosphine as nucleophiles for the activation of the stannylene acetals, although other neutral nitrogen-centered nucleophiles have been used.[6]

Table 5. 2: Selected geometric parameters for the reactant complexes, transition states and product complexes using B3LYP/6-311+G(d,p) and M06-2X/6-311+G(d,p) (r in Å, < in degrees).[a]

Reactant Complex 1

	B3LYP					M06-2X				
	DA(F)	DA(Cl)	DA(Br)	DA(NMe3)	DA(PMe3)	DA(F)	DA(Cl)	DA(Br)	DA(NMe_3)	DA(PMe_3)
r(Sn,O)l	2.123	2.105	2.097	2.019	2.014	2.103	2.085	2.078	2.010	2.000
r(Sn,O)r	2.014	2.009	2.008	1.995	2.002	1.998	1.993	1.991	1.998	1.994
r(Sn,X)	2.004	2.564	2.757	2.593	2.990	1.985	2.534	2.726	2.458	2.914
r(O,H)	2.040	2.076	2.082	2.225	2.227	2.099	2.124	2.135	2.146	2.147
r(C,Br)	1.985	1.984	1.983	1.974	1.974	1.961	1.960	1.958	1.950	1.949
<(O,Sn,O)	80.3	81.0	81.3	83.8	83.8	80.8	81.6	81.9	83.6	84.0
<(O,Sn,X)	88.2	88.0	87.8	75.9	69.6	88.8	88.8	88.5	76.6	69.3
<(C,Sn,C)	119.2	120.0	120.2	119.1	118.7	120.1	121.3	120.9	118.9	120.3

[a] The r(Sn,O)l and r(Sn,O)r, respectively, refer to the intramolecular bonds between tin and dicoordinate oxygen atoms placed on the left and right (see Figure 5.1). X indicates different nucleophilic ions or groups.

5.3.2 Implications for the Reaction Mechanisms

5.3.2.1 Monomeric Intermediate

As B3LYP is considered to be unreliable in predicting for thermochemistry of the organotin compounds, thermochemical results obtained from B3LYP, M06-2X and MP2 single-point energy calculations based on the B3LYP optimized species will be compared. The potential energy surfaces of the alkylation reactions via the monomeric intermediates are revealed in Figures 5.5 to 5.8, while Figures 5.5 to 5.7 display reaction profiles of pathway 1, and Figure 5.8 (a), (b) and (c) exhibits energy changes for pathway 2.

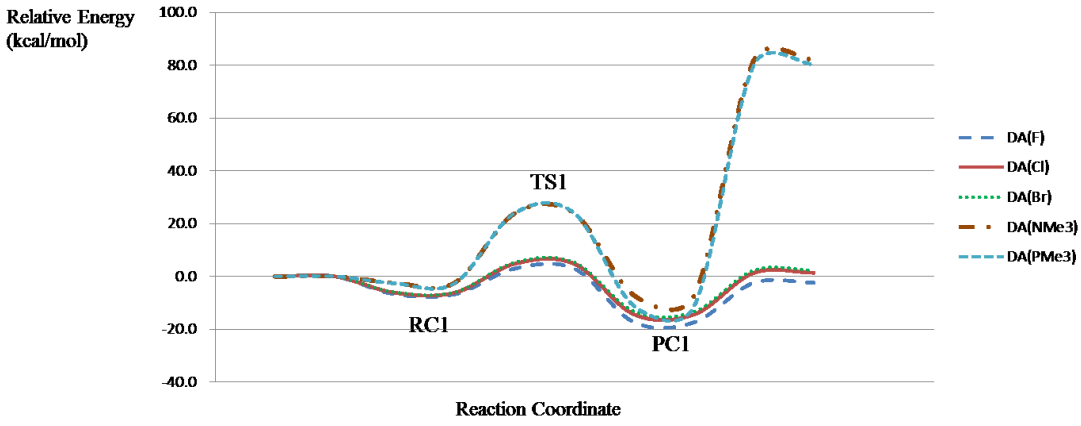

Figure 5. 5: Potential energy profile for pathway 1 of alkylation reactions via monomeric intermediates with various added nucleophiles. Relative energies are in kcal/mol. DA represents the dimethylstannylene acetal, and the groups indicated in the brackets stand for the added nucleophiles. RC1, TS1 and PC1 are short for the reactant complexes, transition states, and product complexes along the pathway 1. All the energies were calculated by using B3LYP/6-311+G(d,p) method.

The energy profile for a S_N2 reaction calculated in the gas-phase usually exhibits a characteristic double-well potential curve, which includes three steps. The reaction starts from the formation of the reaction complex or the ion-molecule complex, then break through the barrier of the transition states, which converts the reactant complex to the product complex. At last, the product complex dissociates to the desired products, which denotes the completion of the S_N2 reaction path (see Chapter 3). From the thermochemical results calculated by B3LYP, the profiles for the systems with added halides provide classic double-well potential curves. Reactant complexes were formed in the first step with a little decrease in energy (e.g. -8.5 kcal/mol for the system with an added fluoride). These complexes overcame the reaction barriers (e.g. 9.7 kcal/mol for the system with an added fluoride), and the structures transformed through the transition

states to the product complexes which break down to yield alkylated product molecules plus the leaving group bromide ion. For the systems with added trimethylamine and trimethylphosphine, the potential surfaces have several distinguishable factors in contrast with others. Their activation energies were higher by approximately 15 kcal/mol, additionally, the relaxation of the product complexes leads to the energy eruption straight to ~80 kcal/mol. This could be understood by analyzing the charges of different systems due to the addition of different nucleophiles. The systems with added halides usually possess one negative charge, while the complexes with added trimethylamine and trimethylphosphine are neutral systems. The relaxation of the product complexes of these systems results in a neutral system that is forced to be separated into a positive charged acetal and a bromide ion. The products yielded from the complexes with an added fluoride are quite stable by comparing to the reactants (-2.4 kcal/mol), while those generated from the complexes with added chloride and bromide are slightly higher in energy than the reactants by 1~2 kcal/mol.

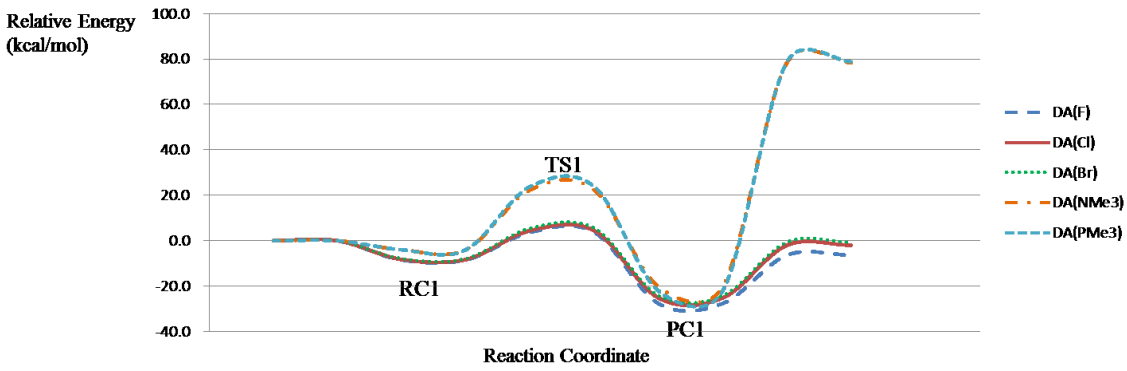

Figure 5. 6: Potential energy profile for pathway 1 of alkylation reactions via monomeric intermediates with various added nucleophiles. Relative energies are in kcal/mol. DA represents the dimethylstannylene acetal, and the group indicated in the brackets stand for the added nucleophiles. RC1, TS1 and PC1 are short for the reactant complexes, transition states, and product complexes along the pathway 1. All the energies were calculated by using M06-2X/6-311+G(d,p) method.

Figure 5.6 demonstrates the energy profile plotted by using M06-2X, similar shapes of the potential energy surfaces were observed. The reaction barriers for the systems with added trimethylamine and trimethylphosphine were higher than other reaction pathways by around 20 kcal/mol. The cleavage of the product complexes generates a straight increase of the energy (~78 kcal/mol). All the products obtained from the systems with added halides are more stable than the corresponding reactants. With the decreasing order of the nucleophilicity from F^- to Br^-, the stability of the products is also decreased (relative energy is reduced from -6.4, -2.0 to -0.7 kcal/mol).

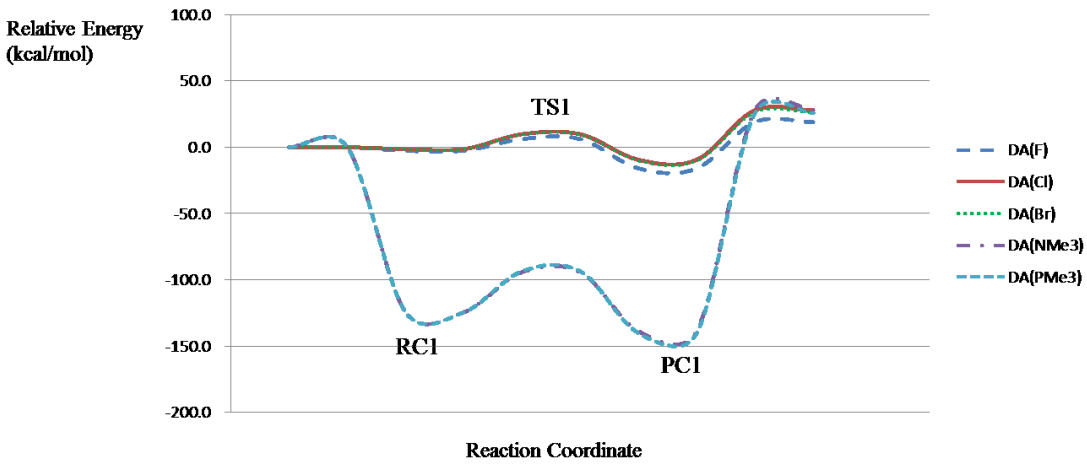

Figure 5. 7: Potential energy profile for pathway 1 of alkylation reactions via monomeric intermediates with various added nucleophiles. Relative energies are in kcal/mol. DA represents the dimethylstannylene acetal, and the groups indicated in the brackets stand for the added nucleophiles. RC1, TS1 and PC1 are short for the reactant complexes, transition states, and product complexes along the pathway 1. All the energies were calculated by using MP2/6-311+G(d,p)//B3LYP/6-311+G(d,p) method.

MP2 single-point energy calculations were carried out based on the B3LYP optimized species, aiming at an expected improvement of the thermochemical predictions. From Figure 5.7, the potential energy surfaces of the systems with added halides are relatively flat in contrast with the other two. Reaction barriers between the reactant complexes and the transition states vary from 8.8 kcal/mol (the system with an added fluoride), 11.3 kcal/mol (the system with an added chloride) to 11.0 kcal/mol (the system with an added bromide). The relaxed products are unstable due to a relatively higher energy (~19 to 28 kcal/mol) than the reactants. The curves of the systems with added trimethylamine and trimethylphosphine show a fairly large energy difference between the complexes and the separated molecules (~ -94 kcal/mol difference between

the reactants and their complexes and ~ -160 kcal/mol between the products and their complexes). According to the previous results, MP2 single-point energy calculations overestimate the relative stabilities of the intermediate complexes, which results in the huge energy gap. Wakamatsu *et al.* proposed that MP2 is too computationally intensive for calculations of reaction paths.[14] Recalling the discussion of the MP2 results in Chapter 3, a point of view was raised that a disagreement could exist between the B3LYP optimizations and those using the MP2 single-point method. Furthermore, there is a possibility that this disagreement is caused by the combined employment of the effective core potential and the Pople basis sets. A related benchmark study focused on examination of the most appropriate level of theories and basis sets for the reaction paths with organotin compounds is urgently necessary.

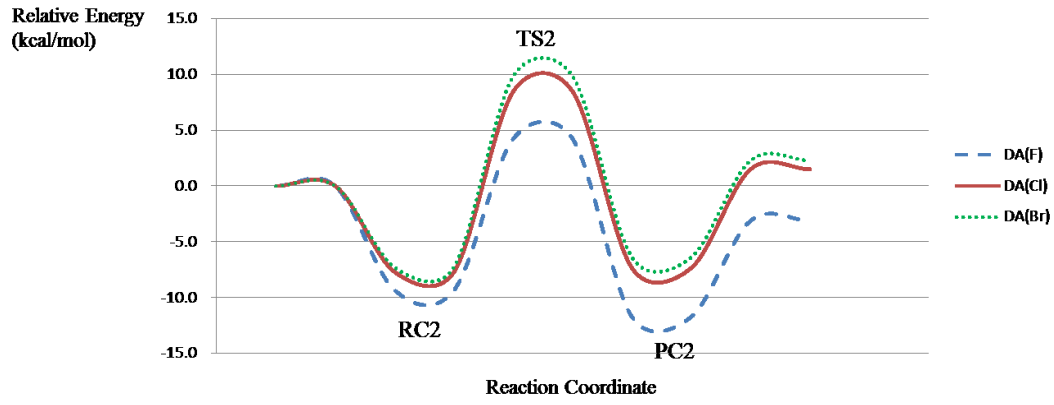

(a)

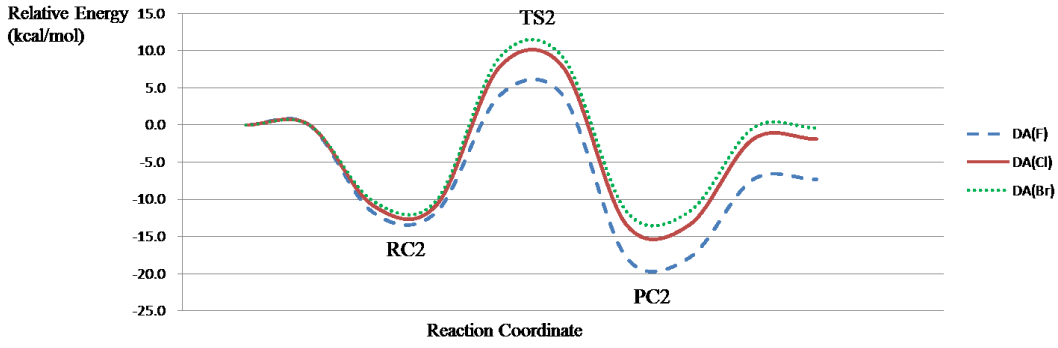

(b)

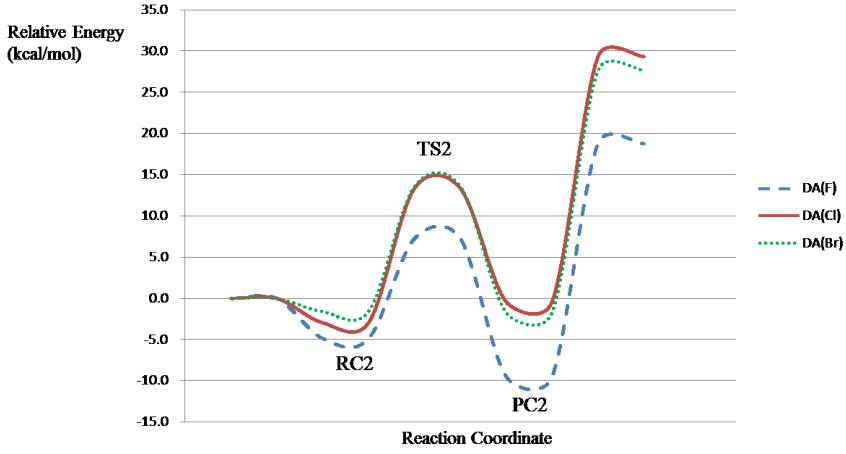

(c)

Figure 5. 8: Potential energy profile for pathway 2 of alkylation reactions via monomeric intermediates with various added nucleophiles. Relative energies are in kcal/mol. DA represents the dimethylstannylene acetal, and the groups indicated in the brackets stand for the added nucleophiles. RC2, TS2 and PC2 are short for the reactant complexes, transition

states, and product complexes along the pathway 2. The energies were calculated by using (a) B3LYP/6-311+G(d,p), (b) M06-2X/6-311+G(d,p) and (c) (MP2/6-311+G(d,p)//B3LYP/6-311+G(d,p) method.

The potential energy surfaces predicted for pathway 2 by different levels of theory are shown in Figure 5.8. These energy profiles clearly show the relationship between the nucleophilicity of the halides and the height of the reaction barriers. The B3LYP and M06-2X results reveal that barriers decreased with the addition of a stronger nucleophile to the tin atom, in the meantime, the stability of the reactant complexes and product complexes are enhanced. A stronger nucleophile has a stronger ability to activate the acetal complex, contributing to a lower reaction barrier and more stable products. In the last profile obtained with MP2 single-point energy calculations, the curve of the system with an added chloride is partially overlapped by the potential energy surface of the system with an added bromide, which turns out a nearly equivalent activation ability of the chloride and bromide. In the step of the relaxation of the product complex to the separated products, an unexpected increasing tendency of the energy curve occurs, which indicates the instability of the products.

5.3.2.2 Dimeric Intermediates

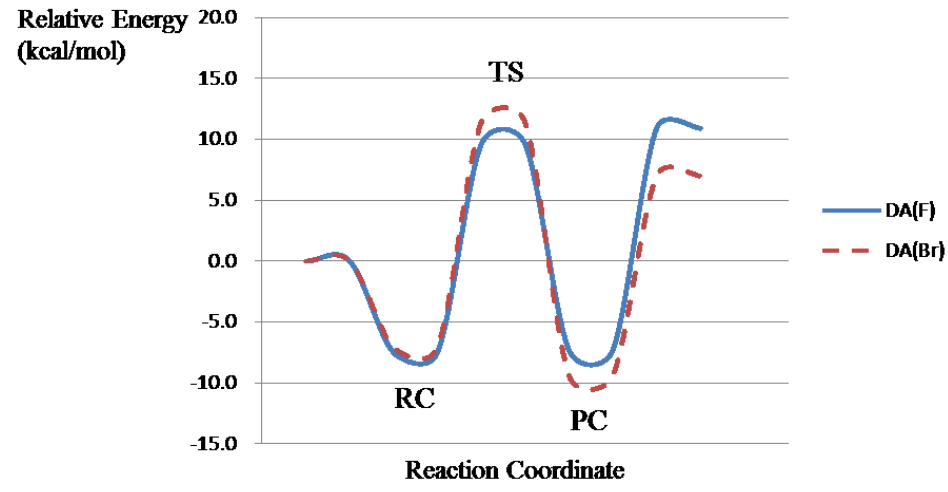

(a)

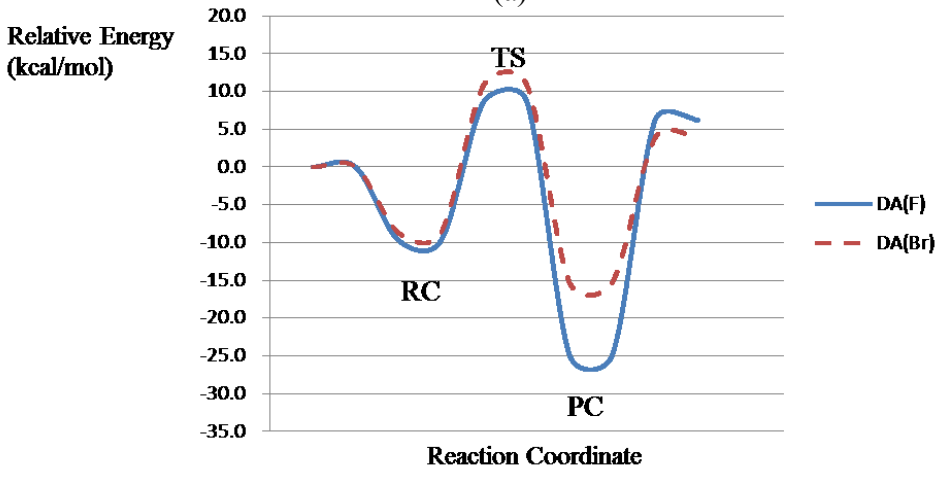

(b)

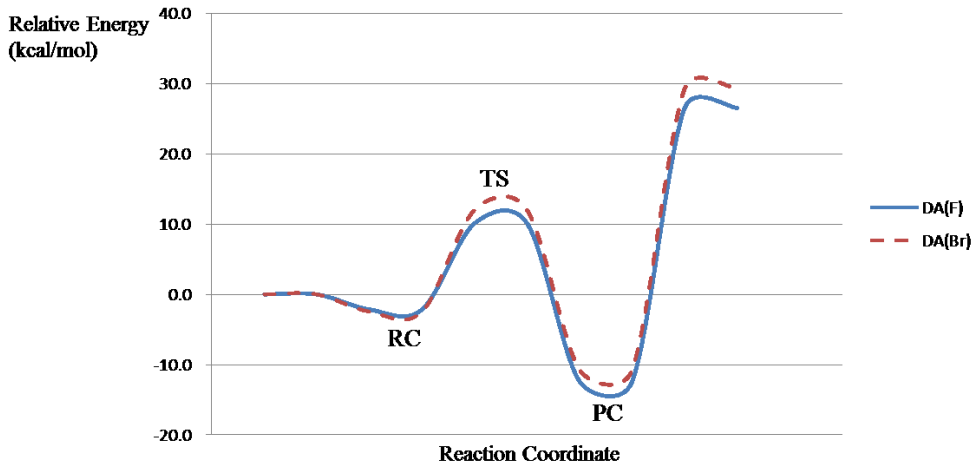

(c)

Figure 5. 9: Potential energy profile for alkylation reactions via dimeric intermediates with various added nucleophiles. Relative energies are in kcal/mol. DA represents the dimethylstannylene acetal, and the groups indicated in the brackets stand for the added nucleophiles. RC, TS and PC are short for the reactant complexes, transition states, and product complexes along the pathway. The energies were calculated by using (a) B3LYP/6-311+G(d,p), (b) M06-2X/6-311+G(d,p) and (c) (MP2/6-311+G(d,p)//B3LYP/6-311+G(d,p) method.

Two nucleophiles were added to the tin atom of the dimeric intermediate, which are F^- and Br^-. For the first profile, the system with an added fluoride involved in the reaction pathway experienced a lower reaction barrier compared to the energy surface of the system with an added bromide. Nevertheless, the product complex and products of the systems containing the fluoride are slightly higher in energy (2.1 kcal/mol and 3.9 kcal/mol). Both of the systems have higher energies of products than reactants. From the results calculated by the M06-2X method, the stronger nucleophile fluoride enhances the activating ability of the acetal by providing a lower reaction barrier, and a more stable product complex. However, the products still have higher energy than reactants by a few

kcal/mol. When analyzing the geometry structures, the bromide moves to the top of the dimer system, forming two hydrogen bonds with two methyl groups. These thermochemical results may be caused by hydrogen bonds that contribute more stabilization to the system with added bromide than to the system with the addition of the fluoride. Profile 5.9 (c) is plotted based on the results obtained from MP2 single-point energy calculations. The curves for the two complex systems change in a similar tendency, slight energy difference of the reaction barriers and stability of the intermediate complexes were found. Similar to the previous MP2 results, a sudden increase of the energy takes place during the relaxation of the product complex.

Table 5. 3: Relative energies (in kcal/mol) of the reaction barriers (energy difference between RCs and TSs) for the different pathways obtained from various levels of theory.

	Nucleophile	Pathway	B3LYP	M06-2X	MP2//B3LYP
Monomer	F	1	9.7	12.2	8.8
		2	13.4	15.6	12.2
	Cl	1	11	12.7	11.3
		2	16.2	18.6	15.2
	Br	1	11.4	13.4	11.0
		2	17.1	19.3	15.2
	$N(CH_3)_3$		26.3	26.4	30.3
	$P(CH_3)_3$		26.6	27.8	30.9
Dimer	F		17.1	18.4	12.3
	Br		18.5	19.6	14.4

According to the geometry analysis and the comparison of the reaction profile calculated by different levels of theory, two mechanisms are proposed to explain the

process of the alkylation reaction and the effect of various added nucleophiles to the activation of the catalytic intermediates. In the two pathways via the monomeric intermediate, with the addition of the nucleophile, the dimethylstannylene acetal approaches the target electrophile (methyl bromide), and then forms the reactant complex in the first step which is stabilized by the presence of the hydrogen bonds. A O-Sn bond cleavage was observed in the process of the alkyl group attachment. The leaving group bromide ion migrates to the bottom space, generating one or two hydrogen bonds with the methyl groups, which largely contributes to the stabilization. The pathway 1 is slightly preferred owing to a lower reaction barrier. The path along the dimeric intermediate suggests a similar mechanism to the monomer. The only difference is that the bromide ion shifts to the top of the system and forms hydrogen bonds from the upper part with the C-H bonds. Nevertheless, a more stable complex structure is believed to produce within the consideration of the polar solvent. In the comparison of the reaction barriers (Table 5.3), the dimer paths were surprisingly less favored than the monomer pathways. With the increasing order of nucleophilicity from Br^- to F^-, gradually increased Sn-O bond lengths were observed in the transition states which illustrates that a stronger nucleophile forms a stronger bond with the tin atom, leading to faster bond cleavage of the O-Sn interaction. On the other hand, in the increasing order of the nucleophiles added, the reaction barrier decreased (Table 5.3) and the generated products are provided with more stability. The nucleophiles trimethylamine and trimethylphosphine reveal close ability in activating the acetal.

5.4 Activation Ability of Nucleophiles

Dong *et al.*[96] conducted experiments exploring the activation ability of halides on benzylation of diols, polyols and carbohydrates. A concept was proposed that the regioselectivity is controlled by the competition or equilibria between the formation and cleavage of Sn-O and Sn-X (halide) bonds. For example, the stronger Sn-X bond, such as the Sn-F bond, indicates the formation of more Sn-X bonds and less Sn-O bonds of acetal molecules in solution, resulting in more stannylene oxygen atoms with rich nucleophilicity. Therefore, F^- should have the greatest activation ability to boost the alkylation reactions. To establish the relationship between the activation ability of a nucleophile and the cleavage of Sn-O bond, the structures of reactant complexes in the monomer reaction pathway 1 were examined and compared (B3LYP/6-311+G(d,p)-LANL2DZdp(Sn)), because the elongation of the Sn-O bond in the path starts from the formation of the reactant complex. It is assumed that the degree of the extension of the bond is associated with the activation ability of the nucleophile. This ability of the promotion also could be reflected as a contribution to the stabilization of the reactant complexes, enhancement of the nucleophilicity on the oxygen atom via the Sn-O bond and overcoming a relatively low reaction barrier.

Recall that a hydrogen bond contributed to the stabilization of the reactant complexes. This intramolecular interaction can be demonstrated in the C-H symmetric stretching frequency shift observed upon complexation. The magnitude of the frequency shift and the hydrogen bond distance could be considered as the measurement of the

strength of the intramolecular hydrogen bond.[128,129] Figure 5.10 summarized a linear correlation between the frequency shifts and the hydrogen bond distance and the Sn-O bond length. Therein, γ(C-H) is the symmetric stretching frequency of the C-H bond of the methyl bromide, while r(O…H) is the bond distance of the hydrogen bond of the reactant complexes and r(Sn-O) describes the Sn-O bond length. As the hydrogen bond distance shortens, the frequency decreases, which means a stronger hydrogen bond causes a redshift of the spectrum. Different added nucleophiles appear to have a striking influence on the O-H distance and the degree of the cleavage of Sn-O bond. The hydrogen bond distance (O···H interaction) is tightened (decreasing γ(C-H)) with the increasing nucleophilicity of the added nucleophile, while the extent of the cleavage becomes greater. This is evidence that the stronger hydrogen bond results from the more nucleophilic oxygen atom whose electron density is enhanced by a stronger nucleophile. Also, a stronger activating agent (nucleophile) causes a larger degree of cleavage of the Sn-O bond, which aids attack by the approaching electrophile. Thus, the reactant complex with the added fluoride has the shortest distance of its hydrogen bond which contributes the most stabilization to the complex structure and the most cleavage of the Sn-O bond. Based on this information provided from Figure 5.10, the fluoride has the strongest activation ability which is much greater than other nucleophiles. The activation ability of chloride and bromide are close, and the ability of trimethylamine and trimethylphosphine are nearly equal.

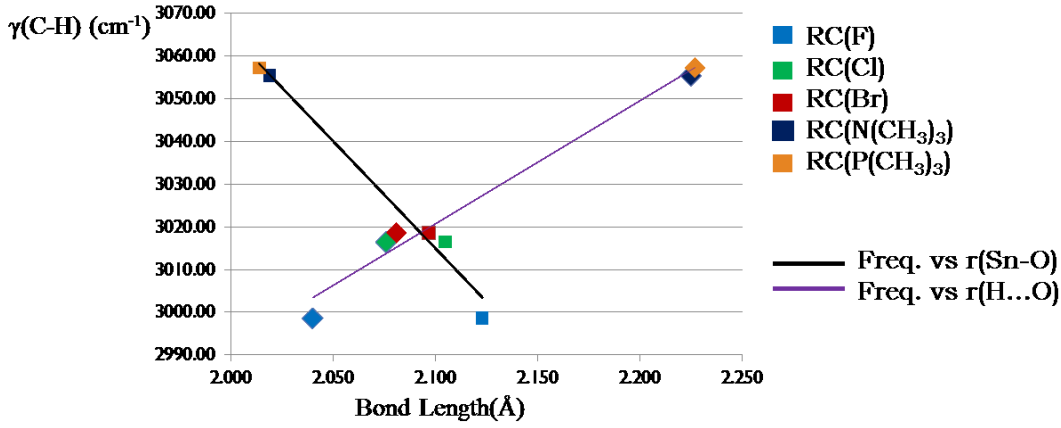

Figure 5. 10: Variation of γ(C-H) with the O···H bonding distance (purple line) and Sn-O bond length (black line) of the reactant complexes from pathway 1 via the monomeric intermediates (B3LYP/6-311+G(d,p)-LANL2DZdp(Sn)). Different color squares represent different reactant complexes with different added nucleophiles.

In order to further prove this relationship, Figure 5.11 summarizes the relation between the Mülliken charge indicated on the oxygen atom which is involved in the hydrogen bond in the reactant complexes and the corresponding reaction barriers of monomers reaction pathway 1. In the previous two sections, based on the reaction profiles sketched for the organotin intermediates with various added nucleophiles, some display a clear indication that a stronger nucleophile gives lower reaction barrier for the reaction path. With the addition of fluoride to the tin-containing system, the most negative charge on the stannylene oxygen indicates the richest nucleophilicity on the atom. Furthermore, the relevant reaction barrier of the pathway is the lowest, which implies the strongest activation to the complex structure resulting in the most ease to overcome the activation energy. Compared to the fluoride, chloride and bromide are slightly weaker activating agents. Trimethylamine and trimethylphosphine are much

weaker than the halides, and these two nucleophiles have the equivalent ability to activate organotin complexes.

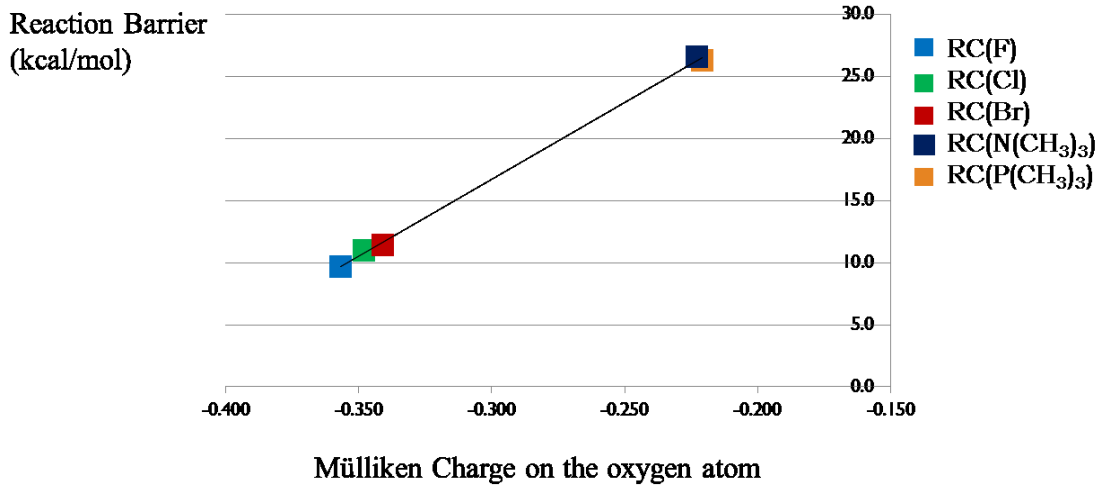

Figure 5. 11: Mülliken charges indicated on the oxygen atoms the reactant complexes versus the corresponding reaction barriers following the pathway 2 via the monomeric intermediates (B3LYP/6-311+G(d,p)). The colored squares from left to right represent reactant complexes with the added fluoride, chloride, bromide, trimethylamine and trimethylphosphine.

The particular outcome of the present work is the quantitative evaluation of the effect of different added nucleophiles to activate the organotin complexes. In order to clarify the influences of the nucleophiles, the relationships between different factors were performed. From the results shown above, the strongest nucleophile fluoride affords the shortest hydrogen bond which contributes to the most stabilization of the reactant complex. Also, the fluoride generates a largest cleavage of the Sn-O bond which provides more chances to proceed the alkylation reaction. Furthermore, the fluoride enhances nucleophilicity on the oxygen atom the most, resulting in more attraction with

the electrophile which further leads to a lower reaction barrier. These computational results partially support Dong group's speculations about the promotional effect of nucleophiles on the reactions of stannylene acetals.[96]

5.5 Summary

This theoretical study demonstrated three emphases in the exploration of reaction pathways via organotin intermediates. First of all, the most reactive stannylene acetal to catalyze the alkylation reactions of diols is the monomer. There are two pathways along the monomeric intermediate, where pathway 1 is kinetically controlled and pathway 2 is thermodynamically controlled. The suggested mechanisms for both monomeric and dimeric intermediates are quite similar. A Sn-O bond cleavage is relevant to the alkylation mechanisms. Secondly, it was illustrated that fluoride, the strongest nucleophile, should possess the strongest ability to activate the acetal. This activation includes the weakening of the Sn-O bond and the enhancement of the nucleophilicity to the stannylene acetal oxygen atoms. Finally, B3LYP and M06-2X provide similar geometric parameters of the optimized structures and identical thermochemical results with the basis set applied.

Chapter 6: Conclusions and Future Work

6.1 Global Conclusions

Computational studies on organotin-mediated alkylation reactions of diols were presented in this thesis, focusing on investigations of geometry analysis, reaction mechanisms and the activating effect of added nucleophiles to the tin center.

A reaction cycle was proposed for the alkylation reaction of 1, 2-diols by assistance of monomeric dialkylstannylene acetals. Chapter 3 aimed to find the most reactive form of fluoridated tin-containing species, which facilitates alkylation reactions by exploration of the reaction paths via monomeric and dimeric forms of dimethylstannylene acetals, using B3LYP/6-31G(d,p)-LANL2DZdp(Sn) for geometry optimization and MP2/6-311G(2d,p)// B3LYP/6-31G(d,p) for thermochemistry. Unexpected thermochemical results were obtained that involved unrealistic large energy differences between reactants and reactant complexes. In Chapter 4, the unreasonable relative energies were examined and a benchmark study was carried out on relevant model systems by using different levels of theory with various basis sets. B3LYP/6-311+G(d,p)-LANL2DZdp(Sn) and M06-2X/6-311+G(d,p)-LANL2DZdp(Sn) were finally selected for the future research and the implications of reaction mechanisms for both monomeric and dimeric form intermediates were suggested. The MP2 method was observed to overestimate the stability of reactant complexes.

In the choice of a new theoretical method, Chapter 5 established the pathway for

alkylation reactions of diols via dimethylstannylene acetals in the presence of different nucleophiles. According to the geometry and thermochemical analysis of reaction paths through both forms of organotin derivatives, the monomeric intermediate was evaluated as the more reactive agent with lower activation energies obtained. The activation effects of five different nucleophiles were examined and corresponding mechanisms of this promotion were proposed through correlation with hydrogen bonds in the reactant complexes.

6.2 Future Work

There are many possibilities for further research relating to topics discussed in this thesis. In particular, the inclusion of solvent effects should be a primary consideration. Due to the presence of a negative charge in the model systems, polar solvents, such as DMF, will contribute significantly to the stabilization of complexes.

Three more main steps should be studied in the reaction cycle, including the addition of the second halide to the tin atom, nucleophilic exchange and separation between tin-containing moiety and the alkylated diol part. The second reaction may be difficult to model. Actually, this reaction step has been explored for the fluoridated monomeric intermediate. It is difficult to locate the transition state because the five-membered ring structure sometimes collapses into fragments.

Obtaining accurate thermochemical results is problematic in computational

organotin chemistry. Major explanation includes a lack of experimental references for benchmarking theoretical methods. Dispersion-corrected density functionals such as B3LYP-gCP-D3 should be considered in the future work. Careful comparisons of all electron calculations with small effective core potentials are required, and large effective core potentials for tin may offer the best potential for major advances in computational organotin chemistry.

References

1. Nicholson, J. W. *J. Chem. Ed.* **1989**, *66*, 621.

2. Davies, A. G. *Organotin Chemistry*; 2nd ed.; Wiley-VCH: Weinheim, 2004.

3. Davies, A. G. In *Tin Chemistry: Fundamentals, Frontiers and Applications*; Davies, A. G., Gielen, M., Pannell, K. H., Tiekink, E. R. T., Eds.; Wiley: Chichester, UK, 2008, p 1.

4. David, S.; Hanessian, S. *Tetrahedron* **1985**, *41*, 643.

5. Pereyre, M.; Quintard, J. P.; Rahm, A. In *Tin in Organic Synthesis*; Butterworths: London, 1987; Vol. 1, p 261.

6. Grindley, T. B. *Adv. Carbohydr. Chem. Biochem.* **1998**, *53*, 17.

7. Grindley, T. B. In *Tin, Fundamentals and Applications*; Gielen, M., Davies, A. G., Tiekink, E. R. T., Pannell, K. H., Eds.; John Wiley: Chichester, UK, 2008, p 491.

8. Dong, H.; Zhou, Y.; Pan, X.; Cui, F.; Liu, W.; Liu, J.; Ramström, O. *J. Org. Chem.* **2012**, *77*, 1457.

9. Muramatsu, W.; Takemoto, Y. *J. Org. Chem.* **2013**, *78*, 2336.

10. Wakamatsu, K.; Orita, A.; Otera, J. *Organometallics* **2008**, *27*, 1092.

11. Whittleton, S. R.; Rolle, A. J.; Boyd, R. J.; Grindley, T. B. *Organometallics* **2010**, *29*, 6384.

12. Yasuda, M.; Chiba, K.; Baba, A. *J. Am. Chem. Soc.* **2000**, *122*, 7549.

13. Whittleton, S. R.; Boyd, R. J.; Grindley, T. B. *J. Phys. Chem. A* **2006**, *110*, 5893.

14. Wakamatsu, K.; Orita, A.; Otera, J. *Organometallics* **2010**, *29*, 1290.

15. Martins, J. C.; Willem, R.; Mercier, F. A. G.; Gielen, M.; Biesemans, M. *J. Am. Chem. Soc.* **1999**, *121*, 3284.

16. De Proft, F.; Vivas-Reyes, R.; Biesemans, M.; Willem, R.; Martin, J. M. L.; Geerlings, P. *Eur. J. Inorg. Chem.* **2003**, 3803.

17. Reginato, G.; Ricci, A.; Roelens, S.; Scapecchi, S. *J. Org. Chem.* **1990**, *55*, 5132.

18. Leigh, D. A.; Martin, R. P.; Smart, J. S.; Truscello, A. M. *J. Chem. Soc., Chem. Comm.* **1994**, 1373.

19. Martinelli, M. J.; Vaidyanathan, R.; Pawlak, J. M.; Nayyar, N. K.; Dhokte, U. P.; Doecke, C. W.; Zollars, L. M. H.; Moher, E. D.; van Khau, V.; Kosmrlj, B. *J. Am. Chem. Soc.* **2002**, *124*, 3578.

20. Smith, P. J.; White, R. F. M.; Smith, L. *J. Organomet. Chem.* **1972**, *40*, 341.

21. Cameron, T. S.; Bakshi, P. K.; Thangarasa, R.; Grindley, T. B. *Can. J. Chem.* **1992**, *70*, 1623.

22. Davies, A. G.; Price, A. J.; Dawes, H. M.; Hursthouse, M. B. *J. Chem. Soc., Dalton Trans.* **1986**, 297.

23. Plasseraud, L.; Cattey, H.; Richard, P. *Z. Naturforsch. Sect. B* **2009**, *64*, 831.

24. Grindley, T. B.; Thangarasa, R.; Bakshi, P. K.; Cameron, T. S. *Can. J. Chem.* **1992**, *70*, 197.

25. Bates, P. A.; Hursthouse, M. B.; Davies, A. G.; Slater, S. D. *J. Organomet. Chem.* **1989**, *363*, 45.

26. Holzapfel, C. W.; Koekemoer, J. M.; Marais, C. F.; Kruger, G. J.; Pretorius, J. A. *South Afr. J. Chem.* **1982**, *35*, 80.

27. Grindley, T. B.; Thangarasa, R. *J. Am. Chem. Soc.* **1990**, *112*, 1364.

28. Grindley, T. B.; Wasylishen, R. E.; Thangarasa, R.; Power, W. P.; Curtis, R. D. *Can. J. Chem.* **1992**, *70*, 205.

29. David, S.; Thiéffry, A.; Forchioni, A. *Tetrahedron Lett.* **1981**, *22*, 2647.

30. Grindley, T. B.; Thangarasa, R. *Can. J. Chem.* **1990**, *68*, 1007.

31. Kong, X.; Grindley, T. B. *Can. J. Chem.* **1994**, *72*, 2405.

32. Glen, A.; Leigh, D. A.; Martin, R. P.; Smart, J. S.; Truscello, A. M. *Carbohydr. Res.* **1993**, *248*, 365.

33. Roelens, S. *J. Org. Chem.* **1996**, *61*, 5257.

34. Grindley, T. B.; Kong, X. *Tetrahedron Lett.* **1993**, *34*, 5231.

35. Kong, X.; Grindley, T. B. *Can. J. Chem.* **1994**, *72*, 2396.

36. David, S.; Thiéffry, A. *J. Chem. Soc., Perkin Trans. 1* **1979**, 1568.

37. Holzapfel, C. W.; Koekemoer, J. M.; Marais, C. F. *South Afr. J. Chem.* **1984**, *37*, 19.

38. Kong, X.; Grindley, T. B. *J. Carbohydr. Chem.* **1993**, *12*, 557.

39. David, S.; Malleron, A. *Carbohydr. Res.* **2000**, *329*, 215.

40. Luchinat, C.; Roelens, S. *J. Org. Chem.* **1987**, *52*, 4444.

41. Nagashima, N.; Ohno, M. *Chem. Pharm. Bull.* **1991**, *39*, 1972.

42. Danishefsky, S. J.; Hungate, R. *J. Am. Chem. Soc.* **1986**, *108*, 2486.

43. David, S.; Thiéffry, A.; Veyrières, A. *J. Chem. Soc., Perkin Trans. 1* **1981**, 1796.

44. Alais, J.; Maranduba, A.; Veyrières, A. *Tetrahedron Lett.* **1983**, *24*, 2383.

45. Kaji, E.; Shibayama, K.; In, K. *Tetrahedron Lett.* **2003**, *44*, 4881.

46. Jenkins, D. J.; Potter, B. V. L. *Carbohydr. Res.* **1994**, *265*, 145.

47. Nagashima, N.; Ohno, M. *Chem. Lett.* **1987**, 141.

48. Cruzado, C.; Martín-Lomas, M. *Carbohydr. Res.* **1988**, *175*, 193.

49. David, S. *Carbohydr. Res.* **2001**, *331*, 327.

50. Kaji, E.; Harita, N. *Tetrahedron Lett.* **2000**, *41*, 53.

51. Iwasaki, F.; Maki, T.; Nakashima, W.; Onomura, O.; Matsumura, Y. *Org. Lett.* **1999**, *1*, 969.

52. Martinelli, M. J.; Vaidyanathan, R.; van Khau, V. *Tetrahedron Lett.* **2000**, *41*, 3773.

53. Gingras, M.; Chan, T. H.; Harpp, D. N. *J. Org. Chem.* **1990**, *55*, 2078.

54. Schrödinger, E. *Ann. Phys.* **1926**, *79*, 361.

55. Schrödinger, E. *Phys. Rev.* **1926**, *28*, 1049.

56. Born, M.; Oppenheimer, R. *Ann. Phys.* **1927**, *84*, 457.

57. Cramer, C. J. *Essentials of Computational Chemistry: Theories and Models*; John

Wiley & Sons Ltd.: Chichester, UK, 2002.

58. Jensen, F. *Introduction to Computational Chemistry*; John Wiley & Sons Ltd.: Chichester, UK, 2007; Vol. 2nd.

59. Ratner, M. A.; Schatz, G. C. *Introduction to Quantum Mechanics in Chemistry*; Prentice-Hall, Inc., 2001.

60. Roothaan, C. C. J. *Rev. Mod. Phys.* **1951**, *23*, 69.

61. Hall, G. G. *Proc. Roy. Soc. A* **1951**, *205*, 541.

62. Slater, J. C. *Phys. Rev.* **1930**, *36*, 57.

63. Boys, S. F. *Proc. Roy. Soc. A* **1950**, *200*, 542.

64. Lewars, E. *Computational Chemistry: Introduction to the Theory and Applications of Molecular and Quantum Mechanics*; Kluwer Academic Publishers: Boston, MA, 2003.

65. Foresman, J. B.; Frisch, A. *Exploring Chemistry with Electronic Structure Methods*; Gaussian Inc., 1996; Vol. Second.

66. Boys, S. F.; Bernardi, F. *Mol. Phys.* **1970**, *19*, 553.

67. Young, D. C. *Computational Chemistry: A Practical Guide for Applying Techniques to Real World Problems*; John Wiley & Sons, Inc., 2001.

68. Szabo, A.; Ostlund, N. S. *Modern Quantum Chemistry: Introduction to Advanced Electronic Structure Theory*; Macmillan Publishing Co., Inc., 1982.

69. Levine, I. N. *Quantum Chemistry*; Prentice Hall: Upper Saddle River, New Jersey, 2000; Vol. 5th.

70. Simons, J. *Introduction to Theoretical Chemistry*; Cambridge University Press, 2003.

71. Hohenberg, P.; Kohn, W. *Phys. Rev.* **1964**, *136*, B864.

72. Kock, W.; Hothausen, M. C. *A Chemist's Guide to Density Functional Theory*; 2nd ed.; Wiley-VCH: Weinheim, 2001.

73. Kohn, W.; Sham, L. J. *Phys. Rev.* **1965**, *140*, A1133.

74. Young, D. C. *Computational Chemistry: A pratical Guide for Applying Techniques to Real World Problems*; John Wiley&Sons, Inc., 2001.

75. Becke, A. D. *J. Chem. Phys.* **1993**, *98*, 5648.

76. Becke, A. D. *J. Chem. Phys.* **1993**, *98*, 1372.

77. Lee, C. H.; Yang, W.; Parr, R. G. *Phys. Rev. B* **1988**, *37*, 785.

78. Redfern, P. C.; Zapol, P.; Curtiss, L. A.; Raghavachari, K. *J. Phys. Chem. A* **2000**, *104*, 5850.

79. Wodrich, M. D.; Corminboeuf, C.; Schleyer, P. v. R. *Org. Lett.* **2006**, *8*, 3631.

80. Schreiner, P. R.; Fokin, A. A.; Pascal, R. A., Jr.; de Meijere, A. *Org. Lett.* **2006**, *8*, 3635.

81. Grimme, S.; Steinmetz, M.; Korth, M. *J. Chem. Theory Comp.* **2007**, *3*, 42.

82. Becke, A. D.; Johnson, E. R. *J. Chem. Phys.* **2005**, *123*.

83. Becke, A. D.; Johnson, E. R. *J. Chem. Phys.* **2007**, *127*.

84. Grimme, S.; Antony, J.; Ehrlich, S.; Krieg, H. *J. Chem. Phys.* **2010**, *132*.

85. Zhao, Y.; Truhlar, D. G. *Acc. Chem. Res.* **2008**, *41*, 157.

86. Cundari, T. R.; Benson, M. T.; Lutz, M. L.; Sommerer, S. O. *Rev. Comp. Chem.* **1996**, *8*, 145.

87. Karni, M.; Apeloig, Y.; Kapp, J.; Schleyer, P. v. R. In *Chemistry of Organic Silicon Compounds*; Rappoport, Z., Apeloig, Y., Eds.; John Wiley: Chichester, UK, 2001.

88. Pyykkö, P. *Chem. Rev.* **1988**, *88*, 563.

89. Gropen, O. In *Methods in Computational Chemistry, Vol. 2: Relativistic Effects in Atoms and Molecules*; Wilson, S., Ed.; Plenum Press: USA, 1988; Vol. 2, p 109.

90. Hay, P. J.; Wadt, W. R. *J. Chem. Phys.* **1985**, *82*, 299.

91. Check, C. E.; Faust, T. O.; Bailey, J. M.; Wright, B. J.; Gilbert, T. M.; Sunderlin, L. S. *J. Phys. Chem. A* **2001**, *105*, 8111.

92. Schlegel, H. B., Computers in Chemistry-Molecular Modeling: Potential Energy Surface. http://www.chem.wayne.edu/~hbs/chm6440/PES.html. (July 13, 2013)

93. Peng, C. Y.; Ayala, P. Y.; Schlegel, H. B.; Frisch, M. J. *J. Comp. Chem.* **1996**, *17*, 49.

94. Gaussian 09; version C.01 ed.; Gaussian, Inc: 2009.

95. Peng, C. Y.; Schlegel, H. B. *Isr. J. Chem.* **1993**, *33*, 449.

96. Zhou, Y.; Li, J.; Zhan, Y.; Pei, Z.; Dong, H. *Tetrahedron* **2013**, *69*, 2693.

97. Xia, L.; Lowary, T. L. *J. Org. Chem.* **2013**, *78*, 2863.

98. Kruse, H.; Goerigk, L.; Grimme, S. *J. Org. Chem.* **2012**, *77*, 10824.

99. Head-Gordon, M.; Pople, J. A.; Frisch, M. J. *Chem. Phys. Lett.* **1988**, *153*, 503.

100. Frisch, M. J.; Head-Gordon, M.; Pople, J. A. *Chem. Phys. Lett.* **1990**, *166*, 275.

101. Frisch, M. J.; Head-Gordon, M.; Pople, J. A. *Chem. Phys. Lett.* **1990**, *166*, 281.

102. Head-Gordon, M.; Head-Gordon, T. *Chem. Phys. Lett.* **1994**, *220*, 122.

103. Saebo, S.; Almlof, J. *Chem. Phys. Lett.* **1989**, *154*, 83.

104. Gonzalez, C. S.; H. B. *J. Phys. Chem.* **1989**, *90*, 2154.

105. Gonzalez, C. S.; H. B. *J. Phys. Chem.* **1990**, *94*, 5523.

106. Whittleton, S. R.; Boyd, R. J.; Grindley, T. B. *Can. J. Chem.* **2009**, *87*, 974.

107. Whittleton, S. R. PhD Thesis, Dalhousie University, 2009.

108. Olmstead, W. N.; Brauman, J. I. *J. Am. Chem. Soc.* **1977**, *99*, 4219.

109. Asubiojo, O. I.; Brauman, J. I. *J. Am. Chem. Soc.* **1979**, *101*, 3715.

110. Pellerite, M. J.; Brauman, J. I. *J. Am. Chem. Soc.* **1980**, *102*, 5993.

111. Martin, J. M. L.; Sundermann, A. *J. Chem. Phys.* **2001**, *114*, 3408.

112. Wadt, W. R.; Hay, P. J. *J. Chem. Phys.* **1985**, *82*, 284.

113. Pople, J. A.; Binkley, J. S.; Seeger, R. *Int. J. Quantum Chem.* **1976**, 1.

114. Pople, J. A.; Seeger, R.; Krishnan, R. *Int. J. Quantum Chem.* **1977**, 149.

115. Krishnan, R.; Pople, J. A. *Int. J. Quantum Chem.* **1978**, *14*, 91.

116. Zhao, Y.; Schultz, N. E.; Truhlar, D. G. *J. Chem. Theory Comp.* **2006**, *2*, 364.

117. Lu, L.; Hu, H.; Hou, H.; Wang, B. *Comput. Theor. Chem.* **2013**, *1015*, 64.

118. Zhao, Y.; Truhlar, D. G. *J. Chem. Theory Comp.* **2008**, *4*, 1849.

119. Van der Kerk, G. J. M. *Adv. Chem. Ser.* **1976**, *157*, 1.

120. Munavu, R. M.; Szmant, H. H. *J. Org. Chem.* **1976**, *41*, 1832.

121. Tsuda, Y.; Nishimura, M.; Kobayashi, T.; Sato, Y.; Kanemitsu, K. *Chem. Pharm. Bull.* **1991**, *39*, 2883.

122. Wagner, D.; Verheyden, J. P. H.; Moffatt, J. G. *J. Org. Chem.* **1974**, *39*, 24.

123. Lou, X. *Asian J. Chem.* **2013**, *25*, 2281.

124. Yang, Y.; Martin, C. E.; Seeberger, P. H. *Chem. Sci.* **2012**, *3*, 896.

125. David, S. *C. R. Acad. Sci., Ser. C* **1974**, *278*, 1051.

126. Nashed, M. A.; Anderson, L. *Tetrahedron Lett.* **1976**, *17*, 3503.

127. Al-Mughaid, H.; Grindley, T. B. *Carbohydr. Res.* **2004**, *339*, 2607.

128. Florio, G. M.; Zwier, T. S.; Myshakin, E. M.; Jordan, K. D.; Sibert, E. L. *J. Chem. Phys.* **2003**, *118*, 1735.

129. Gu, Q.; Trindle, C.; Knee, J. L. *J. Chem. Phys.* **2012**, *137*, 091101.